UNIVERSITY OF AGDER

A Novel Solid Oxide Fuel Cell Anode Substrate Performance and Lifetime Studies

K. A. Chamindi Seneviratne

Thesis Supervisor

Professor Peter Hugh Middleton

University of Agder

This Master's Thesis is carried out as a part of the education at the University of Agder and is therefore approved as a part of this education. However, this does not imply that the University answers for the methods that are used or the conclusions that are drawn.

University of Agder, 2013

Faculty of Engineering and Science

Department of Engineering Sciences

Abstract

The competition in the fuel cell market today is driving improved performance and among the fuel cells types the Solid Oxide fuel cell (SOFC) has a top rank because of its high efficiency in combined heat and power applications. The RoxSolid cell (2-R cell) is a newly invented robust construction developed by Fiaxell – a leading company in SOFC developments and is yet another step to further increasing the performance of current SOFCs.

Before introducing the 2-R cell to the market its performance characteristics need to determined and documented. In particular it is necessary to show that the claims that the 2-R cell is robust are backed up by laboratory tests. The ability of the cell to withstand the effects of redox cycling is essential and therefore redox cycling is one of the main test techniques used in this work. The performance and life time properties of the received 2-R cells were determined by measuring the I-V characteristics during and after redox cycling. In addition, the electrical resistance of the anode substrate material was studied separately under repeated redox cycling.

The test results of the I-V and Power characteristics confirm that the performance of the best 2-R cell is approximately seven times higher than the reference sample (a conventional anode supported SOFC cell). Through the results of resistance value variation of the new anode substrate samples, it was shown that there was an increase of conductivity with the time, converse to the conventional results. The calculated anode conductivity values were approximately 20 % higher than the theoretical data obtained from the percolation theory.

The optical microscopy images taken after redox cycle testing confirmed the higher robustness of the cells compared to the reference SOFC, and also showed a better ability of the 2-R cell to withstand redox cyclings. The results of the conducted experiments confirmed that overall performance and lifetime properties of the Fiaxcell “2-R cell” are considerably better than the conventional SOFCs.

Keywords : Rox Solid, 2-R cell, Anode substrate, Redox cycle testing, Reduction resistance, I-V characteristics, Morphology, Performance, Robustness, Life time

Acknowledgements

I would like to express my sincere gratitude to my thesis supervisor Prof. Peter Hugh Middleton for his guidance and cordial support throughout my work. His support and motivations were invaluable driving forces for me for the successful accomplishment of this study.

I am also very grateful to my master's programme coordinator Stein Bergsmark for his advice on thesis writing and for providing useful suggestions.

I would like to thank my fellow students specially, Mattias Henry Nilsson for his essential scientific and motivational support and Mussie Kiros Weldeab for giving me a helping hand during the laboratory experiments.

Furthermore I would like to thank everybody who has supported me throughout the entire process, both by keeping me harmonious and helping me putting pieces together.

K. A. Chamindi Seneviratne

Contents

Nomenclature

Δg_f	Gibbs Free Energy	[J mol^{-1}]
E_{OCV}	Open circuit voltage	[V]
Z	Number of Electrons	
F	Faraday constant	[C]
E_r	E_{OCV} with pressure correction	[V]
R	Universal Gas constant	[JK^{-1}mol^{-1}]
T	Temperature	[K]
Π	Partial pressure	
Δh_f	Change in enthalpy	[J mol^{-1}]
E_{max}	Maximum electro motive force of cell	[V]
η	Efficiency	
ΔV_{loss}	Potential loss	[V]
ΔV_{act}	Activation potential	[V]
$\Delta V_{act,Cathode}$	Activation potential of cathode	[V]
$\Delta V_{act,Anode}$	Activation potential of anode	[V]
i	Current density of the cell	[A cm^{-2}]
I	Current	[A]
A	Cell area	[cm^2]
$i_{0,C}$	Exchange current densities of cathode	[A cm^{-2}]
$i_{0,A}$	Exchange current densities of anode	[A cm^{-2}]
α_C	Charge transfer coefficient of cathode	
α_A	Charge transfer coefficient of anode	
ΔV_{ohm}	Ohmic potential	[V]
$R_{electrolyte}$	Resistance of electrolyte	[Ω]
$R_{cathode}$	Resistance of cathode	[Ω]
R_{anode}	Resistance of anode	[Ω]
ΔV_{conc}	Concentration potential	[V]
$S_1(T)$, $S_2(T)$	Seebeck coefficients	[VK^{-1}]
ρ	Resistivity	[Ω m]
σ	Conductivity	[Sm^{-1}]
$E_{mixed\ potential}$	Mixed potential	[V]
C, d, P_1, P_2, P, Q	Empirically determined constants	

List of Figures

List of Tables

1

Introduction

This chapter constitutes a brief introduction to evaluating the stability of a novel SOFC towards redox cycle testing, Section 1.1 presents the motivation and the motivation and the importance of the project. Section 1.2 presents the approach adopted in this work to evaluate the new SOFC-called RoxSolid cell or 2-R Cell^{TM}. Section 1.3 is describes the goal and the objectives of the thesis and the section 1.4 introduces the methodology. Section 1.5 includes the key limitations and assumptions of the study and finally, Section 1.6 gives the outline of the thesis.

1.1 Motivation for Testing New SOFCs

Today the world is realizing the need for more efficient and reliable energy supplies without toxic emissions such as NO_x, SO_x and so that the Fuel Cell technology improves day by day with the invention of new cell types. Among the other high temperature fuel cell types the solid oxide fuel cell (SOFC) has hold a top rank because it can be used as a combined heat and power applications with much higher efficiency [1].

Today research is focused on finding new materials for electrodes and electrolyte to increase performance, to reduce the production cost of SOFCs and as well as to make energy production more efficient and reliable [2]. Evaluating the stability of the SOFC is critically important in manufacturing a reliable fuel cell in mass production and commercialization.

The stability tests can be carried out by using different test approaches such as Redox Cycle testing, Thermal or the temperature cycle testing and etc. This thesis is mainly dealing with Redox cycling which occurs when the anode side of the cell is exposed to fuel and air in repeated cycles at operating temperature-typically around 800 ^{0}C.

During Redox Cycles the anode, that is made of Nickel based material which is quite ductile, transforms from its oxide form to the metallic elemental form and vice-versa. Nickel-cermets (Ni-YSZ for example) are sensitive to the presence of sulfur in the fuel they cannot tolerate the oxidation during start-up and shut-down of cycles. They also can be severely damaged by carbon formation on the anode when exposed to hydrocarbon fuels [3].

Due to the morphology variations of metallic Ni compared to its oxide, NiO during redox cycles there can be a build-up of internal stresses within the anode substrate material. The occurrence of these types of sudden state changes weakens the material properties generating cracks and fragmentation. Therefore in order to commercialize this new type of anode support material it is necessary to determine the stability and resistance to cracking during redox cycling.

1.2 The RoxSolid Cell

This thesis mainly deals with the testing of stability and performance of a novel type of redox resistant anode supported SOFCs for industrial purposes. This Master's thesis is part of a Eurostars funded project called RoxSolidCell. The product under test is the new anode supported SOFC, named "2-R Cell™" (trade name) that has been invented by a small company (SME) called Fiaxell, a Swiss-based company. Fiaxcell is the lead SME in the

RoxSolidCell project. Production will be developed by a French ceramic company called CTI and demonstration by a Norwegian company called Prototech, a leading company in fuel cell technology. To achieve the necessary economic criteria for mass production of SOFC stacks, it is necessary to improve the reliability, lifetime and cost of high temperature Solid Oxide Fuel Cell. The 2-R cell is currently the only substrate material able to accomplish these criteria.

1.3 Research Goals

This thesis is mainly dealing with a study of performance and lifetime properties for the 2-R cell specimens. This study provides experimental data and analyzed data for the quality improvements of second stage of the novel anode supported RoxSolid Fuel Cell. The complete study is categorized under two main goals as described below and the objectives under each, were studied during the thesis accordingly to fulfill the goals

- **Research goal 1 – Redox stability properties of the "2-R Cell" Anode Substrate through redox cycle testing.**

  The ability of the new anode substrate material to withstand the harsh changes in environment caused by repeated switching from air to fuel over many accumulated cycles will constitute the first experimental phase of the project. The electrical resistance of the samples will be continually monitored with the time during the redox cycling. The integrity of the specimens after completing the testing will be evaluated by optical microscopy.

- **Research goal 2 – Performance study of the "2-R Cell" samples**

  The electrochemical fuel cell performance will be evaluated on complete cells made from the new anode substrate material. For each test, current-voltage curves will be recorded before and after repeated redox cycles. Lifetime performance will also be determined by running the cells at a fixed output potential over a period of many hours of operation. The integrity of the specimens after completing the testing will be evaluated by optical microscopy. The IV curves of the 2-R cells will be simulated according to the theoretical calculations.

1.4 Research Methodology

To achieve the above research goals the study will be carried out by following the steps:

a. Getting Familiar with Test Equipment and Safety Issues

There will be connections among number of equipment such as test bench, furnace, thermo-computer, thermocouple, fuel flow controller and etc., in-order to build the complete test set-up, to function all together. The test bench in the laboratory is a piece of new equipment and it will be important to study the operation and the procedure of properly mounting the cell on it as well as dismounting. Familiarization with other test equipment and also safety procedures will also be required.

b. Carrying out Redox Cycle Test for Anode Substrates and for 2R Cell specimens

Before attending to the test practically, the redox cycle testing and testing procedure will be studied by analyzing the previous researches. Applying the given testing conditions (heating temperature, fuel flow rates, etc.) properly to the testing specimen, the required measurements will be taken for further analysis.

c. Data Analysis

Finally the data analysis will be done for all the samples that are going to be tested, calculating the required parameters and making plots. The results of the novel 2-R cells will be compared with the results of reference SOFC cell to analyse the performance.

d. Modelling

A model will be created for I-V curves theoretically and by varying the parameters, the simulation output will be tried to fit with the practical results.

1.5 Key Assumptions and Limitations

It is assumed at the beginning, that all the experiments will be conducted according to the test conditions that are given by the Fiaxell Company where the cell was invented. Fiaxell provided a number of specimens to test which included 5 of complete 2-R cells and 5 of 2-R cell anode substrates. Each of them is to be tested over several hours of duration under redox conditions and under a given specific temperature and fuel supply conditions.

The performance analysis will be limited to cope with only the results of the redox cycle tests. To obtain the maximum from the tests with existing short period of time, three and half months, and with the limited number of testing equipments, the number of redox cycles will be limited for a single specimen.

The results will be subsequently compared assuming that all the specimens are tested under the same environmental conditions and thus the theoretical and numerical evaluations will be considered as valid under the applied conditions.

1.6 Thesis Outline

The remaining chapters of the thesis report are organized as follows.

Chapter 2 describes the fundamentals of SOFC with different categorizations. The electro-chemical behavior of SOFC presents in Chapter 3 introducing some of the currently available anode materials. In chapter 4 we discuss the functions of testing equipment and safety facts. Chapter 5 and 6 present the results of redox cycle tests for the anode substrates and for the 2R-cells accordingly with related calculations. Chapter 7 allocates to present the steps of modelling the I-V characteristics. Then in Chapter 8, we discuss the results and observations found from the experiments mentioned in Chapter 5 and 6. Finally the conclusion of the research and possible further work is presented in Chapter 9.

2

SOFC and Background Study

This chapter describes the principles of fuel cells, focusing mainly on SOFCs. A general introduction to the fuel cells is given in Section 2.1, including the basic operation of a FC. The internal function, electro-chemical behaviour with the materials used for electrolyte and electrodes, different categorizations of SOFCs and the development of SOFC from the beginning are the main topics described through Section 2.2.

2.1 The Fuel Cell

2.1.1 Introduction

The energy production and distribution highly affect all the sectors of a country such as industry, transportation, health, etc and finally the economy of the country. The advancement of the technology used to produce energy is important for the quality of life on the earth which depends on all the factors mentioned above.

In the past few decades the fossil fuel supported to fulfill the rapid energy demand increase but with the decrease in the amount of fossil fuel and the higher demand, it has led to elevation of prices. And also the average global temperature rise increased due to the ever increasing emission of green house gases emits while using fossil fuels [4]. Hence the question appears whether these conventional fossil fuels can be converted to electricity in an environmentally benign at prices that can be afforded. As a result the countries started to provide the demand by mixing other energy sources such as wind, photovoltaic, solar thermal systems and ocean wave energy.

As a result of researching more efficient energy production methods, the principle of a fuel cell was invented more than a hundred years ago, in 1838–1839, by William Robert Grove and Christian Schönbein [5].
Major fuel cell types currently in the market are as follows,

- **Proton Exchange Membrane Fuel Cell (PEMFC)**
- **Direct Methanol Fuel Cell (DMFC)**
- **Solid Oxide Fuel Cell (SOFC)**
- **Phosphoric Acid Fuel Cell (PAFC)**
- **Molten Carbonate Fuel Cell (MCFC)**
- **Alkaline Fuel Cell (AFC)**

In future the world will leads to a green energy production reducing the impacts on the environment. The Fuel Cell technology is one of the advance technologies which have the ability to avoid the harm to the environment while producing energy. Today the challenges in front of Fuel Cell industry are cost reduction and increase of durability to be solved by proper material selections and improving design engineering techniques.

2.1.2 Fuel Cell Function

A Fuel Cell is an electrochemical device which can directly convert chemical energy into electrical energy from a reaction between a fuel and an oxidant. Fuel cell technology is able to generate electricity at high efficiencies than other technologies which involves more mechanical equipments. The below Figure 2.1, is a schematic structure of a basic fuel cell and it consists of an electrolyte with porous anode and cathode electrodes.

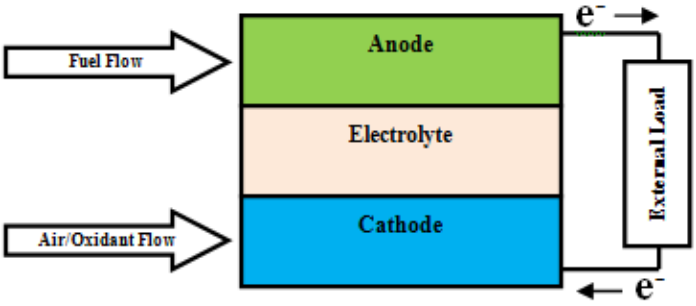

Figure 2.1: Schematic structure of a planar fuel cell

The Fuel and oxidant gases flow along the cathode and anode materials and finally the electro-chemical reaction occurs at both the three-phase-boundary regions established at the gas-electrolyte-electrode interfaces. Hydrogen, methanol, ethanol, natural gas (gaseous fossils) can be used as fuels to the fuel cell and Oxygen or air can be used as the oxidant. From the above mentioned fuel cell types the Solid Oxide Fuel Cell is considered as a High Temperature fuel cell.

2.2 Solid Oxide Fuel Cell

2.2.1 The Structure and function of SOFC

The solid oxide fuel cell is a complete solid state fuel cell and it uses an oxide ion conducting ceramic material as the electrolyte. Because of the solid state the construction is simpler than other fuel cells and also the working concept is simpler as only two phases (solid and gas) are required.

The reduction reaction occurs at the cathode side of the fuel cell and, the fuel oxidation takes place at the anode. Using an external circuit, the electric conduction path is closed while providing a path to guide the electrons through it. The construction and the operation principle of SOFC is as shown in Figure 2.2.

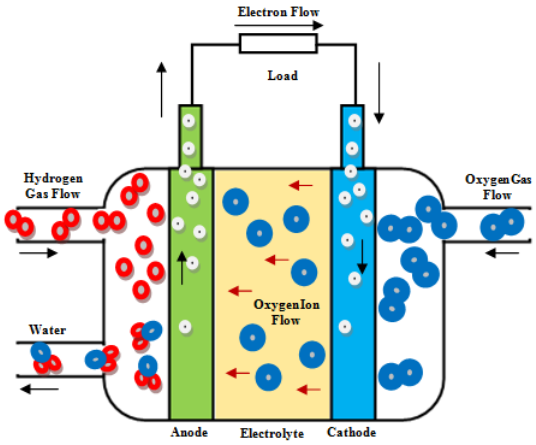

Figure 2.2: Construction and operation of a Solid Oxide Fuel Cell

Commonly the cathode of the solid oxide fuel cell is made up of composition of LSM ($La_x Sr_{1-x} MnO_3$) /YSZ or LSM/SSZ materials and perovskite $Mn(La,Sr)O_3$ is used as the reduction catalyst for Oxygen [6]. The reaction at the cathode is as below,

$$O_2 + 4e \rightarrow 2O^{2-} \quad (2.1)$$

The anode is usually made of a composition of Ni and YSZ cermet (Common anode compositions: NiO-Zr_{1-x} Y_xO2 (YSZ) and NiO-Zr_{1-x} Sc_xO2 (SSZ)) [6]. The anode side does not need current-collecting layer because metal Ni is an excellent electronic conductor and it works as the catalyst to the anode oxidation reaction which is as below,

$$2H_2 + 2O^{2-} \rightarrow 4e + 2H_2O \quad (2.2)$$

Most commonly the Yttria Stabilized Zirconia (YSZ, with a composition of 8 mol % Y_2O_3 and 92 mol % ZrO_2, sometimes referred as 8YSZ) is used as the solid state electrolyte which is an electrically non-conductive, thin, gas tight ceramic membrane.

YSZ-based SOFCs usually operate at high temperatures such as 750–1,000 ^{0}C to be worked at high efficiency because of the limited transport and catalytic properties of the SOFC materials at low temperatures. But by doping Ceria (Ce) into the electrolyte and cathode composites the operating temperature can be reduced up to 700 ^{0}C degrees.
During the operation of fuel cell the Oxygen molecules are absorbed by the cathode surface and they are reduced in to ionic oxygen species. Then these ionic oxygen move through the electrolyte to the anode and combine with fuel molecules to form water.

The combination of the above two reactions yields the overall reaction of the fuel cell,

$$2H_2 + O_2 \rightarrow 2H_2O \quad (2.3)$$

2.2.2 Categorization of SOFCs

Currently SOFCs are being manufactured, using different structures for different types of practical purposes. There are two basic types of cell structures are presented in the market, one is a planar structure and the other one is a tubular structure. The cells are in series in the planar type and connected by the interconnect plates, as schematically shown in Figure 2.3.

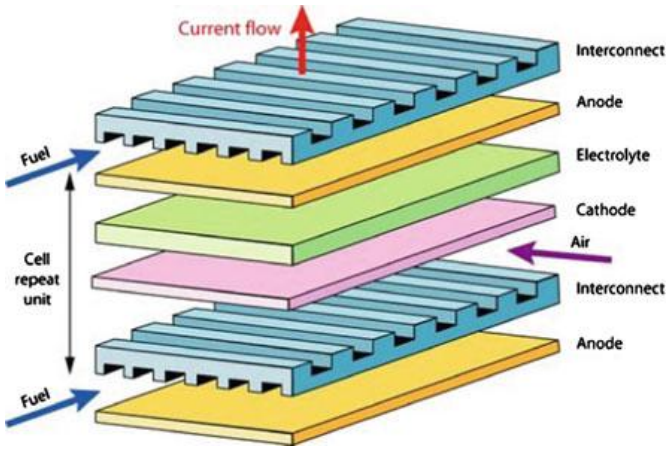

Figure 2.3: Structure of a planar SOFC [1]

In tubular SOFCs, the anode and the cathode electrodes are made as long porous tubes and the cell interconnections are as illustrated in Figure 2.4.

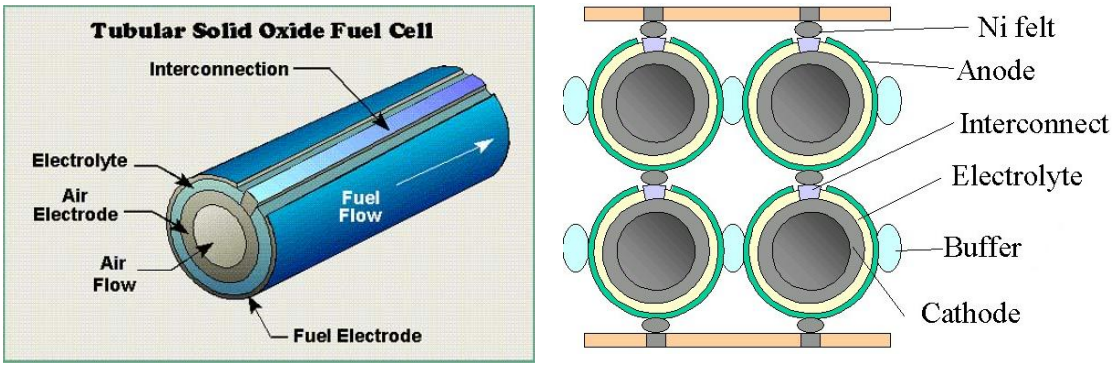

Figure 2.4: Structure of tubular SOFC and cell stacks [2]

Another categorization of SOFCs by the way in which the functional layers are built up is as electrolyte supported, anode supported and metal supported cells. Electrolyte supported cells (ESC) are in general robust; they are stable during redox cycles and can provide high fuel utilization. Because of the higher operation temperature a special high chromium alloy is needed for interconnections and the material cost is higher. The life time of a current electrolyte supported cell is about two years.

Figure 2.3 & 2.4 reffered from [1] www.doitpoms.ac.uk, 23. 01. 2013
[2] www.optics.rochester.edu, 25. 01. 2013

The Anode Supported Cells (ASC), show sufficient electrochemical performances already at low temperature (650 °C), which means that higher output is reached at lower temperature. Because of the lower operation temperature, the degradation and the material cost also reduced. The disadvantage is that the cells are totally destroyed if air enters the anode chamber or even just at the cell edges.

A Metal Supported Cell (MSC) is not a famous cell structure but it shows high electrochemical performances already at low temperature (650 °C), and the redox resistance is good. The degradation is significant in MSC cells due to steel corrosion and inter-diffusion of chromium with the anode material. Also there are some fabrication issues when the electrolyte is a ceria based one.

From the cost perspective the Anode Supported Cells are considered as the best ones, and in the next section the development background of the SOFC is reviewed.

2.2.3 Development of SOFC and Future Goals

The Fuel Cell technology has a very long history nearly of 150 years where in 1839 the first fuel cell was conceived by Sir William Robert Grove, a Welsh judge, inventor and physicist. He mixed hydrogen and oxygen in the presence of an electrolyte, and produced electricity and water. But the term "Fuel Cell" was first coined by Ludwig Mond and Charles Langer, who attempted to build a working fuel cell using air and industrial coal gas.

As in the documents the initial ceramic cell was tested by a Swiss scientist, Emil Baur (1873-1944), and his colleague H. Preis with solid oxide electrolytes in the late 1930s. They used zirconium, yttrium, cerium, lanthanum, and tungsten oxide as the materials to make electrolyte and electrodes [7].

In the early 1960s, there was intensity on research programs on SOFC for energy needs mainly for military, space and transport applications. The second golden era of researching SOFCs began from mid 1980s and going on today to find better electrode, electrolyte materials to suit with the current economy. Currently there are more than 50 huge companies working on SOFCs. To compete with the market by producing SOFCs with high performance, it is advisable to introduce the cells made of new materials avoiding the weaknesses.

For the development of SOFC, in 2001 the Department of Energy (DOE) office of fossil energy initiated a Solid State Energy Conversion Alliance (SECA) program with the industrial sector. Their aims are to produce low cost high efficient, molecular, mass produced fuel cells for stationary, transportation and military markets [8].

2.2.4 Applications of SOFC

There is a broad spectrum of power generation applications of SOFCs, from small scale, light weight, compact devices in the range of few watts to kilowatts to larger applications of SOFCs, in the megawatt range. In addition to the well known applications as stand alone or in CHP (Combined Heat and Power) systems, SOFCs are being developed in an SOFC/gas turbine hybrid systems in 1 to more than 10 MW scale with more than 65 percent efficiency.

Because of the high temperature resultant of the SOFCs, they are mostly found in larger commercial sites as standalone CHP systems with higher efficiency and also for some of the small utility substations, the SOFCs used as hybrid systems [8].

3

Electro Chemistry of SOFC and Anode Materials

This chapter includes the basic principles of electro chemistry of SOFCs. In the beginning a description of anode supported cells is given under Section 3.1 and different types of currently available anode materials mentioned with some fabrication methods in Section 3.2. Finally the section 3.3 covers the electrochemistry principles of SOFCs focusing on the theoretical cell potential with losses and the efficiency of the cell.

3.1 Anode Supported SOFCs

The high power utilization of the solid oxide fuel cells in the combined heat and power applications grabs the attraction of the researchers. As the Ni-cermet anode supported SOFC operates under intermediate temperature conditions and gives higher conductivity it avoids damages to the cells due to thermal expansion mismatch at high processing temperature. The possibility of making much thinner electrolytes for this type of fuel cells provides a higher conductivity [9].

The oxide-ion conductivity of the electrolyte is much smaller than the electronic conductivity of the electrodes and the external circuit and because the electronic and ionic currents must be matched during charge and discharge. For that it is important to make the electrolyte layer as thin as possible. It's an advantage of the anode supported SOFCs because the electrolyte layer can be made as few μms (10–30 μm thickness for intermediate temperature operating FCs) [10].

The anode is the fuel electrode where oxidation occurs by liberating electrons to the external circuit. Most SOFCs can work well with fairly pure H_2 and CO gases that they can be widely produced from hydrocarbons via reforming and the reformation reaction is given below [11],

$$CH_4 + H_2O = CO + 3H_2 \quad (3.1)$$

Sulfur is a constituent of hydrocarbon fuels, and its removal is necessary as it poisons most catalysts. The more sulfur-tolerant the anode, the lower are the requirements for sulfur removal from the feed gas

As a hackneyed fuel, the natural gas can be used as well, so that the overall reactions at the anode can be presented as shown below,

$$H_2 + O^{2-} = H_2O + 2e- \quad (3.2)$$

$$CO + O^{2-} = CO_2 + 2e- \quad (3.3)$$

$$CH_4 + 4O^{2-} = CO_2 + 2H_2O + 8e- \quad (3.4)$$

The electrochemical oxidation of CO at the surface of the anode must be fast enough to prevent formation of coke deposition on it, which can block further reaction.

$$2CO = C + CO_2 \quad (3.5)$$

This can be avoided while making reaction (3) faster than reaction (5) [11]. Therefore the anode material fabrication method and the composition improvements are more important to avoid above effects for whatever fuel is to be used.

3.2 Anode Material Properties and Fabrication Methods

Since the anode operates in the reducing state the metallic catalysts are the suitable materials and among Mn, Fe, Co, Ni, Ru, and Pt the best electrochemical activities present with Hydrogen is by the Ni catalyst [12].The pure Nickel material has the melting point of 1453 $^{\circ}$C, and the thermal expansion coefficient $\alpha = 13.3\times10^{-6}\ K^{-1}$ that is higher than the $\alpha\approx10.5\times10^{-6}\ K^{-1}$ of a YSZ electrolyte. At the oxidation state where the Ni turns to its oxide, NiO, then the thermal expansion coefficient α becomes $13.8\times10^{-6}\ K^{-1}$ [13]. But the better performance can be obtained when the thermal expansion coefficients of the YSZ electrolyte and the cermet are properly matched.

3.2.1 Ni–$ZrO_2(Y_2O_3)$ Cermet

This is the most common low cost chemically stable anode material which is having the thermal coefficient close to the electrolyte. Another importance of this type of anodes is the intrinsic charge transfer resistance that is associated with the electro catalytic activity at Ni/YSZ boundary is low. The electrical conductivity of Ni/YSZ cermet is strongly dependent on its nickel content and it is also affected by size ratio (density) between YSZ and Ni (dYSZ/dNiO).

The first step of common fabrication method is that commercial NiO and YSZ fine powders are coarsened by heat treatment to give desired particle sizes and size distribution. Coerciveness of the YSZ powder is important to increase the porosity of the anode cermet and the triple-phase boundary area. The powders are then homogenized by mechanical mixing, pressed with or without a green electrolyte, then sintered in air and finally annealed in wet H_2 or fuel to reduce the NiO to metallic nickel to form a porous Ni/YSZ anode. But now by using different technologies, the anode cermets can be formed with higher performance and a comparison study of anodes, fabricated using two different processing methods is shown in the figure below [14].

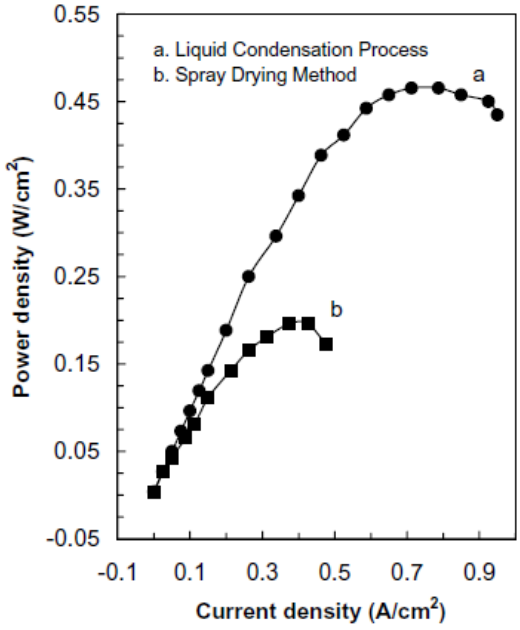

Figure 3.1: Comparison of the power generating characteristics of the unit cell fabricated using two different approaches [14]

3.2.2 Ni/YSZ Cermet Doped with Molybdenum and Gold

This technique is mainly related to mitigate the problems of leaching and delaminating of the anode materials. Also due to the high operating temperature there is a tendency to burn the anode as a result of internal fuel reformation. This doping can reduce the above effect as well as the doped cermets have shown increased resistance to carbon deposition. As the fuel is methane, the new cermet has increased methane conversion, and increased durability, higher performance at lower reforming temperatures and lower methane/steam ratios [14].

3.2.3 Rare Earth-Doped Ceria (CeO_2) Ceramics

Since ceria is an excellent electro catalyst for CH_4 oxidation, it can be used for direct electrochemical oxidation of methane at the anode as shown below.

$$CH_4 + 4O^{2-} = CO_2 + 2H_2O + 8e^- \qquad (3.6)$$

Rare earth oxides such as Gd_2O_3, Sm_2O_3, and Y_2O_3 which can increase the conductivity of the cell as tabulated in the table below.

Table 3.1: Ionic conductivity data for some rare earth-doped ceria ceramics. [14]

Composition	**Dopant**	**Conductivity σ (S cm^{-i})**		
		500^{0}C	**600^{0}C**	**700^{0}C**
$\mathbf{Ce_{0.9}Gd_{0.1}O_{1.95}}$	Gd^{3+}	0.0095	0.0253	0.0544
$\mathbf{Ce_{0.9}Sm_{0.1}O_{1.95}}$	Sm^{3+}	0.0033	0.0090	0.0200
$\mathbf{Ce_{0.88}Y_{0.113}O_{1.9435}}$	Y^{3+}	0.0087	0.0344	0.1015
$\mathbf{Ce_{0.8}Gd_{0.2}O_{1.9}}$	Gd^{3+}	0.0053	0.0180	0.0470

But the ionic conductivity of doped ceria is about one-order of magnitude larger than that of Yttria-doped Zirconia, making it a suitable candidate for the intermediate temperature SOFCs. Ceria-based anodes such as CG4 ($Ce_{0.6}Gd_{0.4}O_{1.8}$) are recognized as effective anode cermets in suppressing carbon deposition [14].

3.2.4 Other Anode Materials

Ni with various Mixed Ionic-Electronic Conductors (MIEC) are being tested to improve the anode performance via increasing the conductivity. Another two famous types of anode cermets are Yttria-Doped Ceria (YDC) and Samaria-Doped Ceria (SDC) mainly for high temperature SOFCs. The fracture strength of Ni–YSZ cermet would increase with increasing the content of YSZ. The electrochemical performance of $La_{0.7}Sr_{0.3}Cr_{0.8}Ti_{0.2}O_3$ and doped $SrTiO_3$ perovskite anode is very much inferior to that of Ni/YSZ cermet [11] [15]. The electrical resistance of the cermet, however, would also increase with the volumetric fraction of YSZ [16].

As the main aim of the anode material is to accelerate the electrode gas reaction, whereas in Ni/YSZ cermet this reaction is only limited to the three-phase contacts between fuel, electrode, and electrolyte. Hence plenty of work remains for the future researches to develop these materials expanding the limitations of thermal expansion coefficient mismatch, sulfidation and carburization tolerance, chemical compatibility with electrolyte as well as catalytic behavior.

3.3 Electro Chemistry of SOFC

To study the practical energy outputs, the electro chemical behavior is important when considering the theoretical energy generation of the SOFCs and the losses characterized by the current voltage curves. A brief discussion of theoretical energy generation of SOFCs is given in the following sections.

3.3.1 Gibbs Free Energy and the Open Circuit Voltage

Gibbs Free energy can be defined as the energy available in the chemical reaction to do any external work neglecting the losses and neglecting any work done by changes in pressure and volume. Change in Gibbs Free energy (Δg_f) for the SOFC overall reaction,

$$H_2 + \frac{1}{2}\, O_2 \rightarrow H_2O \qquad (3.7)$$

at 800^0C is -188.6 KJ mol^{-1}, [17] where the water is at the gaseous stage at this temperature.

The theoretical Open Circuit Voltage (OCV) for a lossless (reversible) H_2 fuel cell is given by the following equation,

$$E_{OCV} = -\frac{\Delta g_f}{zF} \qquad (3.8)$$

Where E is the generated OCV and F is the Faraday constant = 96 485 C
Z is the number of electrons donating to the cell for each molecule of fuel and here at the cathode O_2 is reduced to O^{2-} by taking up 2 electrons from the cathode material and hence here, the z = 2 [18].

As the theoretical cell potential varies with the temperature due to the dependency of Δg_f on temperature, the E also depends on the pressure conditions as well. The above equation is valid only for the atmospheric pressure conditions but it can be operated at any pressure condition. Hence the theoretical potential of a cell can be corrected by the Nernst equation as,

$$E_r = E_{OCV} + \frac{RT}{zF}\left[\frac{\Pi_{H_2}\,\Pi_{O_2}^{0.5}}{\Pi_{H_2O}}\right] \qquad (3.9)$$

Where Π represents the partial pressure components of the reactants and products related to the atmospheric pressure and the above equation is valid for the gaseous stage of all. When the air is used instead of pure oxygen, Π_{O_2} is proportional to its concentration.

3.3.2 Maximum Possible Cell Efficiency

The efficiency of any of the energy conversion device can be defined as the ratio of useful energy output to the supplied or the input energy and for the FC the output is the electrical energy produced and the input is the change in the enthalpy formation ((Δh_f) of the above reaction. At the temperature of 800^0C, the Δh_f = -241.83 kJ / mol (Higher Heating Value) [19].

The maximum possible Electro Motive Force (EMF) of a cell is,

$$E_{max} = -\frac{\Delta h_f}{zF} \tag{3.10}$$

Hence the maximum possible theoretical efficiency of a SOFC cell given by,

$$\eta = \frac{\Delta g_f}{\Delta h_f}\ 100\% = 77.988\ \% \tag{3.11}$$

3.3.3 Actual Fuel Cell Potential

But the actual efficiency is much lower than this because of different types of losses associated with kinetics and dynamics during the complete process. The actual potential can be describe as,

$$V_{cell} = E_r - \Delta V_{loss} \tag{3.12}$$

3.3.4 Voltage Losses

Though the practical open circuit potential of the cell at the given pressure and the temperature conditions, would be expected to be same as the theoretical one, actually it is not and there is a significant reduction of the value. So there are some losses in the fuel cell even the current through the circuit is zero at the open circuit stage. There are different kinds of voltage losses, that effect on a FC caused by several factors.

a. Activation Polarization

At the beginning of the cell reaction, much higher energy is required; which is called as the activation energy to proceed. This can be occurred due to the slowness of the reactions at the anode and the cathode as well. The energy can be supplied as EMF and it is called, the over potential. The activation polarization would be given by the following equation (a combination of Tafel and Butler-Volmer Equations) for both the anode and the cathode,

$$\Delta V_{act} = \Delta V_{act,Cathode} + \Delta V_{act,Anode} \quad (3.13)$$

$$\Delta V_{act} = \frac{RT}{\alpha_C zF} \ln\left[\frac{i}{i_{0,C}}\right] + \frac{RT}{\alpha_A zF} \ln\left[\frac{i}{i_{0,A}}\right] \quad (3.14)$$

Where, i_0 values are the exchange current densities of anode and cathode, T is the operating temperature, R is the gas constant (8.314 J mol / K), α is the transfer coefficient and F is the Faraday constant.

The activation potential loss is higher at the lower current region. At the no load point the voltage of the cell is close to its ideal value, but when the current is slightly increased, the voltage of the cell drops rapidly due to this activation loss.

b. Ohmic or Resistive Losses

Ohmic polarization losses occur in a FC because of the resistance to the flow of ions through the electrolyte and the resistance to flow of the electrons through the electrodes. Ohmic loss can be determined by the Ohm's law,

$$\Delta V_{ohm} = R\, I \quad (3.16)$$

Compared to the resistance of the electrolyte normally the electrode resistance exhibits a negligible value, hence the electrolyte resistance can be evaluated as,

$$R_{ohm} \approx R_{electrolyte} = \frac{L_{el}}{\sigma_{el} A} \quad (3.17)$$

Where L_{el} is the electrolyte thickness A is the area and σ_{el} is the ionic electrolyte conductivity which depends on the temperature and the composition materials as shown below [20],

$$\sigma_{el} = \frac{\sigma_0}{T} \exp\left(-\frac{E_{el}}{RT}\right) \quad (3.18)$$

In this formula, E_{el} is the activation energy for the transportation of ions and σ_0 is the reference conductivity.

The ohmic losses can be reduced by introducing advanced materials with low resistivity, thinner electrolytes and choosing optimal temperature for the operation. For most of the FCs the maximum operating point is in the ohmic loss region of the IV characteristics.

c. Concentration Polarization

At high currents, the mass transportation loss is highly dominant than the other losses. When the fuel cell is subjected to a high current consuming load, the anode reaction is not fast enough to provide the needed output current [21]. When the drawn current by the circuit is higher, the reactant concentration at the catalyst surface is lower and the concentration reaches zero when the rate of consumption exceeds the diffusion rate. The limiting current density that the FC couldn't operate further more is given by,

$$i_L = \frac{zFDC_B}{\delta} \tag{3.19}$$

Where C_B is the bulk concentration of the reactant and D is a proportional constant.

The formula given below is the concentration polarization loss of the FC,

$$\Delta V_{conc} = C \exp\left[\frac{i}{d}\right] \tag{3.20}$$

Where C and d are empirically determined constants (C = 3 x 10^{-5} V and d = 0.125 A cm^{-2} are the suggested values through experiments but it depends on the cell design and operating conditions)

These are the three main types of losses affecting on the FC output, but there are some other losses such as internal currents and crossover losses, not affecting dominantly.

Therefore the actual cell potential can be described as [19],

$$V_{cell} = E_r - \{\Delta V_{act} + \Delta V_{ohm} + \Delta V_{conc}\} \tag{3.21}$$

$$V_{cell} = E_r - \{\Delta V_{act,Cathode} + \Delta V_{act,Anode}\} - \Delta V_{ohm} - \Delta V_{conc} \tag{3.22}$$

$$V_{cell} = E_r - \left\{\frac{RT}{\alpha_C zF} \ln\left[\frac{i}{i_{0,C}}\right] + \frac{RT}{\alpha_A zF} \ln\left[\frac{i}{i_{0,A}}\right]\right\} - R\,I - C \exp\left[\frac{i}{d}\right] \tag{3.23}$$

According to the above equation, the potential variation with the current can be approximately plotted as shown in the figure below, where all the loss regions are mentioned. At the low current region, the Activation loss is highly dominant. In the middle region, the ohmic loss is dominant and the potential varies more linearly in this region. When current leads to a higher value, the concentration loss is dominant in that region [22].

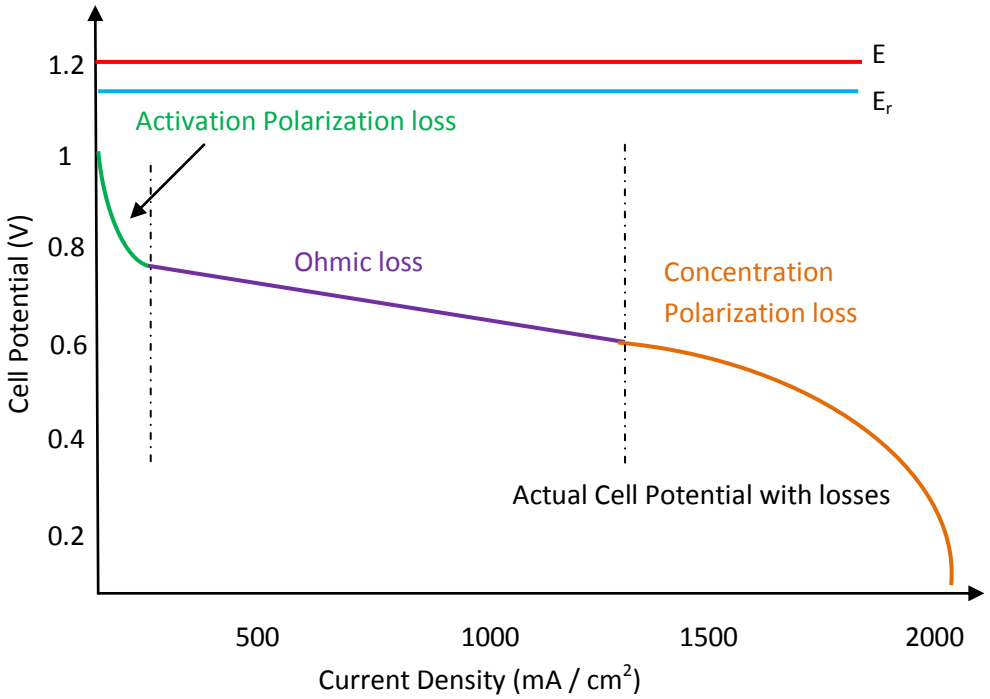

Figure 3.2: I-V characteristic of a SOFC and dominant regions of voltage losses

4

Redox Cycle Testing Equipment

There are different types of equipment used for the redox cycling test, for the solid oxide fuel cell samples and anode substrate materials. This chapter section wise describes the most important types of the equipment; such as test bench, furnace, gas flow controller thermo computer and thermo couple, used during the test and their operating principles. The chapter ends with Section 4.5 that contains safety facts for the complete setup.

4.1 Cell Mounting Test Bench

This is the most important piece of equipment which provides the possibility of mounting the cell providing certain tension on it. The test bench used in the UIA laboratory for this test is a product manufactured by Fiaxcell and operated in an oven manufactured by the Kittec Company [23]. The top side of the test bench is shown in Figure 4.1. The test setup is largely made from Inconel metal which is well known for its high temperature oxidation resistance.

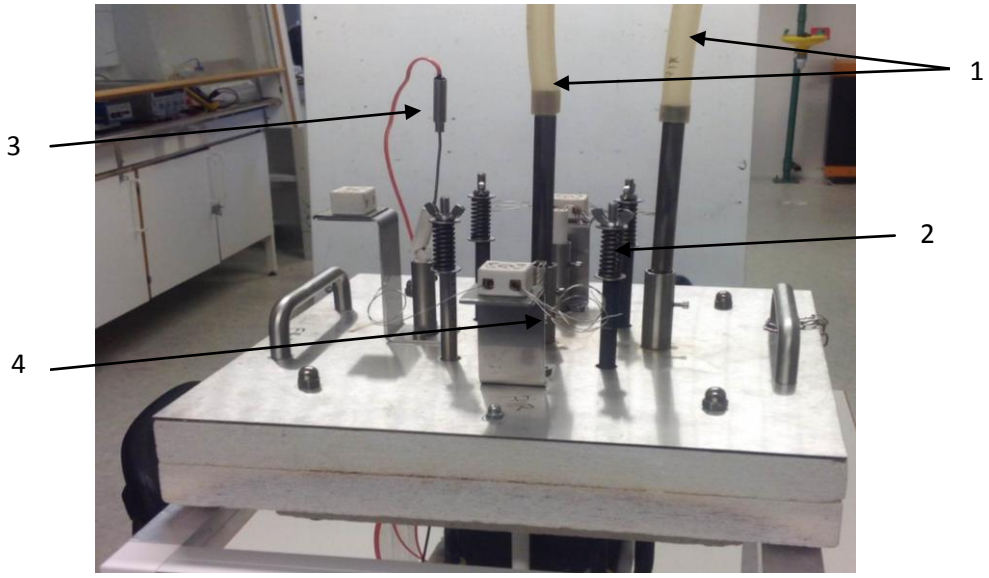

Figure 4.1: The top part of the test bench

The main components as numbered in Figure 4.1 are,

1 – Gas/Fuel Supply to the cell (one tube is for Air Oxygen Supply to the cathode and Hydrogen fuel supply to the anode)

2 – Screws with spring, which is used to mount the cell properly under predefined tension

3 – Thermocouple to measure the actual temperature subjected to the cell/substrate.

4 – Current collector leads/wires for taking current and voltage measurements

The Figure 4.1 below shows the down side of the test bench, which completely goes inside to the oven or the furnace. The cell or the substrate is sandwiched in between the upper and the lower flanges. Both the flanges are fixed together by using four nuts where the springs are attached.

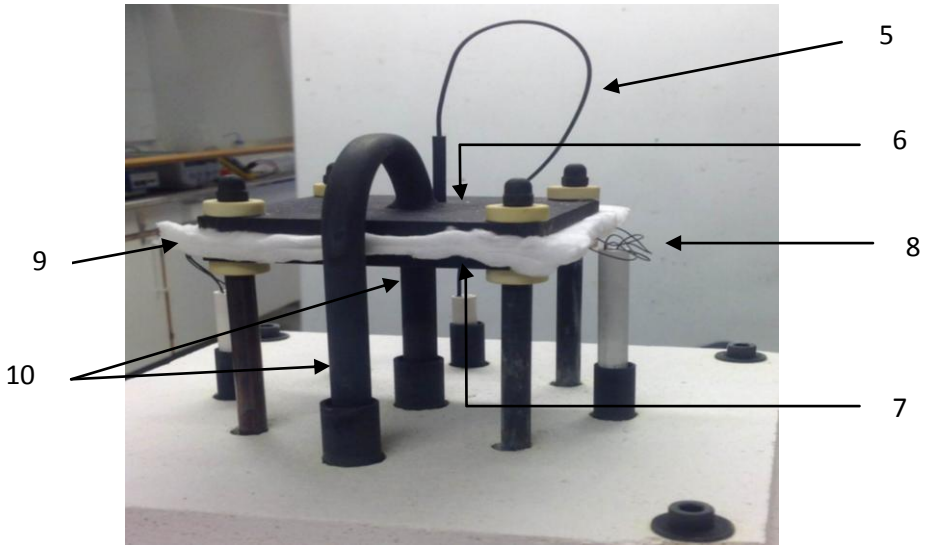

Figure 4.2: The bottom part of the test bench

The main components of the down side of the test bench as numbered above,

5 – Thermocouple heat absorbing lead

6 – Upper Flange

7 – Lower Flange

8 – Current collector leads

9 – Ceramic felts

10 – Gas supply tubes to the cell

4.2 The Furnace

The Furnace in the laboratory is a Kittec-R SQUADRO product and the product name is SQ-11 which is also made according to the German Law VDE. The chamber of the furnace has a volume of 67.24 l and the size is 400 mm x 410 mm x 410 mm (width x depth x height).The maximum temperature that can be obtained in the firing chamber of the furnace is 1320 ^{0}C [23].

There are some safety tips for trouble free safe long time operation of the klin.

The installed room volume should be 600 times greater than the volume of firing chamber and the room should be a dry place where the humidity level is below 80 %. Plugging in the safety

pin before switching on, is very important and to open the kiln the temperature inside must be below 50 ^{0}C. When inserting gases the firing temperature of those must be considered to avoid unnecessary fires. The Figure 4.3 presents the kiln used for this research and an inside view of it.

Figure 4.3: The furnace and the burning coils inside the furnace

4.3 The Gas Flow Controller

The gas flow controller consists of a PID (Propotional Intrigal Derivative) controller to manage the flow accurately. HFC-202 flow controller made by the Teledyne Hastings Instruments company is used in the laboratory for the redox cycle test.

Figure 4.4: The gas flow controller [24]

This pressure controller is designed to accurately measure and control mass flow over the range of 10 sccm to 30 slm, without corrections or compensations for gas pressure and temperature with accuracy of better than ±1% [24].

4.3.1 The Gas Flow Controller Internal Operation

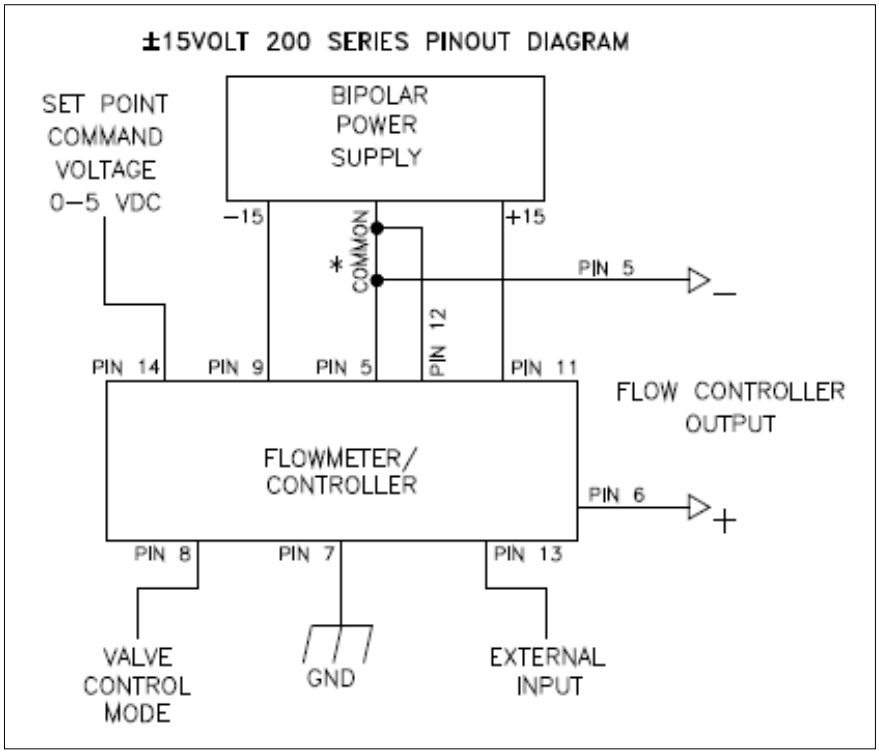

Figure 4.5: The internal circuitry of the flow controller [24]

Hastings Power Pod power supply/display units are available in one and four channel versions which can be used to convert 100, 115 or 230 VAC to the ±15 VDC. This output is required to operate the flow meter and provide a digital indication of the flow rates. Interface terminals for the retransmission of the flow meter analog output signal are located on the rear of the panel [24].

The standard inlet and outlet fittings are of 0.25" and 0.125" diameter and the Viton O-rings used to keep all connections with the rubber tubes to tighten. There is a sensor which can convert the flow rate signal to an electric signal. This electric signal inputs to the pin 13 of the controller and it amplifies inside the circuit, this signal compared with the set point command voltage signal of a 0-5V and the output of 0-5V or 4-20mA is given to the valve inside the piece of equipment. This valve position operates proportionally to this electrical control signal coming out from the pin number 2 where, 0 Volts = zero flow and 5 Volts = 100% of rated flow.

4.3.2 Function of the Sensor

A thermal sensor which consists of a small bore tube shunt with the main flow is used inside the flow controller. The sensor tube is heated by applying an electric current externally to a

predefined temperature and when the flow is above some defined value, the shunt divides the flow so that the flow through the sensor is a precise percentage of the flow through the shunt. There are two coils that are wound around this shunt tube and these coils generate a temperature gradient with the variation of the temperature along the shunt tube due to the pressure variations inside the tube. This resistance variation converts to an electric signal using an internal current source and then this signal inputs to the flow controller circuit with the comparator [25].

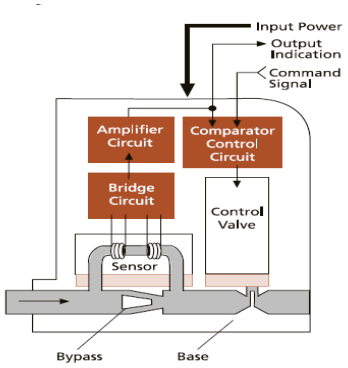

Figure 4.6: Sensor connection [25]

All the equipment operate together as a system to synchronize the flow immediately to the set value and maintain a stable laminar flow to the system.

4.4 Thermal Computer and Thermo-Couple

Thermal computer is already with the furnace and it is made as a bi metal heater with an electronic controller. So that it can control the temperature gradient with a clock pulse generated by the thermal computer [26]. The device consists of a thermal sensor and for each clock pulse the sensor signal is compared with the given gradient value to control the temperature gradient. The profile applied to heat the furnace is shown in Figure 4.7.

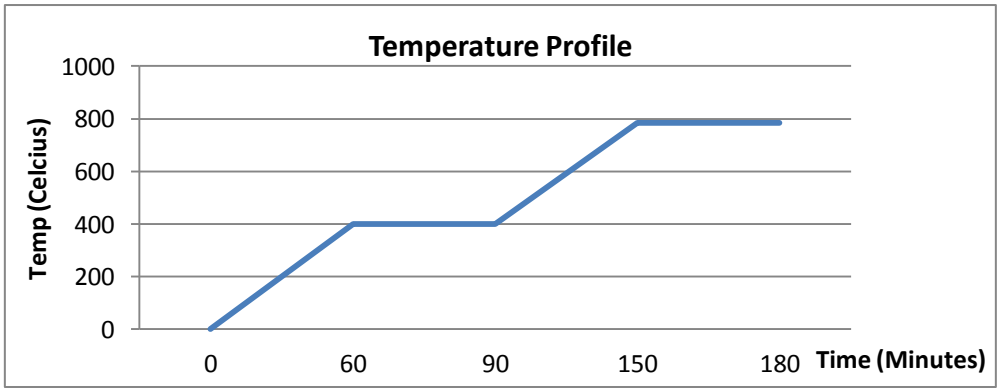

Figure 4.7: Temperature profile set by using thermal computer

The temperature of the copper coils surrounded by the specimen is much different from the actual temperature applicable to the cell and so, a thermocouple is being used to maintain the actual temperature of the cell at a desired value while adjusting the thermal computer set value.

4.4.1 Thermocouple

A thermocouple is a sensor device for measuring temperature and it consists of two dissimilar metal conductors, joined together at one end.

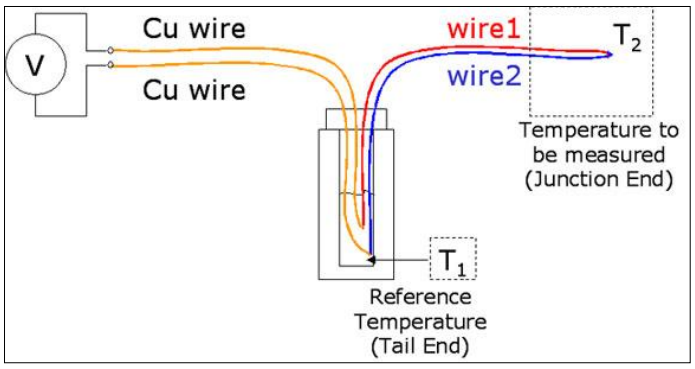

Figure 4.8: Structure of a simple thermocouple

When the junction of the two metals touches the point where the measurement is to be taken, is heated or cooled according to the temperature there. Due to the difference in conductivities a voltage that can be correlated back to the temperature is produced. This effect is called as the Seebeck effect. The voltage gradient of the circuit will be given simply by

$$V_{1-2} = \int_{T_1}^{T_2} (S_1(T) - S_2(T)) \qquad (4.1)$$

where $S_1(T)$ and $S_2(T)$ are the Seebeck coefficients of materials 1 and 2 as a function of temperature, and T_1 and T_2 are the temperatures of the two junctions. If the Seebeck coefficients are effectively constant for the measured temperature range formula can be approximated as below.

$$V_{1-2} = \Delta S \, \Delta T \qquad (4.2)$$

The size of the voltage is dependent on the difference of temperature of the coupled junction with the other parts of the circuit as well as the types of these two heat sensing materials. As the generated voltage, the sensor is calibrated to give the exact temperature at the junction to the accuracy of one degree Celsius (°C).

There are different types of thermocouples such as B, C, E, J, K, N, etc to measure different ranges of temperatures and they are made with different metal compositions. For the purpose of redox testing the N-type of thermocouple which can more accurately measure the range of temperatures from 270 to 1300°C, is used. This thermocouple is made of Nickel-14.2% Chromium-1.4% Silicon vs. Nickel-4.4 % Silicon-0.1 % Magnesium and the reference junction considered to be at 0°C.

Through This chapter most of the important test equipments and measuring devices required for the redox cycle test have been discussed. Another important topic is to discuss the safety issues for assembling all these together considering the precautions.

4.5 Safety Facts for Run the Complete Setup

Safety precautions are very important when dealing with a combustible gas such as Hydrogen at high temperatures. Hydrogen reaction with oxygen to form water at ambient temperature is very slow, but at high temperatures and as well as under catalysts, molecular hydrogen dissociated into free atoms with higher energy. When forming water, by this atomic hydrogen which is a high powerful reductive agent, releases its internal energy even at low temperature and this energy can cause to fires. The worst case is that the hydrogen flame is practically invisible under clean environment.

So, during this laboratory work, because of using heated hydrogen it is important to avoid leakages inside the furnace. Before connecting the thermocomputer there is a safety pin to connect to the furnace to ensure the proper mounting of test bench on top of it. Then the gas supplies connected avoiding the leakages to the outside. The gases were supplied once the furnace reaches to the exact temperature otherwise it will cause to damage the cell and also the external power source is connected after stabilization of the cell with the fuel supply.

The flammable things removed from the surrounding of the furnace to safeguard the emergency fire spreading. The furnace opened to dismantle the test bench subsequently the inside temperature below 50 ^{0}C. These are the main facts that are considered while doing the test.

5

Anode Substrates Test Results and Analysis

This chapter mainly focuses on the results of anode substrate test, including the testing procedure with testing conditions and measurement techniques in Section 5.1. The Section 5.2 discusses the results of the test with required calculations. Result analysis is given in Section 5.3 including graphs.

5.1 Anode Substrate Test Arrangement and Testing Procedure

The anode substrate testing was carried out for the completion of research goal 1. During the test, the substrate was properly mounted on the test bench and the results were taken under the given conditions. The following steps were followed to arrange the complete test setup to test the specimens.

5.1.1 Mounting the Substrate on the Test Bench

First the test bench (Kittec Squadro) was dismantled by removing the connected springs and the upper flange. The small square shaped current collectors which are made of nickel, fixed with the bench using ceramic tubes. The given specimens A-1, A-2, A-3, B-1 and B-2 were properly sandwiched between the current collectors, avoiding the short circuit effects taking one specimen at a time.

The centre of the upper ceramic felt was marked and some small cuts are made for the proper air flow to the specimen. Then the upper flange was fixed by adjusting the spring length to 28.5mm. Finally the thermocouple was mounted and the bench was set inside the furnace. After fixing the safety pin of the furnace, the thermo computer was connected to the furnace using its cable. The furnace temperature controller profile was then set as shown in Figure 5.1 to heat the specimen up to 810 ^{0}C.

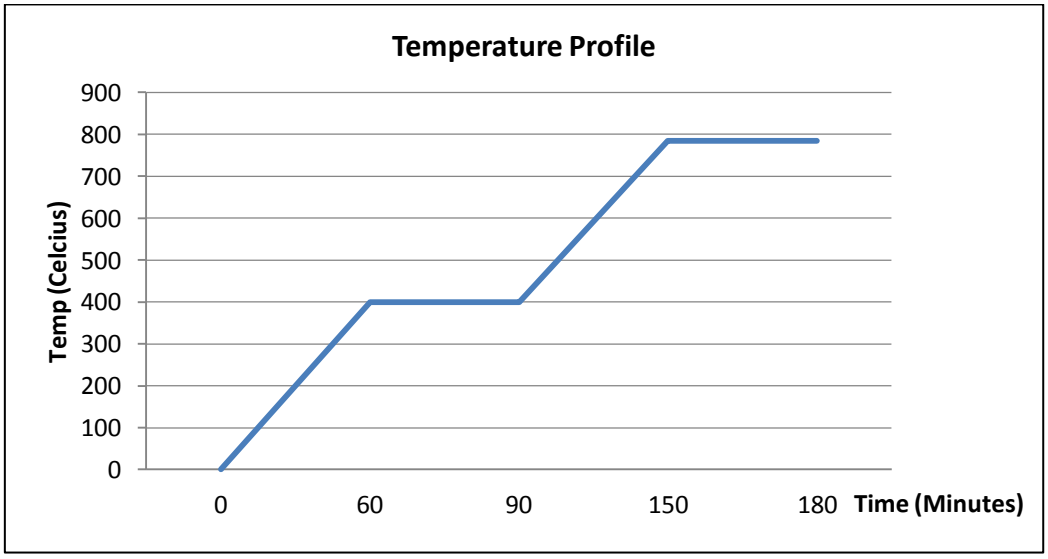

Figure 5.1: The temperature profile set to heat the specimen

When the specimen was heated exactly to the mentioned temperature, the gas flow of Hydrogen, air and Nitrogen were set by using the gas flow controller.

5.1.2 Testing Conditions for the Specimen

The given anode samples were tested under the following test conditions

Room Temperature	19	Celsius
Heated Temperature	810	Celsius
H_2 Flow Rate	18.4	SCCM
N_2 Flow Rate	202.3	SCCM
Air Flow Rate	218.4	SCCM

(H_2 gas was humidified by passing it through water at 23 ^{0}C before supplying to the specimen)

Original spring length	29.5 mm
Adjusted spring length	28.5 mm
Spring Constant	2.8 kg / mm
Force on the substrate	27.468 N

When the system was stabilized, the open circuit resistance was measured and then following current and voltage values were applied to the specimen using a power supply.

Constant Current	0.5	A
Applied Voltage	2.2	V

The 4 wire measurement was taken to calculate the resistance of the specimen under the gas supply (Reduction condition) and then changing the gas supply to Oxygen, readings for the resistance values were directly taken as earlier (under oxidation condition). Then the test was done for several redox cycles and the measurements were taken as tabulated for number of redox cycles.

5.1.3 The Four Wire Measurement to Avoid Connecting Wire Resistance

The direct Ohm meter measurement consists of all the resistance including connectors in the circuit loop. Usually, the wire resistance is very small, but if the connecting wires are very long, and/or the component to be measured has a very low resistance, the error of the measurement will be substantial. The direct resistance can be illustrated by using the circuit in Figure 5.2.

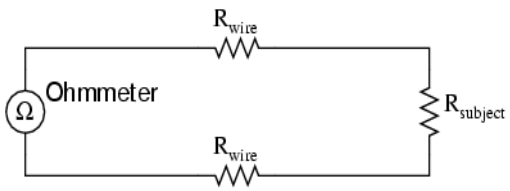

Figure 5.2: Direct Ohm meter measurement method

$$\text{Ohm meter Value} = R_{wire} + R_{subject} + R_{wire} \quad (5.1)$$

By using an ammeter and a volt meter with supplied power as shown below,

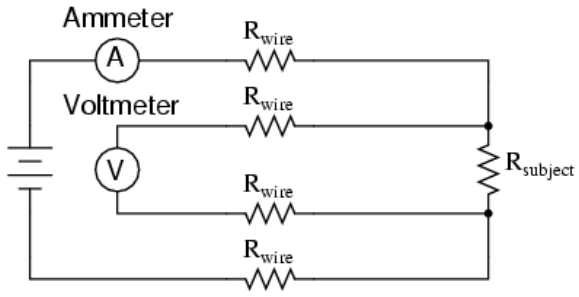

Figure 5.3: Four wire measurement method

Though the voltmeter is far away from the subject, because of the high resistance of the voltmeter, the current through it will be of a negligible value. So the external wire resistance error can be neglected. Then the actual resistance can be taken from Ohm's Law such that the resistance is equal to the voltage reading of the volt meter divided by the current (R = E/I).

5.2 Results

Before starting the test, the resistance value was measured by short circuiting the substrate using upper flange and the substrate area was measured using a micrometer screw gauge.

Considering the specimen sample B_1,

Short Circuit Resistances		
Substrate	1.6	Ohm
Substrate with wires	4.6	Ohm
Substrate area	width cm x length cm = 1.2099 cm^2	

During reduction and oxidation processes the 4 wire setup multimeter reading, which is the actual voltage supplied to the substrate was taken down with the time. Results for the first redox cycle of the specimen sample B_1 are tabulated as shown in Table 5.1 below. The complete results table was attached in the Appendix A.

Table 5.1: Redox test results for first redox cycle of anode specimen B_1

Oxidation or Reduction	Date	Time	Elapsed Time Minutes	Hours	Measured Voltage (mV)	Area Resistance of Substrate (Ohm cm^2)
Reduction	18_02_2013	14.00	0	0	57.6	
		14.05	5	0.083333	51.2	
		14.10	10	0.166667	50.4	
		14.20	20	0.333333	50	
		14.25	25	0.416667	49.6	
		14.30	30	0.5	49.3	
		14.35	35	0.583333	49.1	
		14.40	40	0.666667	49	
		14.45	45	0.75	49	
		14.50	50	0.833333	48.9	
		14.55	55	0.916667	48.9	
		15.00	60	1	48.8	
		15.15	75	1.25	48.6	
		15.30	90	1.5	48.4	
		15.45	105	1.75	48.2	
		16.00	120	2	48.2	
		16.15	135	2.25	48.1	
		16.30	150	2.5	48	
	19_02_2013	9.00	1140	19	25.9	
		9.30	1170	19.5	25.8	
		10.00	1200	20	25.7	
		10.30	1230	20.5	25.6	
		11.00	1260	21	25.5	
		11.20	1280	21.33333	25.4	
Oxidation		11.30	1290	21.5		2000
		11.31	1291	21.51667		1870
		11.32	1292	21.53333		1815
		11.33	1293	21.55		1724
		11.34	1294	21.56667		1634
		11.35	1295	21.58333		1597
		11.36	1296	21.6		1555
		11.37	1297	21.61667		1519
		11.38	1298	21.63333		1492
		11.39	1299	21.65		1485

5.3 Calculations and Results Analysis

Considering the results obtained, the required calculations were done to plot the redox cycle resistance with time.

5.3.1 Calculations

For the measured voltage values under the reduction condition the substrate area resistance can be calculated as given below

Area Resistance of Substrate = Measured cell voltage/ Constant Current

The resistance of the substrate = Area Resistance of Substrate/ Cell Area

But because of the reduction resistance is very low value, the logarithmic values are considered for the comparison.

The Logarithmic value of the Substrate Resistance = 10 log (Substrate Resistance)

The average resistance value is calculated for each sample considering the average of all the measured resistance values during the final reduction phase and the value for sample B1 is 0.0129572 Ω.

The calculated values for first redox cycle of the anode substrate B-1 are tabulated in the Table 5.2. The complete table is included in the Appendix A.

Table 5.2: Table of calculated data for first redox cycle of the anode specimen B_1

Elapsed Time (Hours)	Area Resistance of Substrate (Ohm cm2)	Substrate Resistance (Ohm)	log value of Area Resistance	log value of Substrate Resistance
0	0.1152	0.095214481	-9.38547521	-10.21296998
0.083333333	0.1024	0.084635094	-9.89700043	-10.7244952
0.166666667	0.1008	0.08331267	-9.96539468	-10.79288945
0.333333333	0.1	0.082651459	-10	-10.82749477
0.416666667	0.0992	0.081990247	-10.0348833	-10.86237805
0.5	0.0986	0.081494338	-10.0612309	-10.88872562
0.583333333	0.0982	0.081163733	-10.0788851	-10.90637989
0.666666667	0.098	0.08099843	-10.0877392	-10.91523401
0.75	0.098	0.08099843	-10.0877392	-10.91523401
0.833333333	0.0978	0.080833127	-10.0966115	-10.92410622
0.916666667	0.0978	0.080833127	-10.0966115	-10.92410622
1	0.0976	0.080667824	-10.1055018	-10.93299659
1.25	0.0972	0.080337218	-10.1233374	-10.95083212
1.5	0.0968	0.080006612	-10.1412464	-10.96874119
1.75	0.0964	0.079676006	-10.1592297	-10.98672443

2	0.0964	0.079676006	-10.1592297	-10.98672443
2.25	0.0962	0.079510703	-10.1682493	-10.99574405
2.5	0.096	0.0793454	-10.1772877	-11.00478244
19	0.0518	0.042813456	-12.8567024	-13.68419717
19.5	0.0516	0.042648153	-12.873503	-13.70099775
20	0.0514	0.04248285	-12.8903688	-13.71786358
20.5	0.0512	0.042317547	-12.9073004	-13.73479516
21	0.051	0.042152244	-12.9242982	-13.75179301
21.33333333	0.0508	0.041986941	-12.9413629	-13.76885764
21.5	2000	1653.029176	33.01029996	32.18280519
21.51666667	1870	1545.58228	32.71841607	31.8909213
21.53333333	1815	1500.123977	32.58876629	31.76127153
21.55	1724	1424.91115	32.36537261	31.53787785
21.56666667	1634	1350.524837	32.13252052	31.30502575
21.58333333	1597	1319.943797	32.03304916	31.20555439
21.6	1555	1285.230184	31.91730393	31.08980917
21.61666667	1519	1255.475659	31.81557774	30.98808297
21.63333333	1492	1233.159765	31.73768823	30.91019346
21.65	1485	1227.374163	31.71726454	30.88976977

5.3.2 Data Analysis

Data analysis is done by plotting different curves for the calculated data in the previous section. The Figure 5.4 below is a plot of area Resistance of specimen_B1 vs time.

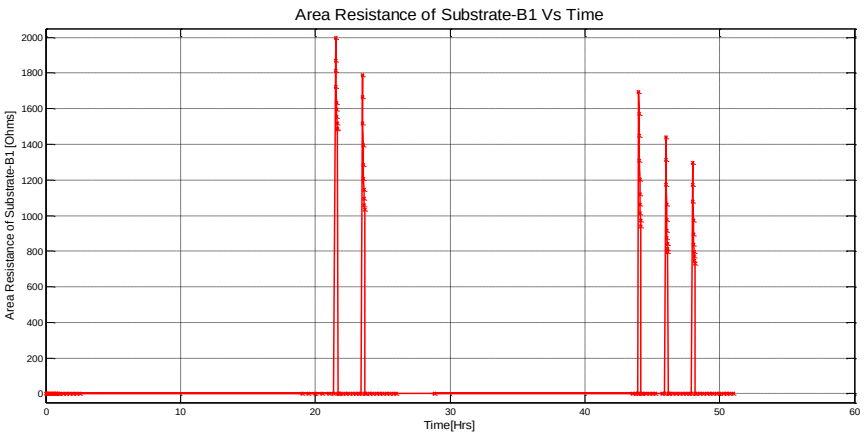

Figure 5.4: Plot of Area Resistance vs time for specimen_B1

The peaks of the curve represent the area resistance values when the specimen is under the oxidation condition and when compared with reduction resistance values, it is much higher. But it can be clearly seen a decrease of resistance values at the oxidation conditions from one redox cycle to the next.

As the reduction resistance values are much smaller, the variation is not clear in the above figure. Hence to get a clear figure let's consider the log value plot for the last three reduction cycles.

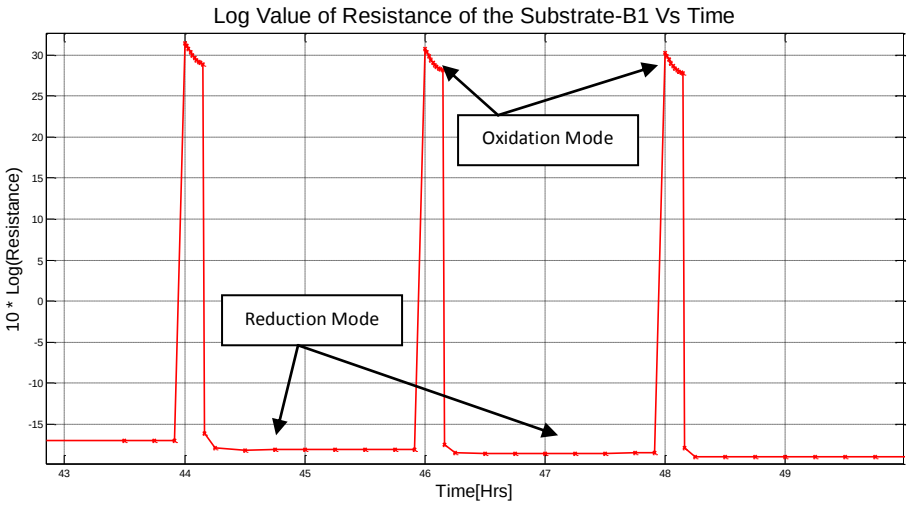

Figure 5.5: Plot of Logarithmic value of Resistance Vs time for specimen_B1

A slight decrease of the reduction mode resistance values with time can be seen from Figure 5.5.

The tables of data obtained for the other four specimens were attached in the appendix A.

The plot of all the tested samples are taken in to a common figure as shown in the below,

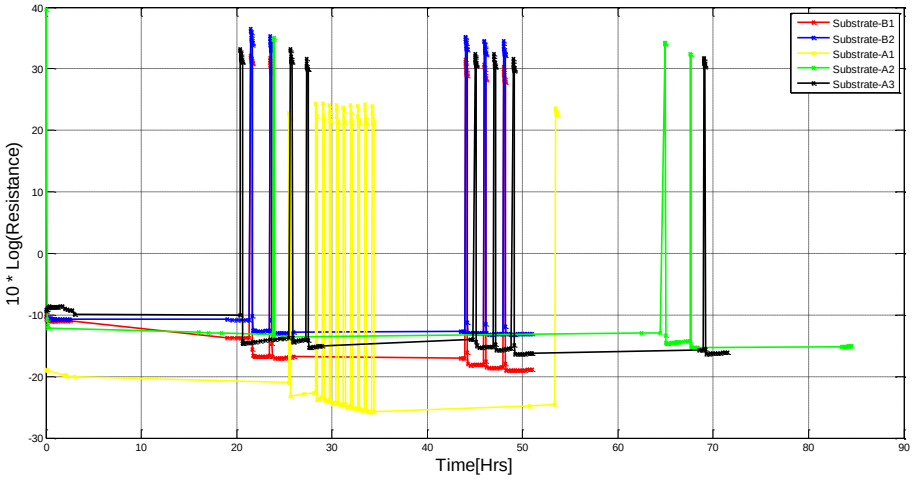

Figure 5.6: Plot of Logarithmic value of Resistance Vs time for specimen all the A and B samples

6

2-R Cell Specimens Test Results and Analysis

This chapter describes the redox cycle test for 2-R cell specimens and reference SOFC. The test procedure and technique used to obtain results for the I-V and power characteristics are mentioned in Section 6.1. Results are tabulated in Section 6.2 giving analysis to the tested data with resultant graphs.

6.1 Anode Substrate Test Arrangement and Testing Procedure

As the anode substrate specimens, the 2-R cell was properly mounted on the test bench and the results were taken under the conditions given by Fiaxell. The target of the redox cycle testing for 2-R cell specimens was to accomplish the research goal 2. The test setup was arranged as follows.

6.1.1 Mounting the Substrate on the Test Bench

Firstly the test bench was dismantled by removing the connected springs and the upper flange. And then the specimen, which was already mounted there, was removed carefully. The small circular shaped current collectors,

Anode current collector – Ni form current collection grid

Cathode current collector – Made of Croffer alloy

that are with four Ni wires were fixed on to the bench using ceramic tubes. The given 2-R cell specimens were properly mounted between the current collectors as shown in Figure 6.1, taking one specimen at a time.

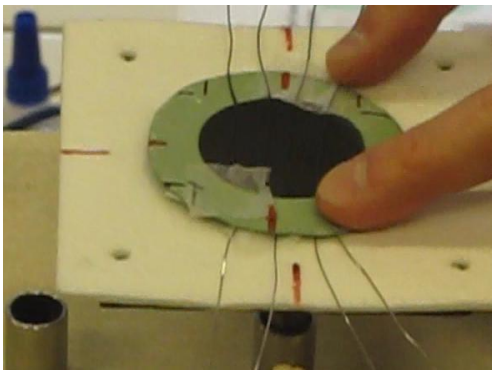

Figure 6.1: Mounting cell in between ceramic flanges with current collectors

Small cuts were made on the ceramic felts to ensure the proper gas flow to the specimen. Then the upper flange was fixed by adjusting the spring length to 28.5mm as earlier. From the four wires of current collectors, one is set for the potential measurement and the other three were together set for the current measurement. The other settings are the same as the previous ones and finally the furnace was heated up to 810 ^{0}C using the thermocomputer. Once the specimen has reached exactly the mentioned temperature, the gas flow of hydrogen, air and nitrogen were set by using the gas flow controller.

6.1.2 Testing Conditions for the Specimen

The 2-R cell specimens were tested under the following test conditions

Room Temperature		19	Celsius

Before supplying the fuel H_2 the cell was run under air supply and Nitrogen supply for about an hour.

For 10% Hydrogen supply condition

Heated Temperature		810	Celsius
H_2	Flow Rate	18.4	SCCM
N_2	Flow Rate	202.3	SCCM
Air	Flow Rate	218.4	SCCM

For 100% Hydrogen supply condition

Heated Temperature		817	Celsius
H_2	Flow Rate	200.1	SCCM
Air	Flow Rate	218.7	SCCM

(Humidified Hydrogen gas was supplied to the specimen)

Force on the substrate 27.468 N

For the Oxidation All the gas supplies switched off

The measurements were taken to analyze the I-V characteristics at the reduction condition and the test was repeated for two redox cycles for each specimen.

6.1.3 Measurement Method

Once after the H_2 supply was connected, the induced voltage was measured with the time until it reaches to a stable value. Then the current measurements were taken for a load while changing the voltage by using an external power supply and the circuit connection is as in the Figure 6.2. The equipment resistance including the resistance of the wires/connecting cables considered as the load R. Then

The voltage across the load $R = V_1 - V_2$

Where $V_2 < V_1$, V_2 is the supplied voltage using external Power supply and V_1 is the cell voltage.

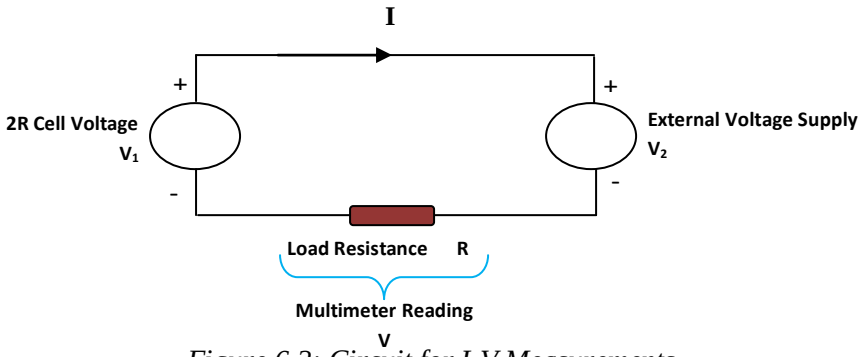

Figure 6.2: Circuit for I-V Measurements

The current through the cable I was measured using clippon meter for desired V values.

6.2 Results and Analysis

The resultant voltage variation with time under fuel supply is tabulated in the below table for sample_2 and the graph is in Figure 6.3.

Table 6.1: Table of cell voltage variation with the time after fuel supplying

Time	Elapsed Time		Induced Voltage(mV)
	Mins	Hours	
11.00	0	0	51.9
11.05	5	0.08333333	90.8
11.10	10	0.16666667	789
11.15	15	0.25	863
11.20	20	0.33333333	927
11.25	25	0.41666667	979
11.30	30	0.5	1003
11.35	35	0.58333333	1012
11.40	40	0.66666667	1019
11.45	45	0.75	1025
11.50	50	0.83333333	1028
11.55	55	0.91666667	1028
12.00	60	1	1028
12.05	65	1.08333333	1028.5
12.10	70	1.16666667	1028.5
12.15	75	1.25	1028.5

Time	Mins	Hours	Induced Voltage(mV)
12.20	80	1.33333333	1028.5
12.25	85	1.41666667	1029
12.30	90	1.5	1029
12.45	105	1.75	1029.5
13.00	120	2	1029.5
13.15	135	2.25	1030
13.30	150	2.5	1030
13.45	165	2.75	1030
14.00	180	3	1030.5
14.15	195	3.25	1030.5
14.30	210	3.5	1030.5
14.45	225	3.75	1030.5
15.00	240	4	1031
15.15	255	4.25	1031
15.30	270	4.5	1031
15.45	285	4.75	1031
16.00	300	5	1031

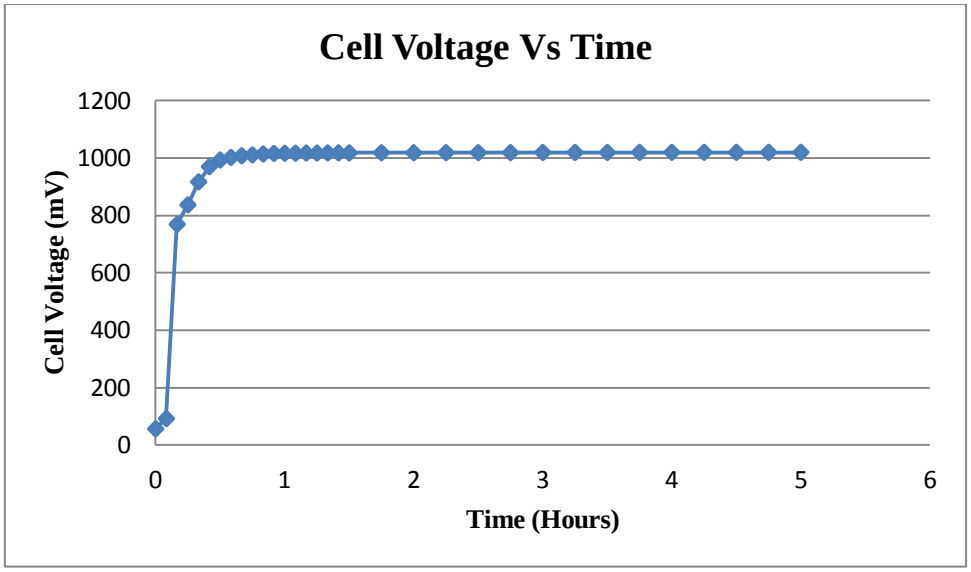

Figure 6.3: The graph of cell voltage variation with the time after fuel supplying

The voltage is slightly increased at the beginning and then there is a rapid rise within 10 minutes. We can assume that this happens at a time when the fuel percentage reach to a certain amount while analyzing results for all the specimens. Finally it takes nearly four hours to stabilize.

During reduction Hydrogen supply the current-voltage measurements for the 2-R cell sample-2 is tabulated as below in Table 6.2. To obtain higher accuracy the current measurements taken while increasing the voltage and then decreasing the voltage as well and the average value is used to plot the I-V and power curves as below.

a. First reduction at 10 % Hydrogen

Table 6.2: Table of I-V values for first reduction at 10% Hydrogen for sample-2

Voltage (V)	Current (A)	Power (W)
0.55	1.430	0.7865
0.6	1.260	0.756
0.65	1.100	0.715
0.7	0.940	0.658
0.75	0.790	0.5925
0.8	0.640	0.512
0.85	0.500	0.425
0.9	0.35	0.315
0.95	0.23	0.2185
1.034	0.00	0

Voltage (V)	Current (A)	Power (W)
0.95	0.23	0.2185
0.9	0.35	0.315
0.85	0.50	0.425
0.8	0.64	0.512
0.75	0.78	0.585
0.7	0.93	0.651
0.65	1.09	0.7085
0.6	1.24	0.744
0.55	1.40	0.77

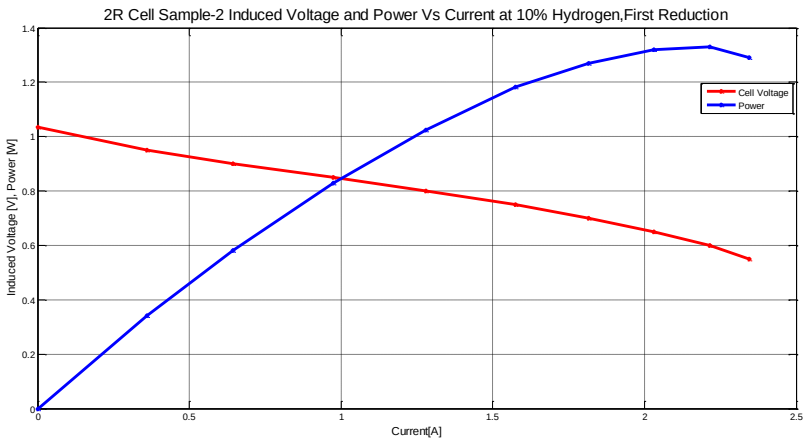

Figure 6.4: The graph of I-V values for first reduction at 10% Hydrogen for sample-2

b. Second reduction at 10 % Hydrogen

Table 6.3: Table of I-V values for second reduction at 10% Hydrogen for sample-2

Voltage (V)	Current (A)	Power (W)
0.55	2.270	1.2485
0.6	2.160	1.296
0.65	1.930	1.2545
0.7	1.630	1.141
0.75	1.340	1.005
0.8	1.080	0.864
0.85	0.780	0.663
0.9	0.52	0.468
0.95	0.28	0.266
1.031	0.00	0

Voltage (V)	Current (A)	Power (W)
0.95	0.28	0.266
0.9	0.52	0.468
0.85	0.77	0.6545
0.8	1.06	0.848
0.75	1.32	0.99
0.7	1.60	1.12
0.65	1.90	1.235
0.6	2.12	1.272
0.55	2.23	1.2265

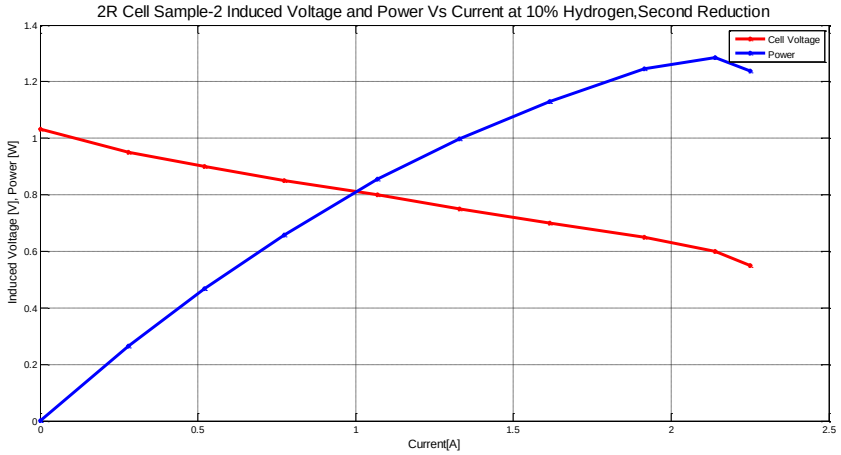

Figure 6.5: The graph of I-V values for second reduction at 10% Hydrogen for sample-2

c. First reduction at 100 % Hydrogen

Table 6.4: Table of I-V values for first reduction at 100% Hydrogen for sample-2

Voltage (V)	Current (A)	Power (W)
0.55	5.060	2.783
0.6	4.770	2.862
0.65	4.230	2.7495
0.7	3.480	2.436
0.75	2.830	2.1225
0.8	2.300	1.84
0.85	1.710	1.4535
0.9	1.29	1.161
0.95	0.81	0.7695
1	0.36	0.36
1.04	0.00	0.000104

Voltage (V)	Current (A)	Power (W)
1	0.36	0.36
0.95	0.81	0.7695
0.9	1.29	1.161
0.85	1.70	1.445
0.8	2.27	1.816
0.75	2.79	2.0925
0.7	3.41	2.387
0.65	4.16	2.704
0.6	4.60	2.76
0.55	4.87	2.6785

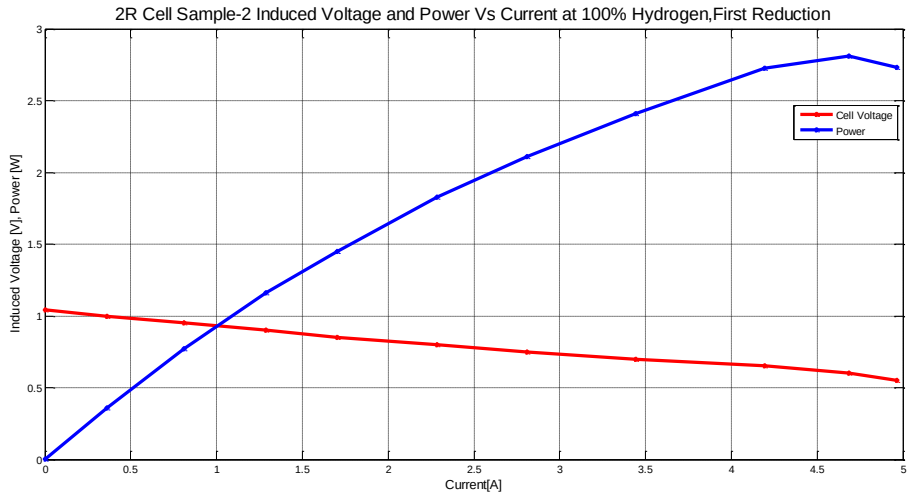

Figure 6.6: The graph of I-V values for first reduction at 100% Hydrogen for sample-2

d. Second reduction at 100 % Hydrogen

Table 6.5: Table of I-V values for second reduction at 100% Hydrogen for sample-2

Voltage (V)	Current (A)	Power (W)
0.55	4.700	2.585
0.6	4.480	2.688
0.65	4.020	2.613
0.7	3.220	2.254
0.75	2.530	1.8975
0.8	1.970	1.576
0.85	1.500	1.275
0.9	1.07	0.963
0.95	0.65	0.6175
1	0.28	0.28
1.04	0.00	0

Voltage (V)	Current (A)	Power (W)
1	0.28	0.28
0.95	0.65	0.6175
0.9	1.06	0.954
0.85	1.48	1.258
0.8	1.95	1.56
0.75	2.50	1.875
0.7	3.18	2.226
0.65	3.98	2.587
0.6	4.42	2.652
0.55	4.62	2.541

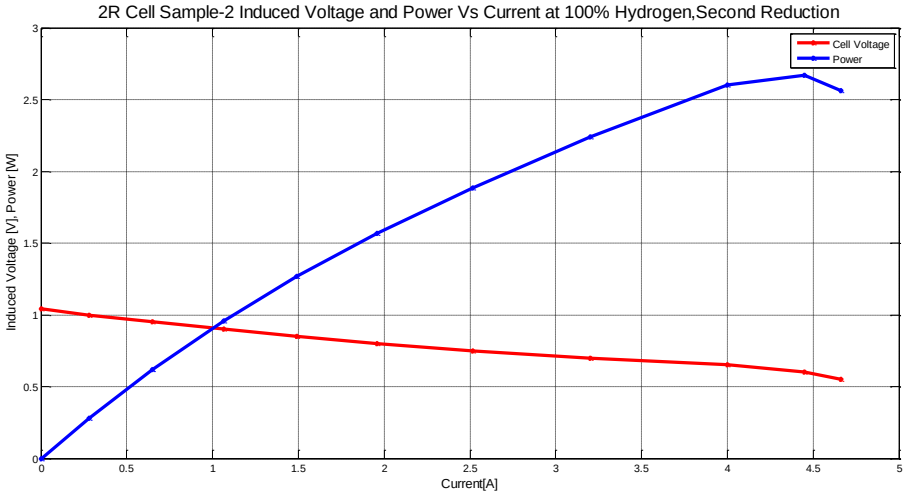

Figure 6.7: The graph of I-V values for second reduction at 100% Hydrogen for sample-2

7

Modelling I-V Characteristics

In this chapter a description is given for the modelling of I-V characteristics for the 2-R cell considering the regions of the curve where the different types of losses are dominant. Section 7.1 presents a small description with the modelling equation. Sections 7.2, 7.3 and 7.4 describe the modelling procedure of the ohmic loss region, activation loss region and concentration loss region, accordingly while showing the parameter calculations.

7.1 Modelling I-V Curve for the RoxSolid Cell

The I-V curve is basically modeled considering the losses of the fuel cell as described under the chapter 3, in section 3.3. From the main three types of losses the effect of concentration loss is very small due to the high rate of fuel and air flow that leads to avoid the pressure drops at the anode and the cathode. The theoretical cell output equation given in the section 3.3 is,

$$V_{cell} = E_r - \left\{\frac{RT}{\alpha_C zF} \ln\left[\frac{i}{i_{0,C}}\right] + \frac{RT}{\alpha_A zF} \ln\left[\frac{i}{i_{0,A}}\right]\right\} - R\,I - C \exp\left[\frac{i}{d}\right] \quad (7.1)$$

The modelling procedure started from the linear or the ohmic loss region as below.

7.2 Modelling the Ohmic Loss Region

7.2.1 Calculations for Modelling the Ohmic Loss Region

The following calculations were considered for the model, making some assumptions.

a. Induced cell voltage, E_r

assuming the partial pressure effect is negligible

$$E_r = -\frac{\Delta g_f}{zF} \quad (7.2)$$

$$E_r = -\frac{(-188.6*1000)}{2*96485} = 0.977354\ V \quad (7.3)$$

b. The resistance of anode,

considering the tested anode substrate sample B_1

The average resistance under the final reduction condition = 0.012957 Ω

c. The resistance of electrolyte

The thickness of the electrolyte is 10 μm and conductivity of YSZ is 4.553 S/m [27].

The resistance of electrolyte = $\frac{\rho l}{A} = \frac{10*10^{-6}}{4.553*44.56622*10^{-4}} = 0.000472\ \Omega$

d. The resistance of cathode

The cathode resistance cannot be obtained directly and therefore it was calculated using the least square method for the linear region of the experimental data plot of the 2R cell specimen 2. (From cell voltage 0.7 V to 0.9 V was considered as the linear region.)

The ohmic loss region is more linear and hence the curve can be represented as in a linear function below,

$$y = P_1 x + P_2$$

Where; y is cell voltage, the x is cell current and P_1 and P_2 are the parameters to be find using least square method.

The linear least square method is a well known method of fitting a mathematical model or a statistical model to fit the practical data where the ideal values of the data points approximately expressed linearly in terms of the unknown parameters such as P_1 and P_2 in above function.

In least square method the system error can be represented as below

$$S = System\ Error = \sum_{i=1}^{n} (y_i - (P_1 x_i + P_2))^2 \qquad (7.5)$$

And then by taking the partial derivatives of the S over P_1 and P_2 choose the parameters to minimize the error (equating $\frac{\partial S}{\partial P_1} = 0$, $\frac{\partial S}{\partial P_2} = 0$)

But by using MATLAB P_1 and P_2 values can be find directly by expressing the data points (x, y) in matrices as below,

$$\begin{pmatrix} y_1 \\ y_2 \\ : \\ : \\ y_n \end{pmatrix} = \begin{pmatrix} x_1 \\ x_2 \\ : \\ : \\ x_n \end{pmatrix} P_1 + \begin{pmatrix} 1 \\ 1 \\ : \\ : \\ 1 \end{pmatrix} P_2 \qquad (7.6)$$

$$\begin{pmatrix} y_1 \\ y_2 \\ : \\ : \\ y_n \end{pmatrix} = \begin{pmatrix} x_1 & 1 \\ x_2 & 1 \\ : & : \\ : & : \\ x_n & 1 \end{pmatrix} \begin{pmatrix} P_1 \\ P_2 \end{pmatrix} \qquad (7.7)$$

$$Y = X * P \qquad (7.8)$$

The matrix P can be found as follows

$$X^T X\ P = X^T\ Y \qquad (7.9)$$

$$(X^T X)^{-1}(X^T X)\ P = (X^T X)^{-1} X^T\ Y \quad \text{but } (X^T X)^{-1}(X^T X) = the\ identity\ matrix$$

Then $P = (X^T X)^{-1} X^T Y$ (7.10)

From the MATLAB using pseudo-inverse command

P = pinv([X ones(size(X))])*Y

Directly obtained the P_1 and P_2 as below,

$$P_1 = -0.16953 \quad \text{and } P_2 = 1.0133$$

Considering these two parameters the $y = P_1 x + P_2$ line plotted with the practical data in the ohmic region in Figure 7.1.

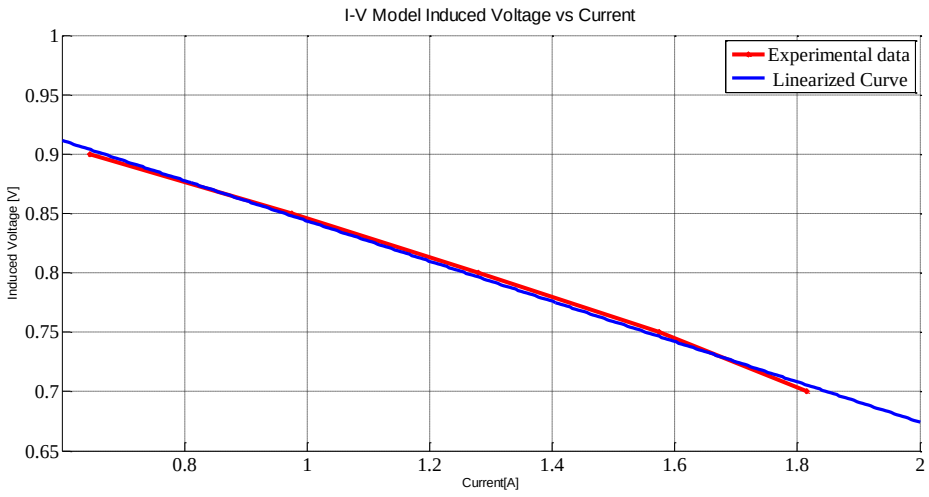

Figure 7.1: Comparison of linear curve and the experimental curve in the ohmic region

The inclination of the curve represents the ohmic loss and hence the total resistance directly equals to the (-P_1) value.

$$R_{total} = -P_1 = 0.16953 \quad (7.11)$$

$$R_{total} = R_{anode} + R_{cathode} + R_{electrolyte} = 0.16953\ \Omega \quad (7.12)$$

$$R_{cathode} = 0.156101\ \Omega \quad (7.13)$$

The comparison of I-V model only with the ohmic loss, with the experimental curve is shown in the Figure 7.2. There is a drop in theoretical model compared to the practical model because in this work only the chemical energy change was used for calculating the cell induced voltage E_r omitting the effect of partial pressure component as in the Nernst equation. Hence an offset of 0.47 V was added to each data point to correct the issue. The model with ohmic loss and this offset voltage is shown in Figure 7.3.

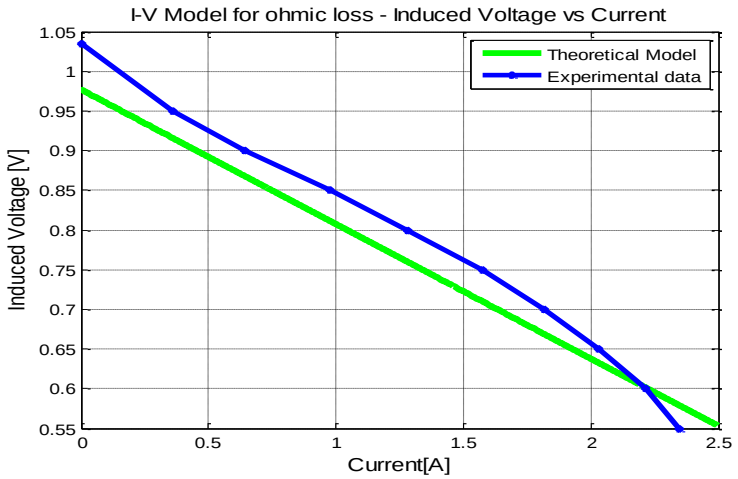

Figure 7.2: Comparison of model for the ohmic loss with experimental data

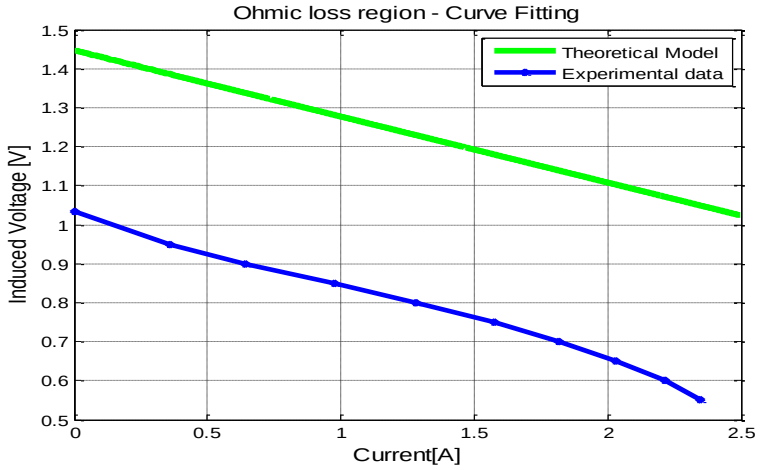

Figure 7.3: The experimental data plot and comparison of model for the ohmic loss with offset voltage

7.3 Modelling the Activation Loss Region

The parameters that are unknown, such as anode and cathode exchange current densities ($i_{0,A}$ and $i_{0,C}$) , charge transfer coefficients (α) of the anode are designed by analyzing the effect of variation of each parameter on the curve. For the hydrogen electrode, the charge transfer coefficient considered to be 0.5 [21].

7.3.1 The effect of Cathode Exchange Current

The effect of cathode exchange current is shown in the below figure while keeping other parameters constantly. The I-V plots for five different values of $i_{0,C}$ are illustrated in Figure 7.4.

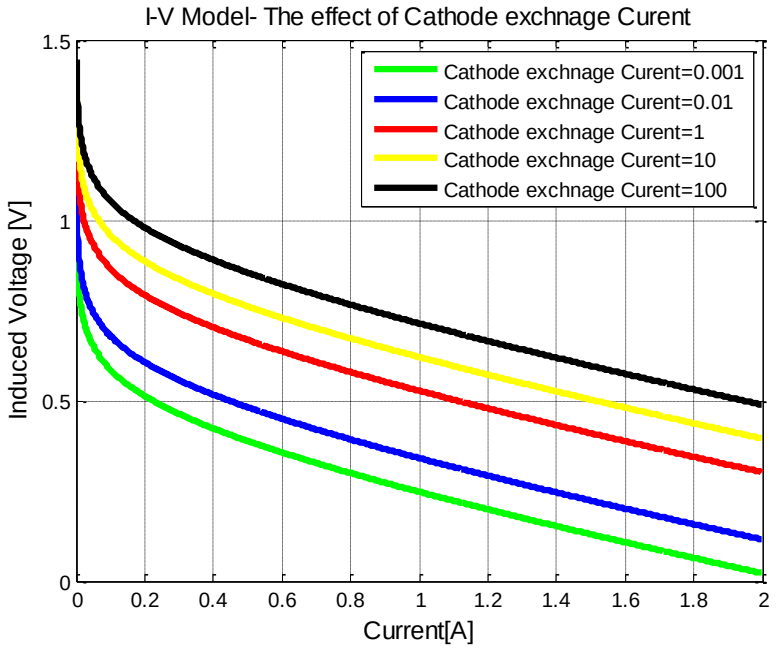

Figure 7.4: The effect of cathode exchange current density on activation loss

As the exchange current density increases the curve shifts upwards without affecting to the curve shape.

7.3.2 The effect of Anode Exchange Current

This effect is also same as above on the curve, because the equation used is the same as the cathode.

7.3.3 The effect of Charge Transfer Coefficient of the Anode

The anode is the fuel electrode for the SOFC and therefore α varies from 0.5 to 1. The effect on the activation loss is shown in the Figure 7.5.

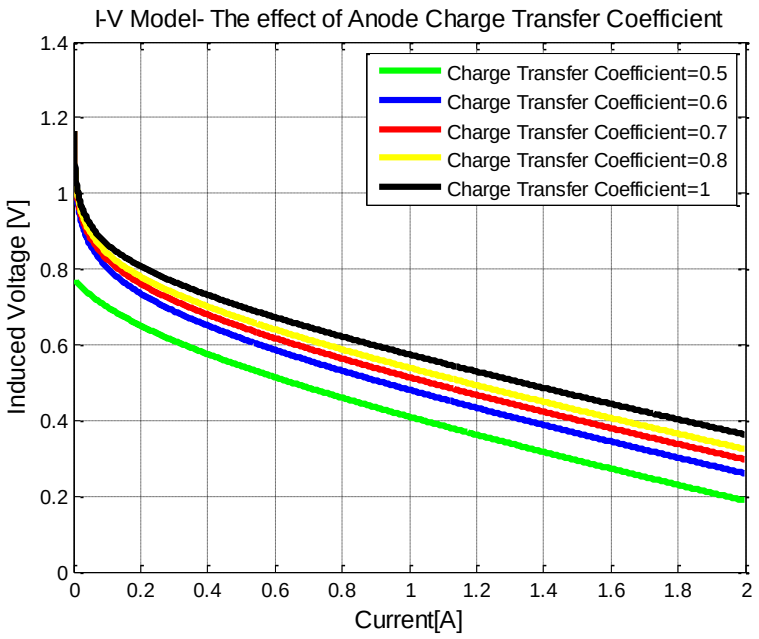

Figure 7.5: The effect of anode charge transfer coefficient on activation loss

The steepness of the curve at low current is reduced with the decrease of charge transfer coefficient.

7.3.4 Model with Ohmic and Activation loss

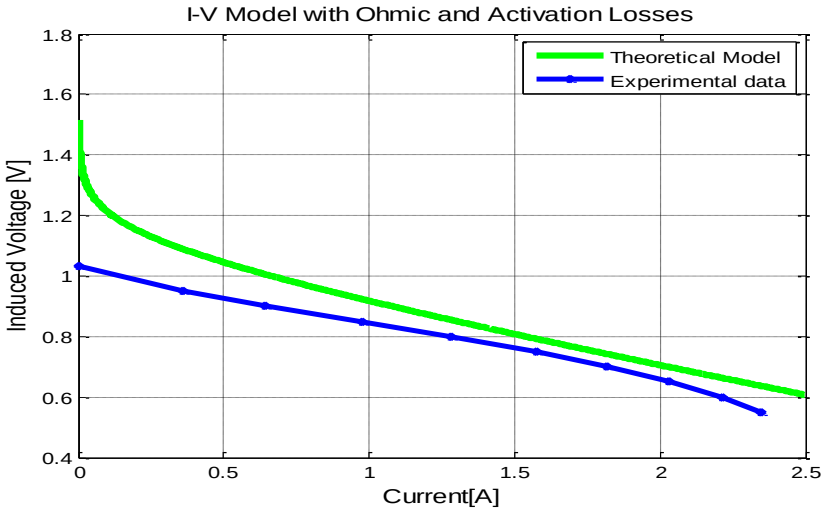

Figure 7.6: The experimental data plot and Comparison of model with ohmic and activation losses

The above figure shows the I-V model with activation and ohmic losses. The parameters that are chosen to fit the curve with experimental data are given below,

Cathode exchange current = 0.003 A

Cathode exchange current = 0.003 A

Charge transfer coefficient of cathode = 0.5

Charge transfer coefficient of cathode = 0.95

There is a large difference at the low current region compared to the experimental curve. Inside the furnace there is no any way to avoid the mixing of gasses, Hydrogen and Air. The gases inject to the center of the cell, but at the edges there is possibility of mixing of gases. Hence at the edges the induced voltage can be lower than the center voltage and this loss is called as the mixed potential loss. Therefore the average induced voltage can be expressed as a function below,

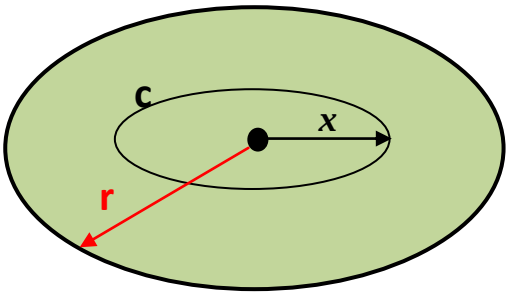

Figure 7.7: Cell geometry

The induced voltage at a small length *dx*, that is x distance is away from the center can be represented as E(x). Therefore the average induced voltage $E_{r,Average}(x)$

$$E_{r,Average}(x) = \frac{1}{A}\oint_{0}^{c}\int^{r} E(x)\,dxdy = \frac{1}{A}\oint_{0}^{c}\int^{r} R * I(x)\,dx\,dy \qquad (7.14)$$

It is difficult to calculate this issue practically but at higher voltage outputs (lower current values) the error is higher. The error basically depends on current and hence it can be represented as an exponential function of the output current.

To reduce this issue from the I-V model, a mathematical expression is designed as below,

$$E_{mixed\ potential} = P * exp[Q - I] \qquad (7.15)$$

Where P and Q are arbitrary constants.

For the above model these values are chosen as follows,

$$P = 10^{-6} \quad and \quad Q = 14.4$$

The model after correcting the mixed potential loss is illustrated in Figure 7.8.

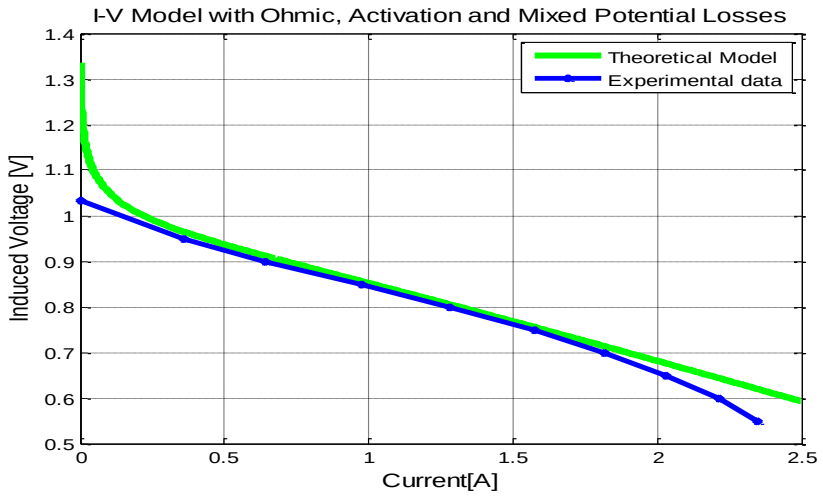

Figure 7.8: The experimental data plot and Comparison of model with ohmic, activation and mixed potential losses

7.4 Modelling the Concentration Loss Region

The concentration loss that discussed in chapter 3, is represented as below,

$$\Delta V_{conc} = C \exp\left[\frac{i}{d}\right] = m \exp\left(n * I\right) \qquad (7.16)$$

For the model the arbitrary constants were selected as,

$$m = 3 * 10^{-5} \qquad and \qquad n = 3.3\ A^{-1}$$

After deducting all the losses from the theoretical output cell voltage, the model fits to the practical data as shown below.

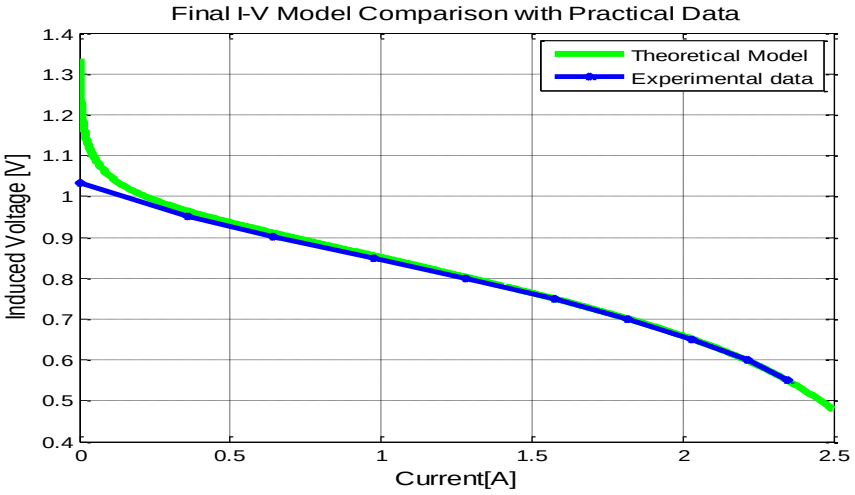

Figure 7.9: The experimental data plot and comparison of final I-V model

7.5 Model Parameters

A summary of model parameters are given in the below table

Table 7.1: The summary of model parameters

Loss	Activation Loss	Ohmic Loss	Concentration Loss	Mixed potential Loss
Equation	$\frac{RT}{\alpha_C zF}\ln\left[\frac{i}{i_{0,C}}\right] + \frac{RT}{\alpha_A zF}\ln\left[\frac{i}{i_{0,A}}\right]$	$(R_{anode} + R_{cathode} + R_{electrolyte})\, i$	$m\exp[nI]$	$P\ exp[Q - I]$
Parameters	$\alpha_C = 0.5$ $\alpha_A = 0.95$ $i_{0,C} = 0.003\ A$ $i_{0,A} = 0.003\ A$	$R_{anode} = 0.013\ \Omega$ $R_{cathode} = 0.156\ \Omega$ $R_{electrolyte} = 0.0005\ \Omega$	$m = 0.00003$ $n = 160\ A^{-1}$	$P = 10^{-6}$ $Q = 14.4$

8

Discussion

This chapter discusses the results that are obtained from all the experiments performed during the thesis for the anode substrates as well as 2-R cell samples and data analysis are given to prove its higher performance. The stability and electrical properties described in Section 8.1 including the comparisons of overall results, average reduction resistance values sample wise as well as with theoretical data. Analysis of performance and lifetime properties of 2-R cells are discussed in Section 8.2. Section 8.3 gives a comparison of I-V model with practical 2-R cell I-V characteristics. Finally the important findings and observations are summarized under Section 8.4.

8.1 The Stability and Electrical Properties of Anode Substrates

The stability of the anode substrate is going to be discussed focusing on the test results mentioned in chapter 5 for the five anode substrates, A-1, A-2, A-3, B-1 and B-2.

8.1.1 Comparison of Overall Result of Five Samples

For all the samples the obtained reduction and oxidation resistance values were plotted in the Figure 5.6 in chapter 5. At the operation condition, the cell is working under the reduction mode and the plot below figures out only the behavior of reduction resistance values for the redox cycles. (Magnification of the latter part of the Figure 5.6)

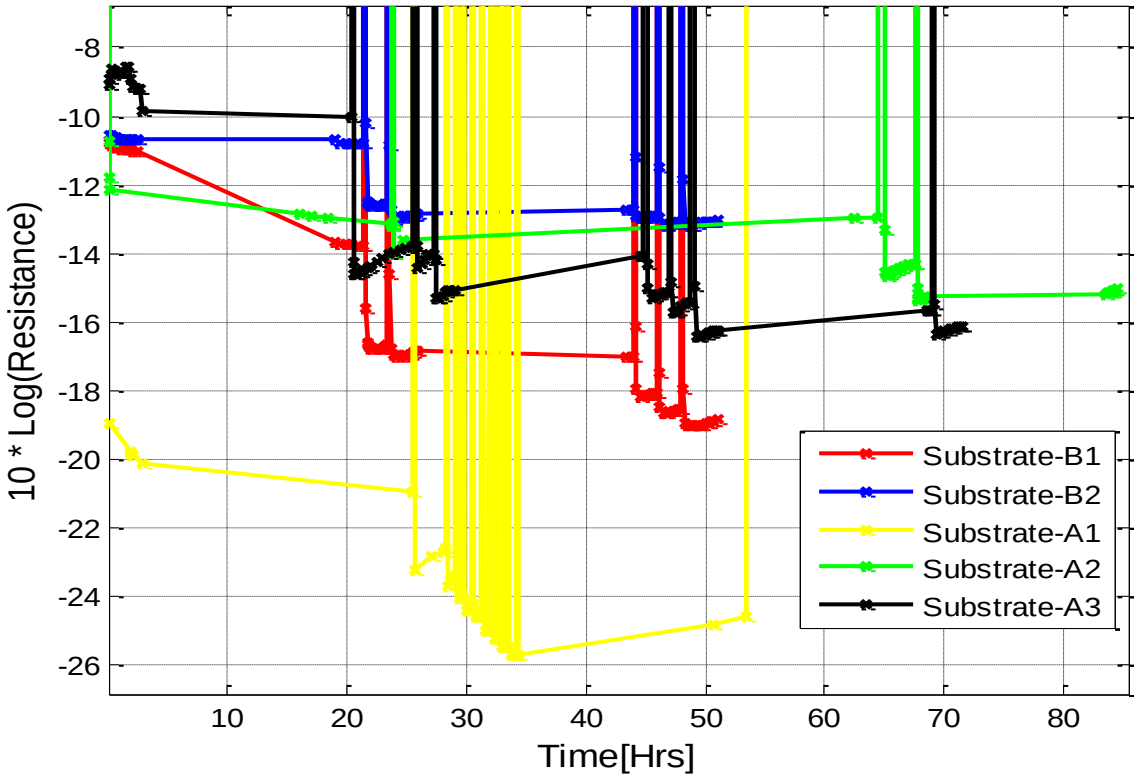

Figure 8.1: The line plot of logarithmic resistance values of all samples under reduction state

A-1 sample is subjected to a many fast redox cycles as well as other samples tested under both fast and slow redox cycles. As seen from the above graph, A-1 sample shows a lower resistance during the whole test, when compared with the other samples. There is a glitch in the behavior shown at the beginning of the A-3 sample and it was due to replacement of Hydrogen cylinder after starting the test. The Figure 8.2 shows the scatter plot of above figure which represents only the data points.

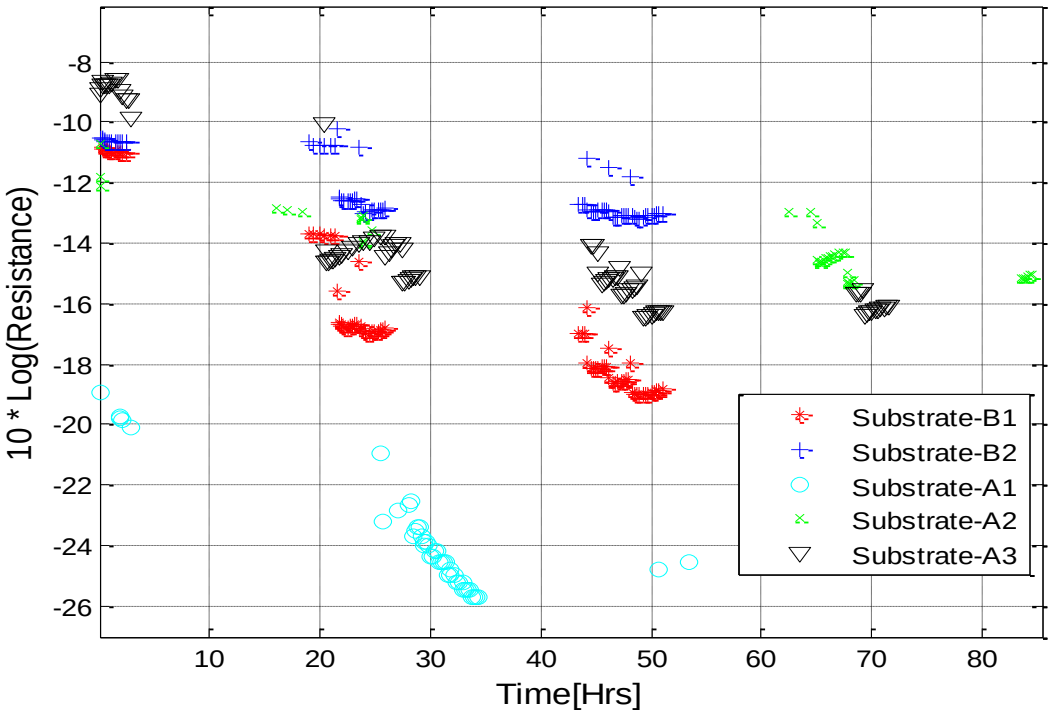

Figure 8.2: The scatter plot of logarithmic resistance values of all samples under reduction state

8.1.2 Comparison of Average Reduction Resistance Values of Five Samples

The average reduction resistance values of all the tested samples for the first five redox cycles are tabulated below.

Table 8.1: Table of Average Resistance values of Anode samples for first five redox cycles

	Anode Substrate Sample Average Resistance (Ω)				
	A-1	**A-2**	**A-3**	**B-1**	**B-2**
Redox Cycle 2	0.005215	0.057955	0.038595	0.021865	0.058953
Redox Cycle 3	0.004464	0.045680	0.033002	0.021331	0.054054
Redox Cycle 4	0.004109	0.036552	0.031176	0.016475	0.053742
Redox Cycle 5	0.003753	0.030231	0.028417	0.014363	0.051575
Redox Cycle 6	0.003556		0.024894	0.012957	0.050354
Average resistance for above 5 cycles	0.004219	0.042605	0.031217	0.017398	0.053736
	Average A sample Resistance 0.026014			Average B sample Resistance 0.035567	

The table shows the average resistance values of each redox cycle separately as well as the sample wise average values. The graphical representation of resistance values against the redox cycles is shown in the figure below,

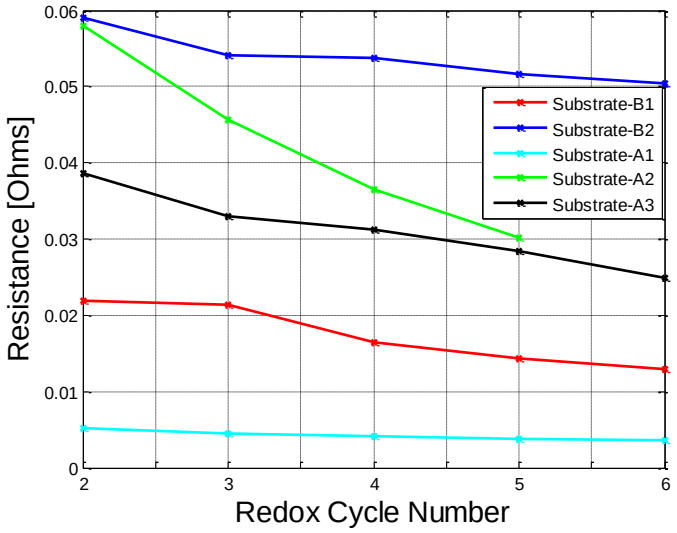

Figure 8.3: Average resistance values of all the samples against redox cycle number

The three A samples show different inclinations as illustrated in the above figure. The practical issues may cause the variations such as,

Instrument errors – The external power source which was used to supply constant current output, is showed the value to the first decimal point only and hence it might cause slight variations for different samples. The same multimeter was not used to measure the voltages for every sample and therefore the internal resistance values of the multimeter could be affected to the above variations.

Compression on the cell – The cell was compressed by tightening the springs, but it was difficult to tighten to the exact value with Vernier calipers. Also there were small dissimilarities in the original length of the springs.

Time scale – For all the samples, the time scale used was different from each other. The test was unable to be started for each specimen, within a similar period after they were heated to the exact temperature.

To clearly identify the difference between A and B type samples, the average of three A sample and two B samples are illustrated in the figure below with linear inclinations

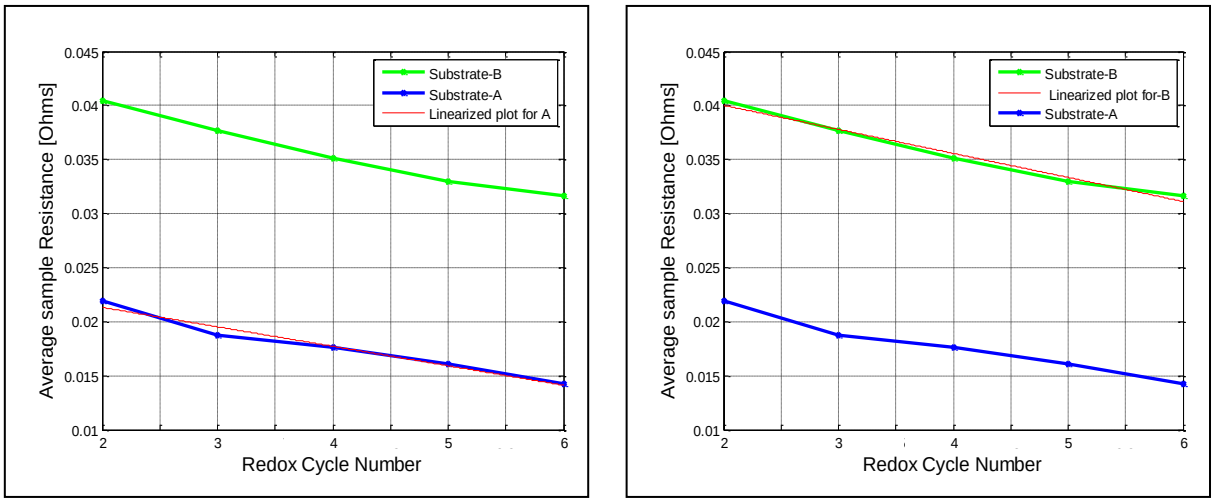

Figure 8.4: Comparison of Average resistance values of sample A and B with their linear approximations

From the above figure it can be seen that the substrate type A has a lower value of average resistance at each redox cycle than that of the type B as well as the inclination is smaller when compared with the anode substrate type B. Hence it can be shown that of these two types, the type A is the best.

8.1.3 Redox Cycle Wise Comparison of Reduction Resistance Values

To compare the reduction resistance value variation from one redox cycle to the other, the 3rd and 4th redox cycles were chosen to obtain most valuable and error free results omitting the very first and final redox cycles. The results were plotted with the inclination as well for all the samples.

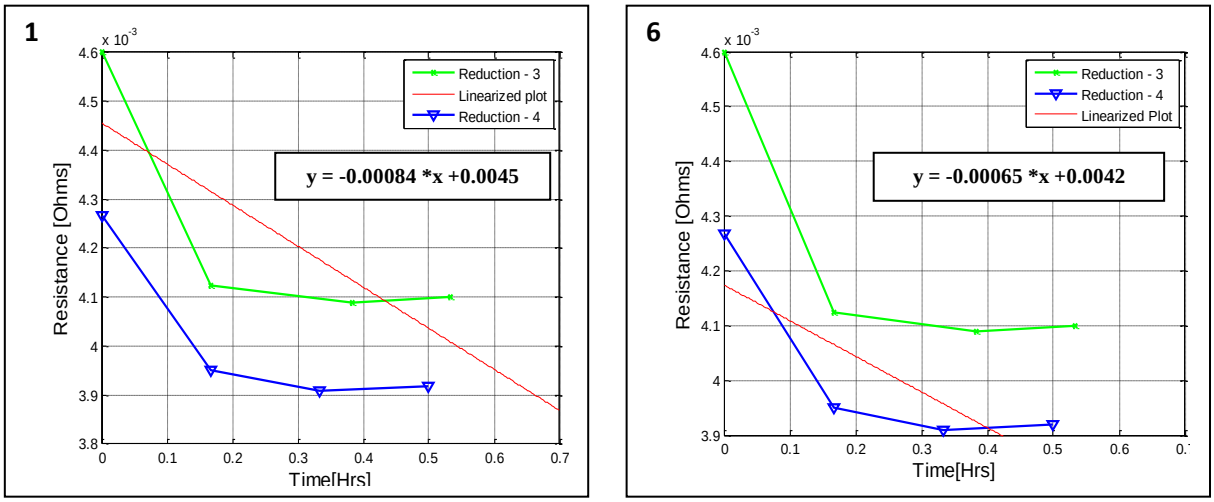

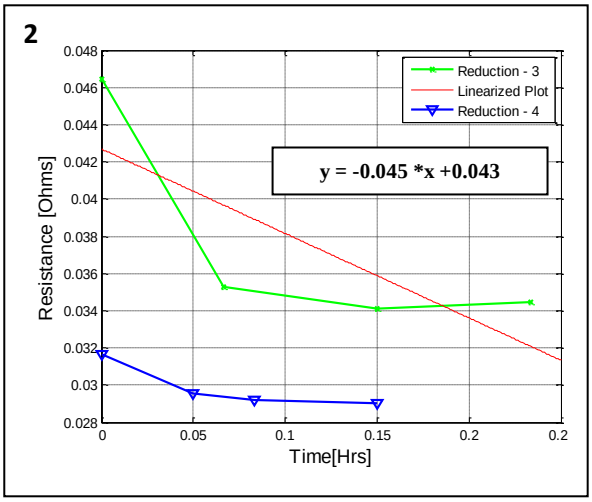
2
Reduction - 3
Linearized Plot
Reduction - 4
y = -0.045 *x +0.043
Resistance [Ohms]
Time[Hrs]

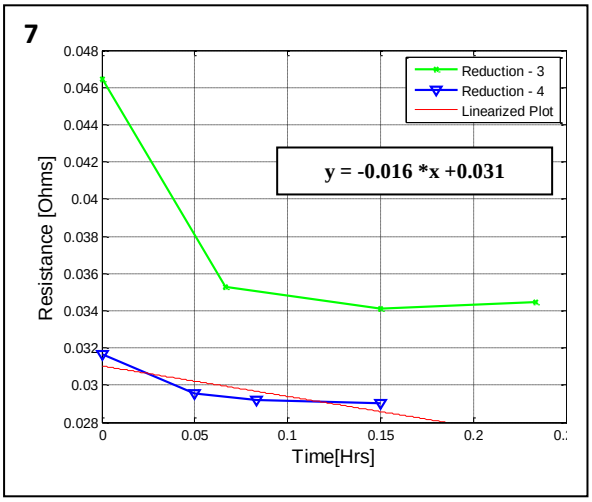
7
Reduction - 3
Reduction - 4
Linearized Plot
y = -0.016 *x +0.031
Resistance [Ohms]
Time[Hrs]

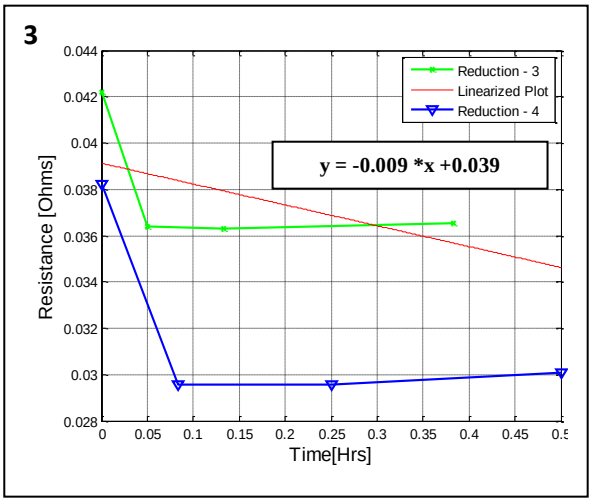
3
Reduction - 3
Linearized Plot
Reduction - 4
y = -0.009 *x +0.039
Resistance [Ohms]
Time[Hrs]

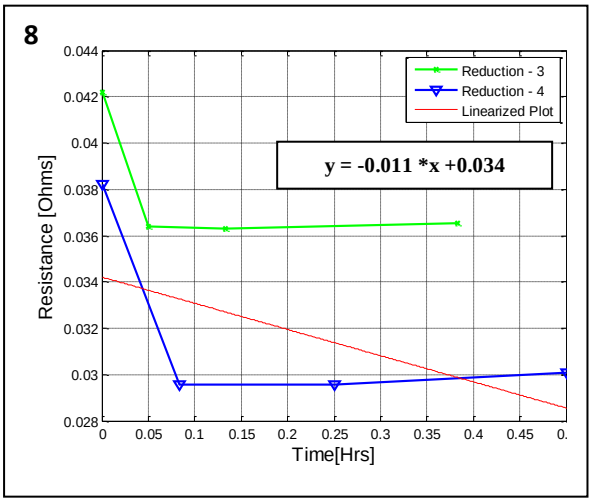
8
Reduction - 3
Reduction - 4
Linearized Plot
y = -0.011 *x +0.034
Resistance [Ohms]
Time[Hrs]

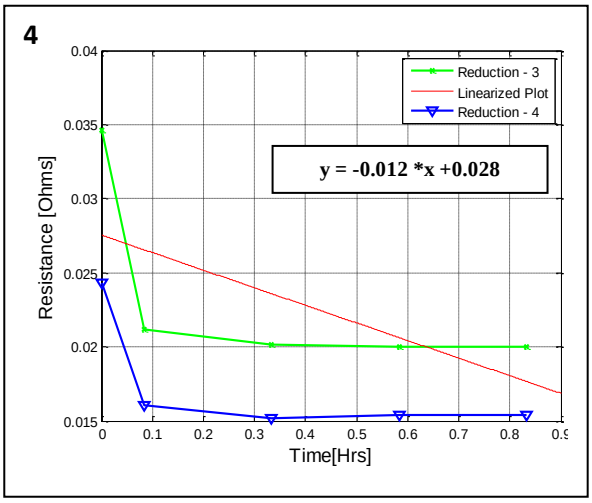
4
Reduction - 3
Linearized Plot
Reduction - 4
y = -0.012 *x +0.028
Resistance [Ohms]
Time[Hrs]

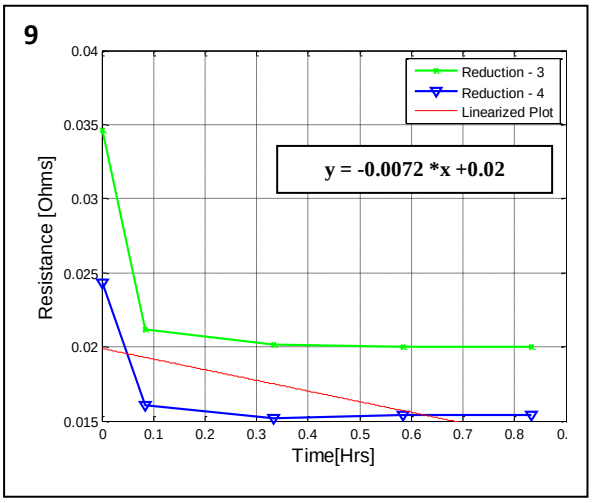
9
Reduction - 3
Reduction - 4
Linearized Plot
y = -0.0072 *x +0.02
Resistance [Ohms]
Time[Hrs]

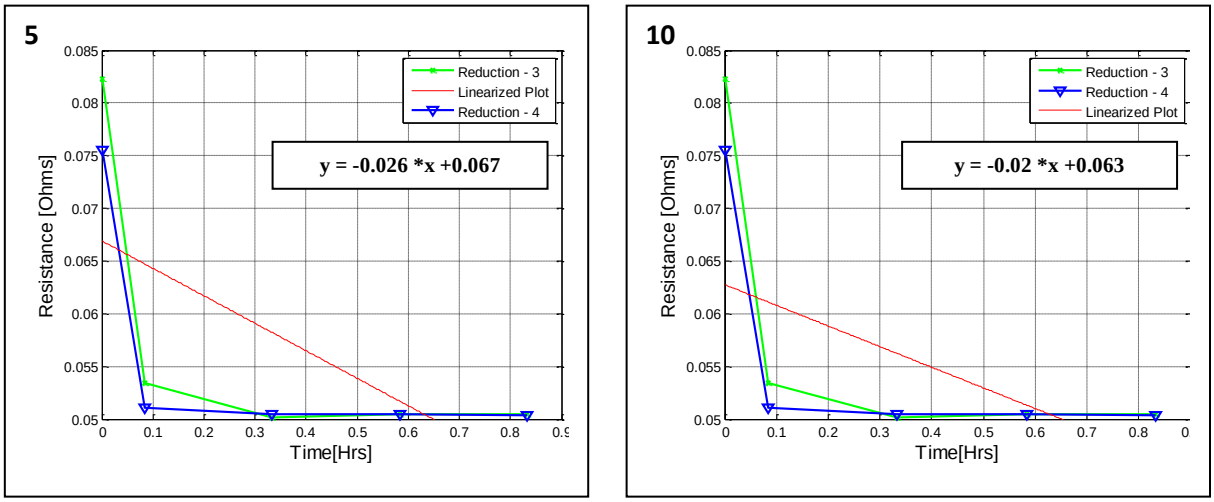

Figure 8.5: The graphs of resistance values of 3rd [1,2,3,4,5] and 4th [6,7,8,9,10] reduction cycles and linearized plots with equations.

From the Figure 8.5, it can be shown that just after changing the conditions from oxidation to reduction there is a steep inclination. At this period all the elements that are used to make the anode, have a trend to change from oxide (NiO, Y_2O_3, ZrO_2, etc.) states to their original element state. In particular there is a large difference in morphology between NiO and metallic Ni. The oxides off all the elements are having higher resistance. The morphology of the anode material, changes with this state change and it stabilizes after a while. Then the resistance value reaches a stable value within a short time period.

8.1.4 Comparison of Reduction Resistance Value variation with the Conventional Test Outputs

As seen from Figure 8.1 and 8.2, the curves were shifted downwards from redox cycle to cycle, showing lower resistance values conflicting with the conventional results. It is difficult to present a clear explanation about that without knowing the exact information about the composition and the manufacturing method. For commercial IP reasons the manufacturing process of the 2-R cell has been withheld from this report. Therefore the manufacturing method and basic elements of these new anode substrates could be assumed as the main reasons. For the sake of interpretation we will assume that the 2R-cell fabrication is made from nickel fibres whereas the conventional nickel cermet is made from nickel powder.

The structures of these two Ni particles are different from each other approximately as drawn below and with the time the particle size variation under reduction conditions can be assumed as shown below,

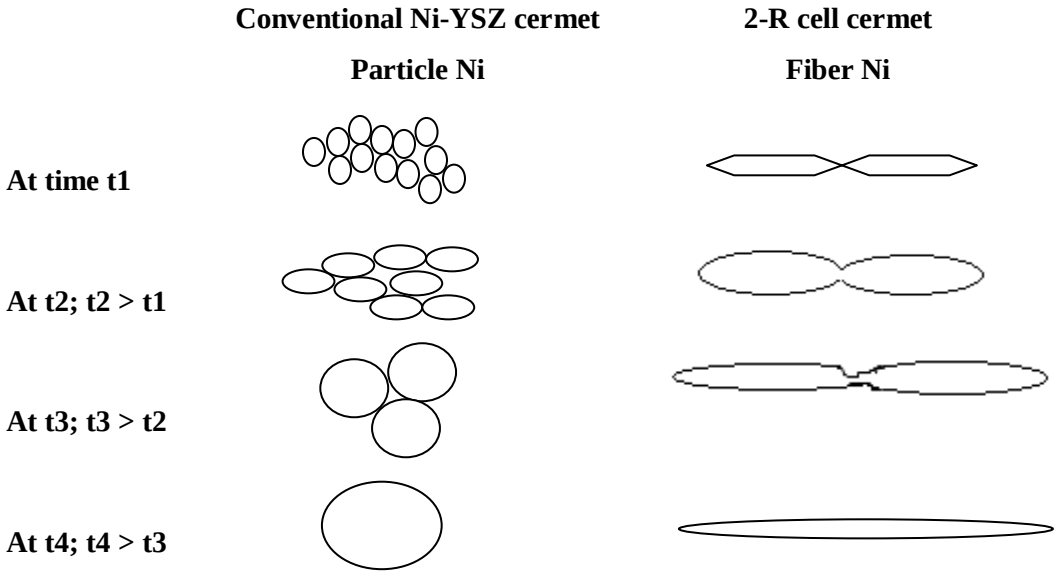

Figure 8.6: Growth of particle Ni and fiber Ni with time under fuel supply

The resistance of Ni substrates depends on the area of contact points of two Ni atoms. The particle type Ni atoms grow under the reduction conditions as shown above while maintaining its spherical shape and hence when it is growing, the number of contact points and the contact area of a single atom with other atoms is increasing. The reason for increase in reduction resistance with time and with number of redox cycles of a conventional SOFC can be explained. Therefore it presents a massive degradation with time.

In the case of 2-R cell which is made of fiber Ni, we observe an increase in its performance with the number of redox cycles from the test results. That opposes the current theoretical explanations. To represent the fiber Ni, we simplify the morphology as a hexagonal shape above and with the time there is a trend to grow these two fibres together as a single fibre. It therefore reduces the constriction in contact area between the fibres. This process is then repeated thought the whole cermet structure so over time the electronic resistance of the 2-R cell decreases.

8.1.5 Comparison of Electrical Properties of Type A and B with Theoretical values.

The calculated average resistance values for Type A and B are mentioned in the table 8.1. To compare performance of the substrate with currently researching specimens, it is important to calculate the resistivity and the conductivity of both the types considering the average substrate area value and the average thickness.

Average substrate area for type A = 1.1905 cm^2

Average substrate area for type B = 1.2099 cm^2

Average thickness = 0.04 cm

Resistivity $\rho = \frac{R*A}{l}$ (8.1)

Conductivity $\sigma = \frac{1}{\rho}$ (8.2)

Table 8.2: Resistance, resistivity and conductivity of anode material samples

	Anode Substrate Sample	
	Type - A	**Type - B**
Average Resistance (Ω)	0.026014	0.035567
Average Resistivity (Ω cm)	0.7742417	1.0758128
Average Conductivity (S/cm)	1.2915864	0.9295297

The conductivity of type A anode substrates varies approximately from 0.9882155 S/cm to 2.399952 S/cm within first five redox cycles.

The electrical conductivity of Ni/YSZ cermet is strongly dependent on its Ni content according to the percolation theory. The conductivity of the cermet as a function of Ni content is an S shaped curve that is predicted by the percolation theory [28]. The graph is shown in the figure below.

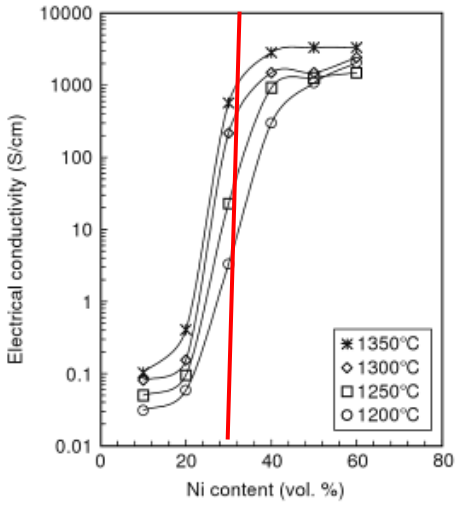

Figure 8.7: The variation of electrical conductivity as a function of Ni concentration at different firing temperatures [28]

The percolation threshold for the conductivity is at about 30 vol % Ni, and at 1200 ^{0}C the electrical conductivity is nearly 2 S/cm. As seen from the figure the conductivity is decreasing with the temperature. The Type A and B samples were tested at 810 ^{0}C and the conductivity was found to increase up to 2.4 S/cm within five redox cycles. Hence, this study proves that the new samples have approximately 20 % higher conductivity than the conventional substrates. It could be more than that when compared with the exact operating temperature.

8.1.6 Stability Analysis of Anode Material Samples.

After testing the samples under several redox cycles, they were tested through the optical microscope. The optical microscope images of A and B anode samples after testing the samples under several redox cycles are shown in Figure 8.8.

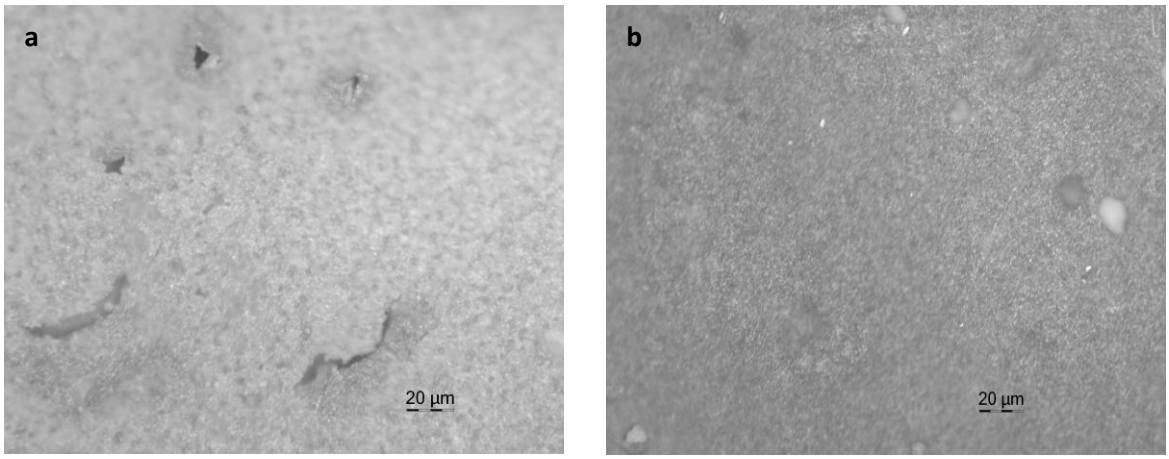

Figure 8.8: Optical Microscope images of (a) A1and (b) B1 after redox cycle testing

The examination of the materials reveals that no cracks were visible in any of the images taken, thus confirming that the 2-R Cells are completely stable and robust towards redox cycling.

8.2 The Performance and Lifetime Properties of 2-R cells

2R cell properties are going to be discussed considering the test results mentioned in chapter 6 for four 2R cells and the reference SOFC.

8.2.1 Comparison of I-V and Power Characteristics of Four 2-R Cell Samples and Reference SOFC

Each of the 2-R cell samples were tested for two redox cycles as mentioned in chapter 6, but the reference cell could withstand for the first reduction only. So the figures below show the I-V curves for the first redox cycle.

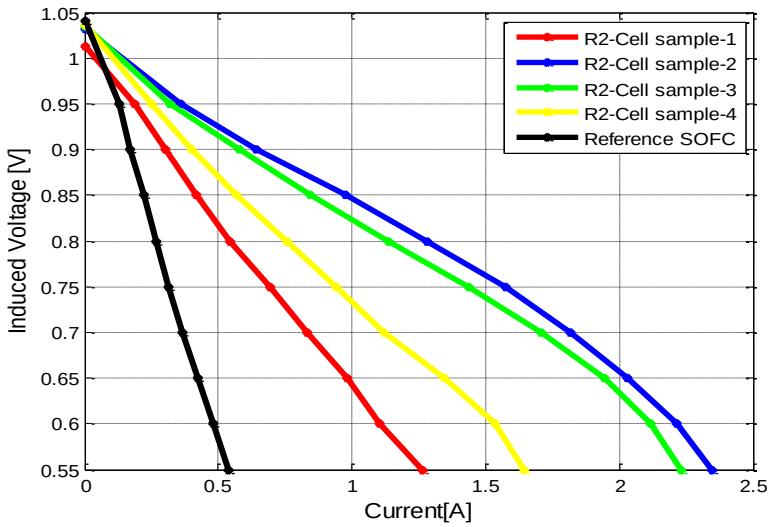

Figure 8.9: The I-V characteristics for all the cells at 10% Hydrogen

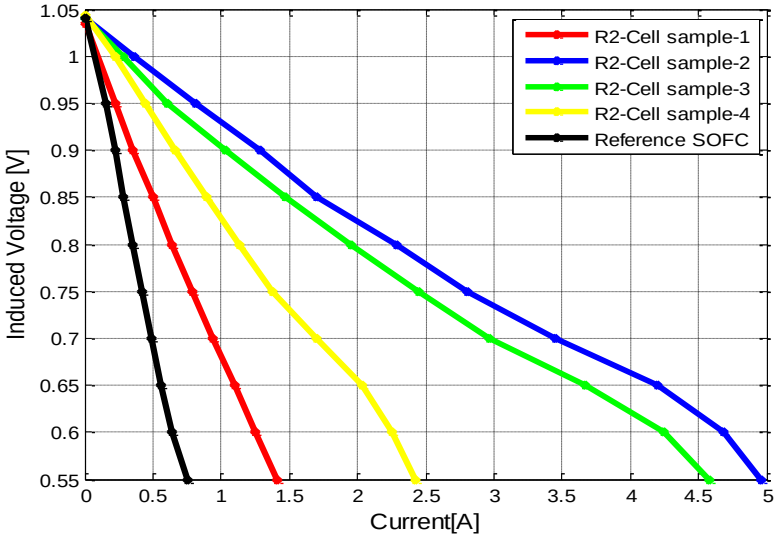

Figure 8.10: The I-V characteristics for all the cells at 100% Hydrogen

The above Figure 8.9 and 8.10 represents the I-V characteristics of all the cells that are tested at 10% and 100% Hydrogen supply. The each cell is different from each other and 2nd and 3rd samples showed similar characteristics. As seen from the figures the reference cell

voltage is highly decreasing with the increase of current. When compared to the reference SOFC, all the 2-R cells performed better I-V characteristics.

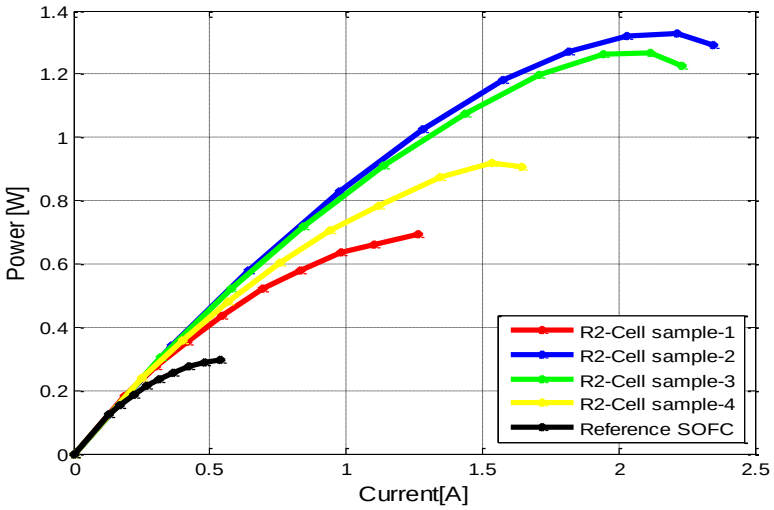

Figure 8.11: The output power Vs current plots for all the cells at 10% Hydrogen

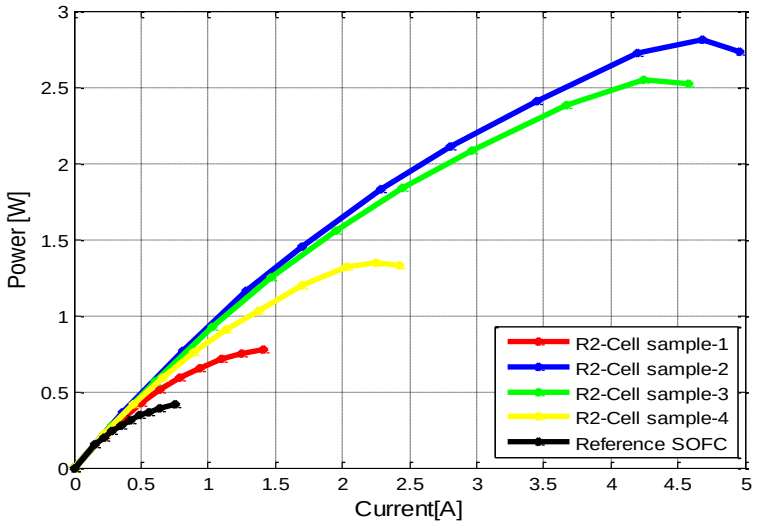

Figure 8.12: The output power Vs current plots for all the cells at 100% Hydrogen

As seen from the two figures above, all the 2-R cells were able to perform better power characteristics than the reference SOFC.

The maximum efficiency can be obtained at the highest power output point and that is the best operating point for all the cells. The operating point characteristics are tabulated below for each cell in Table 8.3.

Table 8.3: Maximum operating point characteristics of cell samples

		The Cell				
		2R-Sample 1	**2R-Sample 2**	**2R-Sample 3**	**2R-Sample 4**	**Reference SOFC**
10% H_2	**Max. power [W]**	**0.696**	**1.329**	**1.269**	**0.921**	**0.297**
	Current [A]	1.265	2.215	2.115	1.535	0.54
	Voltage [V]	0.550	0.600	0.600	0.600	0.550
100% H_2	**Max. power [W]**	**0.778**	**2.811**	**2.544**	**1.350**	**0.413**
	Current [A]	1.415	4.685	4.24	2.250	0.750
	Voltage [V]	0.550	0.600	0.600	0.600	0.550

8.2.2 Redox Cycle Wise Comparison of I-V and Power Characteristics

To compare the Voltage and Power outputs, the second 2-R sample, which is having the highest performance among the tested samples, was chosen. Comparison of I-V and power curves for first and second reduction at 10% Hydrogen is shown in Figure 8.13.

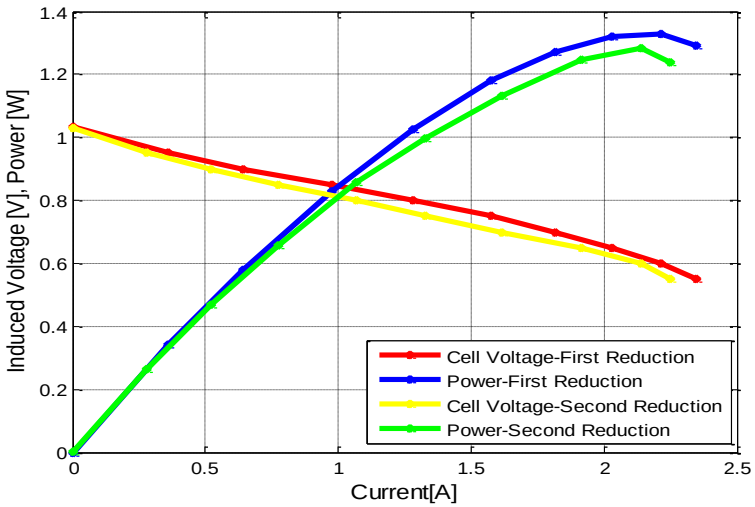

Figure 8.13: The graph of I-V and Power results comparison for first and second reduction at 10% Hydrogen for sample-2

Comparison of I-V and power curves for first and second reduction at 100% Hydrogen is shown in Figure 8.14.

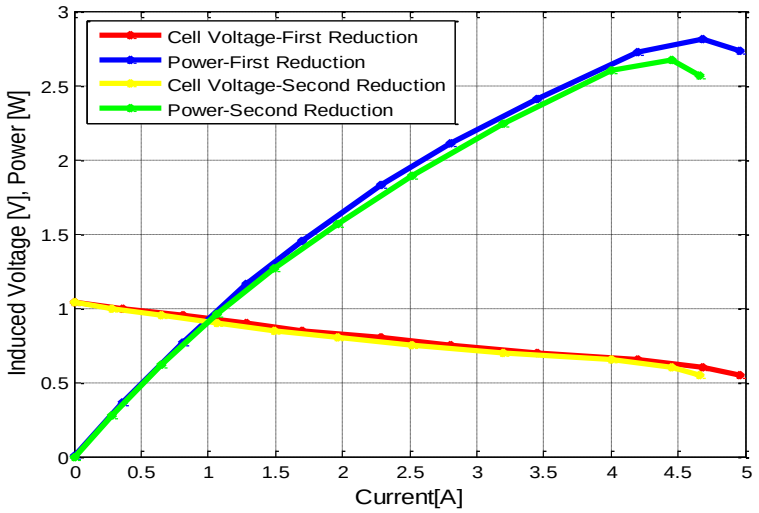

Figure 8.14: The graph of I-V and Power results comparison for first and second reduction at 100% Hydrogen for sample-2

There is a slight reduction of voltage and power in the second reduction than the values in the first reduction but it is a value of milivolts. Also the maximum operating point is slightly shifted below.

8.2.3 Stability and Lifetime Properties of 2-R Cells

From the above studies it's shown that the performance under redox cycles is considerably stable and therefore it can be predicted that the 2-R cells will have longer lifetime than the conventional SOFCs. The physical structure of 2-R cell compared to the reference SOFC is shown in the below figure.

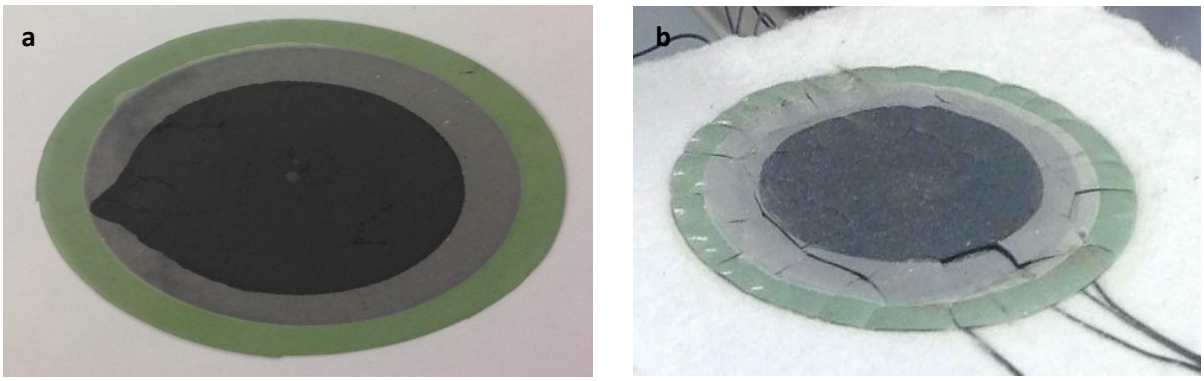

Figure 8.15: The physical structure of (a) 2R cell and (b) Reference cell after redox testing

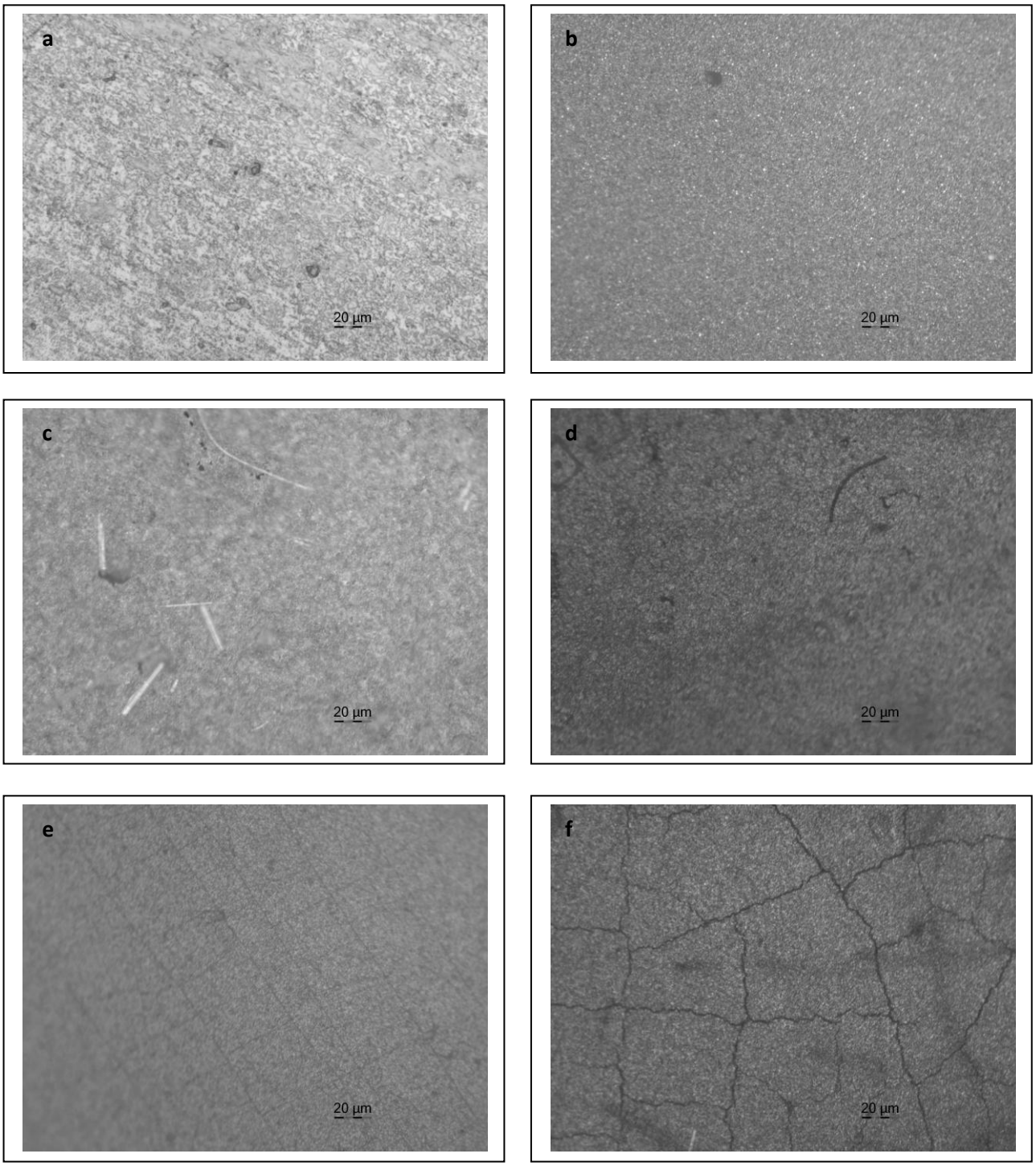

Figure 8.16: The optical microscope images of (a) anode and (b) cathode substrates of 2R cell before testing, (c) anode and (d) cathode substrates of 2-R cell after testing and (e) anode and (f) cathode substrates of reference cell after testing

The above figure shows the optical microscope images for anode and cathode substrate for the 2-R cell as well as for the reference cell. As seen from the figures, the 2-R cell shows a very few smaller cracks on its anode and cathode substrates after the redox cycle test when compared with the reference cell. So it can be mentioned that the 2-R cell is more reliable and can with stand more redox cycles than the conventional products.

After the two redox cycles, every 2-R cell was kept under reduction condition for 72 hours. During this period no significant decrease in cell voltage was observed, thus confirming that the 2-R cell is very stable and does not show any signs of degradation

8.3 Comparison of Model with Practical I-V Characteristics

The modeling procedure of I-V characteristics was described in detailed in chapter 7 with the found parameter values to fit the model to the practical curve. The Figure 7.9 in chapter 7 represents the final model that was created with a comparison of practical output as well.

As seen from the figure the model fits well to the practical characteristics at the higher current region and also the ohmic loss region as well. The maximum operating points of all the tested 2-R cells were within this region.

In the activation loss region there is a considerable difference between the two curves at the open circuit voltage (zero current). There may be some uncertainty in determining the true EMF because of small leakage currents caused by fuel and air mixing at the outer edge of the cell, giving rise to a mixed potential (this is a consequence of the open flange arrangement of the test housing). Also the actual effect of partial pressure components was not be able to measure inside the closed furnace that used for the test. The mixed potential loss is another component that highly affects to the lower current region that was not be able to measure during the test. As explained in the chapter 7, the mixed potential loss was modeled using a mathematical expression (equation 7.15) with exponentially reducing term with the increase of current.

Compared to the existing models developed by other research papers, this model fits well to the 2-R cell characteristics.

8.4 Summary of Discussion

Below is the main outcome from this thesis

- The results obtained for the redox cycle resistance of the anode substrates showed that the substrate type A showed better characteristics than the type B.
- The graphs of the reduction stage resistance values of both the substrate types A and B with time were shifted downwards from one redox cycle to the next showing a decrease of resistance value converse to the conventional results. The decrease of resistance values represents an increase of the conductivity with the time.
- It was proven that the new samples have approximately 20 % higher conductivity than the conventional substrates according to the percolation theory.
- All the 2-R cells were able to withstand for the redox cycles without showing any considerable reduction of its performance with redox cycles.
- The maximum power output of the best 2-R cell among the four samples studied, the cell number 2 was approximately seven times higher than the reference cell.
- From the optical microscope results, it was shown that the cell degradation is negligible of the 2-R cells compared to the reference SOFC cell which has showed a number of cracks on it even after the first redox cycle**.**
- The 2-R cells were able to maintain a constant stable open circuit voltage during a considerable time period showing the ability of higher reliability.
- The I-V model created for the best 2-R cell sample was nicely fits with its practical I-V characteristics at ohmic and concentration loss regions with a small variation at the activation loss region.

9

Conclusion

The conclusion and topics for future work are given accordingly in Section 9.1 and 9.2

9.1 Conclusion

The thesis has dealt with a study of performance and life time properties of 2-R cell samples manufactured by the Fiaxcell Company, through redox cycle testing. The 2-R cell is a novel anode supported RoxSolid fuel cell and the sample cells were subjected to a series of redox cycles to study the performance in comparison with the provided reference SOFC sample.

The A and B types of Anode substrate samples were tested under several redox cycles and the results of the reduction stage resistance values were the opposite of the conventional test results. The reduction resistance values decreased with time for the new anode samples, increasing the conductivity from one redox cycle to the other. So that it can be concluded that the performance of these new anode samples is increasing with time without showing degradation. The integrity of the tested samples was analyzed by optical microscopy. The images obtained were free of cracks and hence this study can prove the higher ability of the tested samples to withstand the redox cycling.

From the tested anode substrate samples, lower average reduction resistance values were obtained from the type A. The average conductivity of sample type A was approximately 1.4 times higher than of the type B and so the type A has the better conductivity properties. At the fifth redox cycle the average conductivity of the substrate type A showed 2.399952 S/cm conductivity, which is 20% better than the theoretical value obtained from the percolation theory on conventional cermet anode substrates.

In the second phase of the work, four compete 2-R cells and a single conventional SOFC sample were tested under fuel cell conditions and their I-V performance characteristics determined both before and after redox cycling. Comparison was made with a conventional anode supported cell (reference SOFC).

From all the five samples the best I-V and power characteristics were obtained from the second 2-R cell sample. The power output at the maximum operating point was approximately seven times higher than the reference SOFC.

All the 2-R cell samples were able to withstand all redox cycles without showing any significant degradation of output power where as the reference cell was unable to withstand even its first redox cycle. The images, taken from the optical microscope after redox cycle testing proved the robustness of the 2-R cells compared to the reference SOFC. The images showed many cracks on the reference cell but there were very few on the tested 2-R cells.

All the 2-R cells were able to maintain their original open circuit voltages after returning the cell to fuel conductions, and keeping cells under the fuel condition for a long period of time as well.

The overall result of the thesis was to be able to confirm higher robustness of the 2-R cell and better performance compared to the reference conventional SOFC.

As the final stage of the thesis an I-V model was created successfully to coincide with the practical 2-R cell characteristics considering the theoretical cell output with losses.

9.2 Future Work

This thesis has focused specifically on the ability of the 2-R cell to withstand redox cycling.

In future work, testing could be extended to cover the robustness of the 2-R cell towards thermal cycling.

In addition a more in-depth electrochemical study using Electrochemical Impedance Spectroscopy (EIS) could be made to assist in establishing a more sophisticated model for the time dependency of the new 2-R cell substrate material.

Bibliography

[1]. **Arnab Choudhury, H.Chandra, A.Arora.** *Application of solid oxide fuel cell technology for power generation - Review.* Department of Mechanical Engineering, Bhilai Institute of Technology. India : 2012 ElsevierLtd, 2012. Renewable and Sustainable Energy Reviews 20(2013)430–442.

[2]. **L.L. Zhenga, J.J. Lia, M.S. Lia, Y.C. Zhoua.** *Investigation on the properties of Nb and Al doped Ti3SiC2 as a new interconnect material for IT-SOFC.* henyang National Laboratory for Materials Science, Institute of Metal Research, Chinese Academy of Sciences. China : ScienceDirect, 2012. international journal of hydrogen energy 371084e1088.

[3]. **Kyung Bin Yoo, Byung Hyun Park, Gyeong Man Choi.** *Stability and performance of SOFC with SrTiO3-based anode in CH4 fuel.* Fuel Cell Research Center/Department of Materials Science and Engineering , Pohang University of Science and Technology (POSTECH). Republic of Korea : ScienceDirect, 2012. Solid State Ionics 225 (2012) 104–107.

[4]. **Kaarstad, Olav.** *Fossil fuels and responses to global warming.* Statoil R&D Centre. Norway : ScienceDirect, 1995. Second International Conference on Carbon Dioxide Removal. Energy Conversion and Management, 0196-8904(95)00141.

[5]. **J.M. Andu jar, F. Segura.** *Fuel cells History and updating A walk along two centuries.* Department of Electronic, Computer Science and Automatic Engineering, University of Huelva Crta. Spain : ScienceDirect, 2009. Renewable and Sustainable Energy Reviews, 13 (2009) 2309–2322.

[6]. **C.H.Zhao, R.Z.Liu, S.R.Wang, T.L.Wen.** *Effect of Ag-(La0.8 Sr 0.2)0.95MnO3 current-collecting layer on the stability of anode-supported solid oxide fuel cell.* CAS Key Laboratory of Materials for Energy Conversion, Shanghai Institute of Ceramics. China : ScienceDirect, 2010. Journal of Alloys and compounds, 0925-8388.

[7]. **Behling, Noriko Hikosaka.** *Fuel Cells, Current Technology challengers and Future Research Needs.* Japan : Elsevier B. V. , 2013. 978-0-444-56325-5.

[8]. **National Research Council, National Academy of Engineering.** *The Hydrogen Economy.* Washington, United States of America : National Academies, 2009. 0-309-09163-2.

[9]. **Toshio Suzuki-a, Masanobu Awano-a, Piotr Jasinski-b, Vladimir Petrovsky-c, Harlan U. Anderson-c.** *Composite (La, Sr)MnO3–YSZ cathode for SOFC.* a-Advanced Manufacturing Research Institute, AIST , Moriyama-ku Nagoya, Japan. b-Department of Biomedical Engineering, Gdansk University of Technology, Poland, c-Electronic Materials Applied Research Center, University of Missouri-Rolla., Missouri, U.S.A : Science Direct , 2005. Journal of Solid State Ionics 177 (2006) 2071 – 2074.

[10]. **N.S. Sochugov-a, A.A. Soloviev-a, A.V. Shipilova-a, V.P. Rotshtein-b.** *An ion-plasma technique for formation of anode-supported thin electrolyte films for IT-SOFC applications.* Laboratory of Applied Electronics(a) and Laboratory of Vacuum Electronics (b), Institute of High Current Electronics, Siberian Branch of Russian Academy of Sciences, 2/3 Akademichesky ave., Tomsk 634055, Russia : Science Direct, 2011. international journall of hydrogen energy 36(2011)5550e5556.

[11]. **John B. Goodenough, Yun-Hui Huang.** *Alternative anode materials for solid oxide fuel cells.* Texas Materials Institute, ETC 9.102, 1 University Station, C2200, The University of Texas at Austin, Austin, TX 78712, USA : Science Direct, 2007. Journal of Oower Sources 173 (2007) 1-10.

[12]. **Q.X. Fu-a, F. Tietz-a, P. Lersch-b, D. Stöver-a.** *Evaluation of Sr- and Mn-substituted LaAlO3 as potential SOFC anode materials.* a-Institute for Materials and Processes in Energy Systems (IWV-1), Forschungszentrum Jülich GmbH, 52425 Jülich, Germany, b-Institute for Materials and Processes in Energy Systems (IWV-2), Forschungszentrum Jülich GmbH, 52425 Jülich, Germany : Science Direct, 2006. Journal of Solid State Ionics 177 (2006) 1059–1069.

[13]. **Chang Rong He, Wei Guo Wang, Jianxin Wang, Yejian Xue.** *Effect of alumina on the curvature, Young's modulus, thermal expansion.* Division of Fuel Cell and Energy Technology, Ningbo Institute of Materials Technology and Engineering, Chinese Academy of Sciences, 519 Zhuangshi Road, Ningbo 315201, PR China : Science Direct, 2011. Journal of Power Sources 196 (2011) 7639– 7644.

[14]. **W.Z. Zhu, S.C. Deevi.** *A review on the status of anode materials for solid oxide fuel cells.* Research and Development Center, Chrysalis Technologies Incorporated, 7801 Whitepine Road, Richmond, VA 23237, USA : Elsevier, 2003. Materials Science and Engineering A362 (2003) 228–239.

[15]. **Qianli Ma, Frank Tietz.** *Comparison of Y and La-substituted SrTiO3 as the anode materials for SOFCs.* Forschungszentrum Jülich, Institute of Energy and Climate Research (IEK-1), 52425 Jülich, Germany : Science Direct, 18th International Conference on Solid State Ionics Warsaw, Poland, 2012. Solid State Ionics journal, 225 (2012) 108–112.

[16]. **Ji Haeng Yu, Gun Woo Park, Shiwoo Lee, Sang Kuk Woo.** *Microstructural effects on the electrical and mechanical.* Korea Institute of Energy Research (KIER), Jang-dong 71-2, Daejeon 305-343, Republic of Korea : Science Direct, Papers presented at the FUEL PROCESSING FOR HYDROGEN PRODUCTION SYMPOSIUM at the 230th American Chemical SocietyNational Meeting, Washington, 2006. Journal of Power Sources 163 (2007) 926–932.

[17]. **James Larminie-a, Andrew Dicks-b.** *Fuel Cell Systems Explained (Second Edition).* a-Oxford Brookes University, UK, b-University of Queensland, Australia : John Wiley & Sons Ltd, The Atrium, Southern Gate, Chichester,West Sussex PO19 8SQ, England, 2003. ISBN 0-470-84857-X.

[18]. **Andre, Leonide.** *SOFC Modeling and Parameter Identification by means of Impedance Spectroscopy.* KarlsruherInstitute of Technology, Germany : KIT Scientific Publishers, 2010. 978-3-86644-538-3.

[19]. **S. Kalac, A. Pramuanjaroenkij, L. Vasiliev.** *Mini Micro Fuel Cells - Fundamentals and Applications.* Cesme-Lzmir, Turkey : Springer, Netherlands, 2007. ISBN 978-1-4020-8295-5.

[20]. **Stanislaw Sieniutycz, Jacek Jezowski.** *Energy Optimization in Process Systems and Fuel Cells.* The Boulevard, Langford Lane, Kidlington, Oxford OX5 1GB, UK : Oxford : Elsevier Science, 2013. ISBN: 978-0-08-098221-2.

[21]. **M., Sammes Nigel.** *Fuel cell technology: reaching towards commercializatio.* Department of Metallurgical and Materials Engineering, Colarado School of Mines, USA : Springer, Technology & Engineering -, 2006. ISBN-10: 185-23397-48.

[22]. **El-Sharkawi, Mohamed A.** *Electric Energy: An Introduction (Third Edition).* 6000, Broken Sound Parkway NW, Boca Raton, United States of America : CRC Press-Taylor & Francis Group, 2012. ISBN: 978-1-4665-0303-8.

[23]. **Kittec-R Squadro (User manual for Klin and test bench)**. Kittec GmbH, St.-Georg Strasse 69, D-83024, Rosenheim, Germany : www.kittec.de, Standard 2007.

[24]. **Instruments, Teledyne Hastings.** HFC-202 Flow Controller-User Guide. *Standad: ISO 9001*. Teledyne Hastings Instruments 804 Newcombe Ave, Hampton, VA 23669 : www.teledyne-hi.com, 2011.

[25]. **MFC, Advanced Energy-R Aera.** Fundamentals of Mass Flow Control- Critical Terminology and Operation Principles for Gas and Liquid MFCs . *White Paper*. Advanced Energy Industrie, inc., 1625 Sharp Point Drive, Colorado : www.advanced-energy.com, 2005.

[26]. **Bentup TC 505 Thermocomputer - User Guide**. Bentup Industrial Controls, inc., U.S.A. : www.bentup.de, 2001.

[27]. **S.C. Singhal, K. Eguchi.** *Solid Oxide Fuel Cells 12 (SOFC-XII) Volume 35 no1*. USA : The Electrical Society 65, South Streat, Penington, Newjersy, 2011. ISBN-978-1-60768-212-7 (PDF).

[28]. **Sorensen, Bent.** *Hydrogen and Fuel Cells.* United Kingdom : Elsevier Ltd, Langford, Kidlington, Oxford OX5 1GB, 2005 (First Edition). ISBN : 0-08-044696-5.

Appendix A

The appendix A contains the results obtained from the redox cycle testing of all the five anode substrates with calculated values.

A.1 Redox Cycle Test Results for Anode Substrate Sample B-1

Table A.1: Redox test results for anode specimen B_1

Oxidation or Reduction	Time	Elapsed Time Minutes	Elapsed Time Hours	Measured Voltage (mV)	Area Resistance of Substrate (Ohm cm^2)
Reduction	14.00	0	0	57.6	
	14.05	5	0.083333	51.2	
	14.10	10	0.166667	50.4	
	14.20	20	0.333333	50	
	14.25	25	0.416667	49.6	
	14.30	30	0.5	49.3	
	14.35	35	0.583333	49.1	
	14.40	40	0.666667	49	
	14.45	45	0.75	49	
	14.50	50	0.833333	48.9	
	14.55	55	0.916667	48.9	
	15.00	60	1	48.8	
	15.15	75	1.25	48.6	
	15.30	90	1.5	48.4	
	15.45	105	1.75	48.2	
	16.00	120	2	48.2	
	16.15	135	2.25	48.1	
	16.30	150	2.5	48	
	9.00	1140	19	25.9	
	9.30	1170	19.5	25.8	
	10.00	1200	20	25.7	
	10.30	1230	20.5	25.6	
	11.00	1260	21	25.5	
	11.20	1280	21.33333	25.4	
Oxidation	11.30	1290	21.5		2000
	11.31	1291	21.51667		1870
	11.32	1292	21.53333		1815
	11.33	1293	21.55		1724

	11.34	1294	21.56667		1634
	11.35	1295	21.58333		1597
	11.36	1296	21.6		1555
	11.37	1297	21.61667		1519
	11.38	1298	21.63333		1492
	11.39	1299	21.65		1485
Reduction	11.40	1300	21.66667	16.7	
	11.45	1305	21.75	13.2	
	11.50	1310	21.83333	13	
	11.55	13.15	0.219167	12.9	
	12.00	1320	22	12.8	
	12.15	1335	22.25	12.7	
	12.30	1350	22.5	12.7	
	12.45	1365	22.75	12.8	
	13.00	1380	23	12.8	
	13.15	1395	23.25	12.9	
	13.25	1405	23.41667	13	
Oxidation	13.30	1410	23.5		1789
	13.31	1411	23.51667		1668
	13.32	1412	23.53333		1520
	13.33	1413	23.55		1396
	13.34	1414	23.56667		1286
	13.35	1415	23.58333		1209
	13.36	1416	23.6		1146
	13.37	1417	23.61667		1096
	13.38	1418	23.63333		1061
	13.39	1419	23.65		1034
Reduction	13.40	1420	23.66667	20.96	
	13.45	1425	23.75	12.8	
	14.00	1440	24	12.2	
	14.15	1455	24.25	12.1	
	14.30	1470	24.5	12.1	
	14.45	1485	24.75	12.2	
	15.00	1500	25	12.2	
	15.15	1515	25.25	12.3	
	15.30	1530	25.5	12.4	
	15.45	1545	25.75	12.5	
	16.00	1560	26	12.6	
	9.30	2610	43.5	12.1	
	9.45	2625	43.75	12.1	
	9.55	2635	43.91667	12.1	
Oxidation	10.00	2640	44		1694
	10.01	2641	44.01667		1574
	10.02	2642	44.03333		1448
	10.03	2643	44.05		1311
	10.04	2644	44.06667		1201

	10.05	2645	44.08333		1122
	10.06	2646	44.1		1064
	10.07	2647	44.11667		1016
	10.08	2648	44.13333		974
	10.09	2649	44.15		941
Reduction	10.10	2650	44.16667	14.7	
	10.15	2655	44.25	9.7	
	10.30	2670	44.5	9.2	
	10.45	2685	44.75	9.3	
	11.00	2700	45	9.3	
	11.15	2715	45.25	9.3	
	11.30	1730	28.83333	9.4	
	11.45	2745	45.75	9.4	
	11.55	2755	45.91667	9.4	
Oxidation	12.00	2760	46		1441
	12.01	2761	46.01667		1314
	12.02	2762	46.03333		1174
	12.03	2763	46.05		1062
	12.04	2764	46.06667		978
	12.05	2765	46.08333		917
	12.06	2766	46.1		873
	12.07	2767	46.11667		841
	12.08	2768	46.13333		815
	12.09	2769	46.15		796
Reduction	12.10	2770	46.16667	10.8	
	12.15	2775	46.25	8.6	
	12.30	2790	46.5	8.3	
	12.45	2805	46.75	8.3	
	13.00	2820	47	8.4	
	13.15	2835	47.25	8.4	
	13.30	2850	47.5	8.4	
	13.45	2865	47.75	8.5	
	13.55	2875	47.91667	8.5	
Oxidation	14.00	2880	48		1298
	14.01	2881	48.01667		1176
	14.02	2882	48.03333		1082
	14.03	2883	48.05		972
	14.04	2884	48.06667		896
	14.05	2885	48.08333		840
	14.06	2886	48.1		799
	14.07	2887	48.11667		771
	14.08	2888	48.13333		747
	14.09	2889	48.15		730
Reduction	14.10	2890	48.16667	9.7	
	14.15	2895	48.25	7.7	
	14.30	2910	48.5	7.6	

14.45	2925	48.75	7.6	
15.00	2940	49	7.6	
15.15	2955	49.25	7.6	
15.30	2970	49.5	7.6	
15.45	2985	49.75	7.6	
16.00	3000	50	7.7	
16.15	3015	50.25	7.7	
16.30	3030	50.5	7.8	
16.45	3045	50.75	7.8	
17.00	3060	51	7.9	

A.2 Redox Cycle Test Results and Calculations for Anode Substrate Sample B-1

Table A.2: Redox test results for anode specimen B_1

Elapsed Time (Hours)	Area Resistance of Substrate (Ohm cm2)	Substrate Resistance (Ohm)	log value of Area Resistance	log value of Substrate Resistance
0	0.1152	0.095214481	-9.38547521	-10.21296998
0.083333333	0.1024	0.084635094	-9.89700043	-10.7244952
0.166666667	0.1008	0.08331267	-9.96539468	-10.79288945
0.333333333	0.1	0.082651459	-10	-10.82749477
0.416666667	0.0992	0.081990247	-10.0348833	-10.86237805
0.5	0.0986	0.081494338	-10.0612309	-10.88872562
0.583333333	0.0982	0.081163733	-10.0788851	-10.90637989
0.666666667	0.098	0.08099843	-10.0877392	-10.91523401
0.75	0.098	0.08099843	-10.0877392	-10.91523401
0.833333333	0.0978	0.080833127	-10.0966115	-10.92410622
0.916666667	0.0978	0.080833127	-10.0966115	-10.92410622
1	0.0976	0.080667824	-10.1055018	-10.93299659
1.25	0.0972	0.080337218	-10.1233374	-10.95083212
1.5	0.0968	0.080006612	-10.1412464	-10.96874119
1.75	0.0964	0.079676006	-10.1592297	-10.98672443
2	0.0964	0.079676006	-10.1592297	-10.98672443
2.25	0.0962	0.079510703	-10.1682493	-10.99574405
2.5	0.096	0.0793454	-10.1772877	-11.00478244
19	0.0518	0.042813456	-12.8567024	-13.68419717
19.5	0.0516	0.042648153	-12.873503	-13.70099775
20	0.0514	0.04248285	-12.8903688	-13.71786358
20.5	0.0512	0.042317547	-12.9073004	-13.73479516
21	0.051	0.042152244	-12.9242982	-13.75179301

21.33333333	0.0508	0.041986941	-12.9413629	-13.76885764
21.5	2000	1653.029176	33.01029996	32.18280519
21.51666667	1870	1545.58228	32.71841607	31.8909213
21.53333333	1815	1500.123977	32.58876629	31.76127153
21.55	1724	1424.91115	32.36537261	31.53787785
21.56666667	1634	1350.524837	32.13252052	31.30502575
21.58333333	1597	1319.943797	32.03304916	31.20555439
21.6	1555	1285.230184	31.91730393	31.08980917
21.61666667	1519	1255.475659	31.81557774	30.98808297
21.63333333	1492	1233.159765	31.73768823	30.91019346
21.65	1485	1227.374163	31.71726454	30.88976977
21.66666667	0.0334	0.027605587	-14.7625353	-15.5900301
21.75	0.0264	0.021819985	-15.7839607	-16.6114555
21.83333333	0.026	0.021489379	-15.8502665	-16.67776129
0.219166667	0.0258	0.021324076	-15.8838029	-16.71129771
22	0.0256	0.021158773	-15.9176003	-16.74509511
22.25	0.0254	0.020993471	-15.9516628	-16.7791576
22.5	0.0254	0.020993471	-15.9516628	-16.7791576
22.75	0.0256	0.021158773	-15.9176003	-16.74509511
23	0.0256	0.021158773	-15.9176003	-16.74509511
23.25	0.0258	0.021324076	-15.8838029	-16.71129771
23.41666667	0.026	0.021489379	-15.8502665	-16.67776129
23.5	1789	1478.634598	32.52610341	31.69860864
23.51666667	1668	1378.626333	32.22196046	31.3944657
23.53333333	1520	1256.302174	31.81843588	30.99094111
23.55	1396	1153.814365	31.44885418	30.62135942
23.56666667	1286	1062.89776	31.09240969	30.26491492
23.58333333	1209	999.2561369	30.82426301	29.99676824
23.6	1146	947.1857178	30.59184618	29.76435141
23.61666667	1096	905.8599884	30.39810554	29.57061077
23.63333333	1061	876.9319778	30.25715384	29.42965907
23.65	1034	854.616084	30.14520539	29.31771062
23.66666667	0.04192	0.034647492	-13.7757873	-14.60328203
23.75	0.0256	0.021158773	-15.9176003	-16.74509511
24	0.0244	0.020166956	-16.1261017	-16.9535965
24.25	0.0242	0.020001653	-16.1618463	-16.98934111
24.5	0.0242	0.020001653	-16.1618463	-16.98934111
24.75	0.0244	0.020166956	-16.1261017	-16.9535965
25	0.0244	0.020166956	-16.1261017	-16.9535965
25.25	0.0246	0.020332259	-16.0906489	-16.9181437
25.5	0.0248	0.020497562	-16.0554832	-16.88297796
25.75	0.025	0.020662865	-16.0205999	-16.84809468
26	0.0252	0.020828168	-15.9859946	-16.81348936
43.5	0.0242	0.020001653	-16.1618463	-16.98934111
43.75	0.0242	0.020001653	-16.1618463	-16.98934111
43.91666667	0.0242	0.020001653	-16.1618463	-16.98934111

44	1694	1400.115712	32.28913406	31.46163929
44.01666667	1574	1300.933961	31.97004728	31.14255251
44.03333333	1448	1196.793123	31.60768562	30.78019085
44.05	1311	1083.560625	31.17602692	30.34853215
44.06666667	1201	992.6440202	30.79543007	29.96793531
44.08333333	1122	927.3493677	30.49992857	29.6724338
44.1	1064	879.4115216	30.26941628	29.44192151
44.11666667	1016	839.7388214	30.06893708	29.24144231
44.13333333	974	805.0252087	29.88558957	29.0580948
44.15	941	777.7502273	29.73589623	28.90840147
44.16666667	0.0294	0.024299529	-15.3165267	-16.14402146
44.25	0.0194	0.016034383	-17.1219827	-17.94947747
44.5	0.0184	0.015207868	-17.3518218	-18.17931654
44.75	0.0186	0.015373171	-17.3048706	-18.13236533
45	0.0186	0.015373171	-17.3048706	-18.13236533
45.25	0.0186	0.015373171	-17.3048706	-18.13236533
28.83333333	0.0188	0.015538474	-17.2584215	-18.08591627
45.75	0.0188	0.015538474	-17.2584215	-18.08591627
45.91666667	0.0188	0.015538474	-17.2584215	-18.08591627
46	1441	1191.007521	31.58663981	30.75914504
46.01666667	1314	1086.040169	31.18595365	30.35845888
46.03333333	1174	970.3281263	30.69668097	29.8691862
46.05	1062	877.7584924	30.26124517	29.4337504
46.06666667	978	808.331267	29.90338855	29.07589378
46.08333333	917	757.9138772	29.62369336	28.79619859
46.1	873	721.5472353	29.41014244	28.58264767
46.11666667	841	695.0987685	29.24795996	28.42046519
46.13333333	815	673.6093892	29.11157609	28.28408132
46.15	796	657.905612	29.00913068	28.18163591
46.16666667	0.0216	0.017852715	-16.6554625	-17.48295726
46.25	0.0172	0.014216051	-17.6447155	-18.4722103
46.5	0.0166	0.013720142	-17.7989191	-18.62641389
46.75	0.0166	0.013720142	-17.7989191	-18.62641389
47	0.0168	0.013885445	-17.7469072	-18.57440195
47.25	0.0168	0.013885445	-17.7469072	-18.57440195
47.5	0.0168	0.013885445	-17.7469072	-18.57440195
47.75	0.017	0.014050748	-17.6955108	-18.52300555
47.91666667	0.017	0.014050748	-17.6955108	-18.52300555
48	1298	1072.815935	31.13274692	30.30525216
48.01666667	1176	971.9811555	30.70407322	29.87657845
48.03333333	1082	894.2887842	30.34227261	29.51477784
48.05	972	803.3721795	29.87666265	29.04916788
48.06666667	896	740.5570708	29.5230801	28.69558533
48.08333333	840	694.2722539	29.24279286	28.41529809
48.1	799	660.3851558	29.02546779	28.19797303
48.11666667	771	637.2427473	28.87054378	28.04304901

48.13333333	747	617.4063972	28.73320602	27.90571125
48.15	730	603.3556492	28.6332286	27.80573383
48.16666667	0.0194	0.016034383	-17.1219827	-17.94947747
48.25	0.0154	0.012728325	-18.1247928	-18.95228756
48.5	0.0152	0.012563022	-18.1815641	-19.00905889
48.75	0.0152	0.012563022	-18.1815641	-19.00905889
49	0.0152	0.012563022	-18.1815641	-19.00905889
49.25	0.0152	0.012563022	-18.1815641	-19.00905889
49.5	0.0152	0.012563022	-18.1815641	-19.00905889
49.75	0.0152	0.012563022	-18.1815641	-19.00905889
50	0.0154	0.012728325	-18.1247928	-18.95228756
50.25	0.0154	0.012728325	-18.1247928	-18.95228756
50.5	0.0156	0.012893628	-18.068754	-18.89624878
50.75	0.0156	0.012893628	-18.068754	-18.89624878
51	0.0158	0.01305893	-18.013429	-18.8409239

A.3 Redox Cycle Test Results and Calculations for Anode Substrate Sample B-2

Table A.3: Redox test results and calculations for anode specimen B_2

Oxidation or Reduction	Elapsed Time Hours	Measured Voltage (mV)	Area Resistance of Substrate (Ohm cm2)	Substrate Resistance (Ohm)	log value of Area Resistance	log value of Substrate Resistance
Reduction	0	56.1	0.1122	0.092734937	-9.50007143	-10.3275662
	0.083333333	53.5	0.1122	0.092734937	-9.50007143	-10.3275662
	0.166666667	53.4	0.107	0.088437061	-9.70616222	-10.533657
	0.333333333	53	0.1068	0.088271758	-9.71428747	-10.5417822
	0.416666667	52.6	0.106	0.087610546	-9.74694135	-10.5744361
	0.5	52.6	0.1052	0.086949335	-9.7798426	-10.6073374
	0.583333333	52.4	0.1052	0.086949335	-9.7798426	-10.6073374
	0.666666667	52.4	0.1048	0.086618729	-9.79638717	-10.6238819
	0.75	52.2	0.1048	0.086618729	-9.79638717	-10.6238819
	0.833333333	52.2	0.1044	0.086288123	-9.81299501	-10.6404898
	0.916666667	52.2	0.1044	0.086288123	-9.81299501	-10.6404898
	1	52.1	0.1044	0.086288123	-9.81299501	-10.6404898
	1.25	52.1	0.1042	0.08612282	-9.82132281	-10.6488176
	1.5	52.1	0.1042	0.08612282	-9.82132281	-10.6488176
	1.75	52.1	0.1042	0.08612282	-9.82132281	-10.6488176
	2	52	0.1042	0.08612282	-9.82132281	-10.6488176

	2.25	52	0.104	0.085957517	-9.82966661	-10.6571614
	2.5	52	0.104	0.085957517	-9.82966661	-10.6571614
	19	50.7	0.104	0.085957517	-9.82966661	-10.6571614
	19.5	50.7	0.1014	0.083808579	-9.93962045	-10.7671152
	20	50.7	0.1014	0.083808579	-9.93962045	-10.7671152
	20.5	50.7	0.1014	0.083808579	-9.93962045	-10.7671152
	21	50.7	0.1014	0.083808579	-9.93962045	-10.7671152
	21.33333333	50.7	0.1014	0.083808579	-9.93962045	-10.7671152
Oxidation	21.5		5350	4421.853046	37.28353782	36.45604305
	21.51666667		4990	4124.307794	36.98100546	36.15351069
	21.53333333		4610	3810.232251	36.63700925	35.80951449
	21.55		4260	3520.952145	36.29409599	35.46660122
	21.56666667		3930	3248.202331	35.9439255	35.11643074
	21.58333333		3650	3016.778246	35.62292864	34.79543388
	21.6		3410	2818.414745	35.32754379	34.50004902
	21.61666667		3240	2677.907265	35.1054501	34.27795533
	21.63333333		3110	2570.460369	34.92760389	34.10010912
	21.65		2990	2471.278618	34.75671188	33.92921712
Reduction	21.66666667	57.6	0.1152	0.095214481	-9.38547521	-10.21297
	21.75	34.1	0.0682	0.056368295	-11.6621563	-12.489651
	21.83333333	33.7	0.0674	0.055707083	-11.713401	-12.5408958
	0.219166667	33.5	0.067	0.055376477	-11.739252	-12.5667467
	22	33.3	0.0666	0.055045872	-11.7652577	-12.5927525
	22.25	33.1	0.0662	0.054715266	-11.7914201	-12.6189149
	22.5	33.1	0.0662	0.054715266	-11.7914201	-12.6189149
	22.75	33.2	0.0664	0.054880569	-11.7783192	-12.605814
	23	33.4	0.0668	0.055211174	-11.7522354	-12.5797301
	23.25	33.6	0.0672	0.05554178	-11.7263073	-12.553802
	23.41666667	33.7	0.0674	0.055707083	-11.713401	-12.5408958
Oxidation	23.5		4080	3372.179519	36.10660163	35.27910686
	23.51666667		3740	3091.164559	35.72871602	34.90122125
	23.53333333		3320	2744.028432	35.21138084	34.38388607
	23.55		2990	2471.278618	34.75671188	33.92921712
	23.56666667		2760	2281.180263	34.40909082	33.58159605
	23.58333333		2590	2140.672783	34.13299764	33.30550287
	23.6		2470	2041.491032	33.92696953	33.09947477
	23.61666667		2390	1975.369865	33.78397901	32.95648424
	23.63333333		3320	2744.028432	35.21138084	34.38388607
	23.65		3270	2702.702703	35.14547753	34.31798276
Reduction	23.66666667	49.8	0.0996	0.082320853	-10.0174066	-10.8449014
	23.75	32.3	0.0646	0.053392842	-11.8976748	-12.7251696
	24	30.3	0.0606	0.050086784	-12.1752738	-13.0027685
	24.25	30.5	0.061	0.05041739	-12.1467016	-12.9741964
	24.5	30.7	0.0614	0.050747996	-12.1183163	-12.9458111
	24.75	30.9	0.0618	0.051078602	-12.0901152	-12.91761
	25	31	0.062	0.051243904	-12.0760831	-12.9035779

	25.25	31.1	0.0622	0.051409207	-12.0620962	-12.8895909
	25.5	31.2	0.0624	0.05157451	-12.0481541	-12.8756489
	25.75	31.2	0.0624	0.05157451	-12.0481541	-12.8756489
	26	31.3	0.0626	0.051739813	-12.0342567	-12.8617514
	43.5	32.5	0.065	0.053723448	-11.8708664	-12.6983612
	43.75	32.5	0.065	0.053723448	-11.8708664	-12.6983612
	43.91666667	32.5	0.065	0.053723448	-11.8708664	-12.6983612
Oxidation	44		4020	3322.588644	36.04226053	35.21476576
	44.01666667		3920	3239.937185	35.93286067	35.1053659
	44.03333333		3630	3000.247954	35.59906625	34.77157148
	44.05		3340	2760.558724	35.23746467	34.4099699
	44.06666667		3100	2562.195223	34.91361694	34.08612217
	44.08333333		2900	2396.892305	34.62397998	33.79648521
	44.1		2750	2272.915117	34.39332694	33.56583217
	44.11666667		2640	2181.998512	34.21603927	33.3885445
	44.13333333		2550	2107.612199	34.0654018	33.23790704
	44.15		2490	2058.021324	33.96199347	33.1344987
Reduction	44.16666667	45.7	0.0914	0.075543433	-10.390538	-11.2180328
	44.25	30.9	0.0618	0.051078602	-12.0901152	-12.91761
	44.5	30.5	0.061	0.05041739	-12.1467016	-12.9741964
	44.75	30.5	0.061	0.05041739	-12.1467016	-12.9741964
	45	30.6	0.0612	0.050582693	-12.1324858	-12.9599805
	45.25	30.9	0.0618	0.051078602	-12.0901152	-12.91761
	28.83333333	31.1	0.0622	0.051409207	-12.0620962	-12.8895909
	45.75	31.2	0.0624	0.05157451	-12.0481541	-12.8756489
	45.91666667	31.2	0.0624	0.05157451	-12.0481541	-12.8756489
Oxidation	46		3480	2876.270766	35.41579244	34.58829767
	46.01666667		3290	2719.232994	35.17195898	34.34446421
	46.03333333		2960	2446.48318	34.71291711	33.88542234
	46.05		2750	2272.915117	34.39332694	33.56583217
	46.06666667		2540	2099.347053	34.04833717	33.2208424
	46.08333333		2380	1967.104719	33.76576957	32.9382748
	46.1		2260	1867.922969	33.54108439	32.71358962
	46.11666667		2150	1777.006364	33.3243846	32.49688983
	46.13333333		2090	1727.415489	33.20146286	32.37396809
	46.15		2020	1669.559468	33.05351369	32.22601893
Reduction	46.16666667	42.9	0.0858	0.070914952	-10.6651271	-11.4926219
	46.25	30.7	0.0614	0.050747996	-12.1183163	-12.9458111
	46.5	29.3	0.0586	0.048433755	-12.3210238	-13.1485186
	46.75	29.2	0.0584	0.048268452	-12.3358715	-13.1633663
	47	29.5	0.059	0.048764361	-12.2914799	-13.1189747
	47.25	29.6	0.0592	0.048929664	-12.2767829	-13.1042777
	47.5	29.8	0.0596	0.049260269	-12.2475374	-13.0750322
	47.75	29.9	0.0598	0.049425572	-12.2329882	-13.0604829
	47.91666667	29.9	0.0598	0.049425572	-12.2329882	-13.0604829
Oxidation	48		3450	2851.475329	35.37819095	34.55069618

	48.01666667		3170	2620.051244	35.01059262	34.18309785
	48.03333333		2740	2264.649971	34.37750563	33.55001086
	48.05		2550	2107.612199	34.0654018	33.23790704
	48.06666667		2400	1983.635011	33.80211242	32.97461765
	48.08333333		2290	1892.718406	33.59835482	32.77086006
	48.1		2180	1801.801802	33.38456494	32.55707017
	48.11666667		2110	1743.945781	33.24282455	32.41532979
	48.13333333		2050	1694.354905	33.11753861	32.29004384
	48.15		2013	1663.773866	33.03843775	32.21094298
Reductiion	48.16666667	39.8	0.0796	0.065790561	-10.9908693	-11.8183641
	48.25	29.9	0.0598	0.049425572	-12.2329882	-13.0604829
	48.5	29.5	0.059	0.048764361	-12.2914799	-13.1189747
	48.75	29	0.058	0.047937846	-12.3657201	-13.1932148
	49	29	0.058	0.047937846	-12.3657201	-13.1932148
	49.25	29.4	0.0588	0.048599058	-12.3062267	-13.1337215
	49.5	29.7	0.0594	0.049094967	-12.2621356	-13.0896303
	49.75	29.8	0.0596	0.049260269	-12.2475374	-13.0750322
	50	29.9	0.0598	0.049425572	-12.2329882	-13.0604829
	50.25	29.9	0.0598	0.049425572	-12.2329882	-13.0604829
	50.5	30	0.06	0.049590875	-12.2184875	-13.0459823
	50.75	30	0.06	0.049590875	-12.2184875	-13.0459823
	51	30.1	0.0602	0.049756178	-12.2040351	-13.0315299

A.4 Redox Cycle Test Results and Calculations for Anode Substrate Sample A-1

Table A.4: Redox test results and calculations for anode specimen A_1

Oxidation or Reduction	Elapsed Time (Hours)	Measured Voltage(mV)	Area Resistance of Substrate (Ohm cm2)	Substrate Resistance (Ohm)	log value of area Resistance	log value of Substrate Resistance
Reduction	0.00	8.3	0.0166	0.013116308	-17.79891912	-18.82188378
	0.17	8.1	0.0162	0.012800253	-17.90484985	-18.92781452
	1.88	6.7	0.0134	0.010587863	-18.72895202	-19.75191668
	2.05	6.6	0.0132	0.010429836	-18.79426069	-19.81722535
	2.18	6.5	0.013	0.010271808	-18.86056648	-19.88353114
	3.03	6.2	0.0124	0.009797724	-19.06578315	-20.08874781
	25.45	5.1	0.0102	0.008059418	-19.91399828	-20.93696294
Oxidation	25.52		244	192.7939317	23.87389826	22.8509336
	25.67		193	152.4968394	22.85557309	21.83260843
Reduction	25.68	3.0	0.006	0.004740834	-22.2184875	-23.24145216
	27.10	3.3	0.0066	0.005214918	-21.80456064	-22.82752531

	28.08	3.4	0.0068	0.005372946	-21.67491087	-22.69787553
	28.30	3.5	0.007	0.005530973	-21.5490196	-22.57198426
Oxidation	28.30		351	277.3388116	25.45307116	24.4301065
	28.47		211	166.7193426	23.24282455	22.21985989
Reduction	28.47	2.7	0.0054	0.004266751	-22.6760624	-23.69902706
	28.63	2.8	0.0056	0.004424779	-22.51811973	-23.54108439
	28.85	2.9	0.0058	0.004582807	-22.36572006	-23.38868473
	29.00	2.9	0.0058	0.004582807	-22.36572006	-23.38868473
Oxidation	29.05		349	275.7585335	25.42825427	24.40528961
	29.22		189	149.3362832	22.76461804	21.74165338
Reduction	29.22	2.7	0.0054	0.004266751	-22.6760624	-23.69902706
	29.38	2.5	0.005	0.003950695	-23.01029996	-24.03326462
	29.55	2.6	0.0052	0.004108723	-22.83996656	-23.86293123
	29.72	2.6	0.0052	0.004108723	-22.83996656	-23.86293123
Oxidation	29.75		329	259.9557522	25.17195898	24.14899432
	29.78		253	199.9051833	24.03120521	23.00824055
	29.82		223	176.2010114	23.48304863	22.46008397
	29.85		184	145.3855879	22.64817823	21.62521357
	29.88		179	141.4348925	22.52853031	21.50556565
	29.92		178	140.6447535	22.50420002	21.48123536
Reduction	29.92	2.5	0.005	0.003950695	-23.01029996	-24.03326462
	30.08	2.3	0.0046	0.00363464	-23.37242168	-24.39538634
	30.25	2.3	0.0046	0.00363464	-23.37242168	-24.39538634
	30.42	2.4	0.0048	0.003792668	-23.18758763	-24.21055229
Oxidation	30.47		326	257.585335	25.132176	24.10921134
	30.50		272	214.9178255	24.34568904	23.32272438
	30.53		211	166.7193426	23.24282455	22.21985989
	30.57		180	142.2250316	22.55272505	21.52976039
	30.60		174	137.4841972	22.40549248	21.38252782
	30.63		174	137.4841972	22.40549248	21.38252782
Reduction	30.67	2.4	0.0048	0.003792668	-23.18758763	-24.21055229
	30.83	2.2	0.0044	0.003476612	-23.56547324	-24.5884379
	31.00	2.2	0.0044	0.003476612	-23.56547324	-24.5884379
	31.17	2.2	0.0044	0.003476612	-23.56547324	-24.5884379
Oxidation	31.22		295	233.091024	24.69822016	23.6752555
	31.25		261	206.2262958	24.16640507	23.14344041
	31.28		203	160.3982301	23.07496038	22.05199572
	31.32		173	136.6940582	22.38046103	21.35749637
	31.35		167	131.9532238	22.22716471	21.20420005
	31.38		167	131.9532238	22.22716471	21.20420005
Reduction	31.42	2.2	0.0044	0.003476612	-23.56547324	-24.5884379
	31.58	2	0.004	0.003160556	-23.97940009	-25.00236475
	31.75	2	0.004	0.003160556	-23.97940009	-25.00236475
	31.92	2.1	0.0042	0.003318584	-23.7675071	-24.79047176
Oxidation	31.97		323	255.2149178	25.09202522	24.06906056

	32.00		244	192.7939317	23.87389826	22.8509336
	32.03		195	154.0771176	22.90034611	21.87738145
	32.07		174	137.4841972	22.40549248	21.38252782
	32.10		167	131.9532238	22.22716471	21.20420005
	32.13		165	130.3729456	22.17483944	21.15187478
Reduction	32.17	2	0.004	0.003160556	-23.97940009	-25.00236475
	32.33	1.9	0.0038	0.003002528	-24.20216403	-25.2251287
	32.50	1.9	0.0038	0.003002528	-24.20216403	-25.2251287
	32.67	1.9	0.0038	0.003002528	-24.20216403	-25.2251287
Oxidation	32.72		316	249.6839444	24.99687083	23.97390616
	32.75		215	169.8798989	23.3243846	22.30141994
	32.78		197	155.6573957	22.94466226	21.9216976
	32.82		174	137.4841972	22.40549248	21.38252782
	32.85		165	130.3729456	22.17483944	21.15187478
	32.88		163	128.7926675	22.12187604	21.09891138
Reduction	32.92	1.9	0.0038	0.003002528	-24.20216403	-25.2251287
	33.08	1.8	0.0036	0.002844501	-24.43697499	-25.45993965
	33.25	1.8	0.0036	0.002844501	-24.43697499	-25.45993965
	33.42	1.8	0.0036	0.002844501	-24.43697499	-25.45993965
Oxidation	33.47		337	266.2768647	25.27629901	24.25333435
	33.50		275	217.2882427	24.39332694	23.37036228
	33.53		211	166.7193426	23.24282455	22.21985989
	33.57		184	145.3855879	22.64817823	21.62521357
	33.60		170	134.323641	22.30448921	21.28152455
	33.63		163	128.7926675	22.12187604	21.09891138
Reduction	33.67	1.8	0.0036	0.002844501	-24.43697499	-25.45993965
	33.83	1.7	0.0034	0.002686473	-24.68521083	-25.70817549
	34.00	1.7	0.0034	0.002686473	-24.68521083	-25.70817549
	34.17	1.7	0.0034	0.002686473	-24.68521083	-25.70817549
Oxidation	34.22		315	248.8938053	24.98310554	23.96014088
	34.25		242	191.2136536	23.83815366	22.815189
	34.28		192	151.7067004	22.83301229	21.81004763
	34.32		173	136.6940582	22.38046103	21.35749637
	34.35		164	129.5828066	22.14843848	21.12547382
	34.38		161	127.2123894	22.06825876	21.0452941
Reduction	34.42	1.7	0.0034	0.002686473	-24.68521083	-25.70817549
	50.75	2.1	0.0042	0.003318584	-23.7675071	-24.79047176
	53.42	2.2	0.0044	0.003476612	-23.56547324	-24.5884379
Oxidation	53.47		292	230.7206068	24.65382851	23.63086385
	53.50		275	217.2882427	24.39332694	23.37036228
	53.53		249	196.7446271	23.96199347	22.93902881
	53.57		236	186.4728192	23.72912003	22.70615537
	53.60		231	182.5221239	23.6361198	22.61315514
	53.63		229	180.9418458	23.59835482	22.57539016

A.5 Redox Cycle Test Results and Calculations for Anode Substrate Sample A-2

Table A.5: Redox test results and calculations for anode specimen A_2

Oxidation or Reduction	Elapsed Time (Hours)	Measured Voltage(mV)	Area Resistance of Substrate (Ohm cm2)	Substrate Resistance (Ohm)	log value of Unit Area Resistance	log value of Area Resistance
Oxidation	0		10800	9216.983145	40.33423755	39.64588793
Reduction	0.166667	51.8	0.099615385	0.085014196	-10.01673584	-10.70508546
	0.2	40.5	0.077884615	0.066468628	-11.0854832	-11.77383283
	0.233333	37.5	0.072115385	0.061545026	-11.41972076	-12.10807038
	16.03333	31.6	0.060769231	0.051861942	-12.16316261	-12.85151223
	17.03333	31.2	0.06	0.051205462	-12.2184875	-12.90683712
	18.43333	31	0.059615385	0.050877222	-12.2464165	-12.93476612
	23.76667	29.6	0.056923077	0.048579541	-12.44711633	-13.13546595
	23.78333	29.3	0.056346154	0.048087181	-12.49135723	-13.17970685
Oxidation	23.9		3500	2986.985278	35.44068044	34.75233082
	23.91667		3700	3157.670151	35.68201724	34.99366762
Reduction	23.93333	30	0.057692308	0.049236021	-12.38882089	-13.07717051
	23.95	24.6	0.047307692	0.040373537	-13.25068237	-13.93903199
	24.03333	24.2	0.046538462	0.039717057	-13.32187978	-14.0102294
	24.76667	26.7	0.051346154	0.043820059	-12.89492082	-13.58327044
	62.46667	30.7	0.059038462	0.050384862	-12.28864968	-12.9769993
	64.4	30.8	0.059230769	0.050548982	-12.27452627	-12.96287589
Oxidation	64.93333		2960	2526.136121	34.71291711	34.02456749
	64.95		3170	2705.355238	35.01059262	34.322243
	64.96667		3120	2662.68402	34.94154594	34.25319632
	64.98333		3060	2611.478558	34.85721426	34.16886464
Reduction	65	28.3	0.054423077	0.04644598	-12.64216908	-13.3305187
	65.06667	21.5	0.041346154	0.035285815	-13.83564884	-14.52399846
	65.15	20.8	0.04	0.034136975	-13.97940009	-14.66774971
	65.23333	21	0.040384615	0.034465215	-13.93784049	-14.62619011
	65.31667	21.1	0.040576923	0.034629335	-13.91720888	-14.60555851
	65.65	21.4	0.041153846	0.035121695	-13.8558957	-14.54424532
	65.81667	21.6	0.041538462	0.035449935	-13.81549592	-14.50384555
	66.06667	21.8	0.041923077	0.035778175	-13.7754685	-14.46381812
	66.15	21.9	0.042115385	0.035942295	-13.75559229	-14.44394191
	66.31667	22.1	0.0425	0.036270536	-13.7161107	-14.40446032
	66.65	22.3	0.042884615	0.036598776	-13.67698481	-14.36533443
	67.06667	22.6	0.043461538	0.037091136	-13.61894904	-14.30729867
	67.31667	22.7	0.043653846	0.037255256	-13.59977486	-14.28812449
	67.56667	22.7	0.043653846	0.037255256	-13.59977486	-14.28812449
Oxidation	67.6		2020	1723.917218	33.05351369	32.36516407
	67.63333		1980	1689.780243	32.9666519	32.27830228

	67.65		1960	1672.711756	32.92256071	32.23421109
Reduction	67.66667	19.3	0.037115385	0.031675174	-14.30446035	-14.99280997
	67.71667	18	0.034615385	0.029541613	-14.60730839	-15.29565801
	67.75	17.8	0.034230769	0.029213373	-14.65583341	-15.34418304
	67.81667	17.7	0.034038462	0.029049252	-14.68030077	-15.36865039
	67.85	17.8	0.034230769	0.029213373	-14.65583341	-15.34418304
	67.98333	17.9	0.034423077	0.029377493	-14.63150313	-15.31985275
	68.15	18	0.034615385	0.029541613	-14.60730839	-15.29565801
	68.31667	18.2	0.035	0.029869853	-14.55931956	-15.24766918
	83.48333	18.5	0.035576923	0.030362213	-14.48831615	-15.17666577
	83.65	18.6	0.035769231	0.030526333	-14.46490399	-15.15325362
	83.81667	18.7	0.035961538	0.030690453	-14.44161737	-15.12996699
	83.98333	18.8	0.036153846	0.030854573	-14.41845494	-15.10680457
	84.15	18.9	0.036346154	0.031018693	-14.39541539	-15.08376502
	84.31667	19	0.036538462	0.031182813	-14.37249743	-15.06084705
	84.48333	19.1	0.036730769	0.031346933	-14.34969976	-15.03804939

A.6 Redox Cycle Test Results and Calculations for Anode Substrate Sample A-3

Table A.6: Redox test results and calculations for anode specimen A_3

Oxidation or Reduction	Elapsed Time (Hours)	Measured Voltage(mV)	Area Resistance of Substrate (Ohm cm2)	Substrate Resistance (Ohm)	log value of Area Resistance	log value of Substrate Resistance
Reduction	0	66.1	0.129607843	0.114272477	-8.87368717	-9.420583596
	0.083333	70.6	0.138431373	0.122051995	-8.58765475	-9.13455118
	0.166667	71.6	0.140392157	0.123780777	-8.52657154	-9.073467967
	0.25	74.5	0.146078431	0.128794244	-8.35413903	-8.901035463
	0.333333	76.9	0.150784314	0.13294332	-8.21643836	-8.763334792
	0.416667	79.1	0.155098039	0.13674664	-8.09393693	-8.640833356
	0.5	77.5	0.151960784	0.133980589	-8.18268474	-8.729581165
	0.583333	77.5	0.151960784	0.133980589	-8.18268474	-8.729581165
	0.666667	77.4	0.151764706	0.133807711	-8.18829215	-8.735188584
	0.75	77.4	0.151764706	0.133807711	-8.18829215	-8.735188584
	0.833333	77.4	0.151764706	0.133807711	-8.18829215	-8.735188584
	1	77.4	0.151764706	0.133807711	-8.18829215	-8.735188584
	1.083333	77.4	0.151764706	0.133807711	-8.18829215	-8.735188584
	1.166667	77.7	0.152352941	0.134326346	-8.17149157	-8.718388002
	1.25	78.6	0.154117647	0.135882249	-8.1214763	-8.66837273
	1.5	80.8	0.158431373	0.139685569	-8.00158815	-8.548484583
	1.75	80.9	0.158627451	0.139858447	-7.99621654	-8.543112974

	2	74.3	0.145686275	0.128448487	-8.36581362	-8.912710053
	2.25	70.6	0.138431373	0.122051995	-8.58765475	-9.13455118
	2.5	69.4	0.136078431	0.119977457	-8.66210706	-9.209003486
	2.75	69.1	0.135490196	0.119458822	-8.68092129	-9.227817717
	3	59.9	0.11745098	0.10355403	-9.30143354	-9.848329967
	20.33333	57.2	0.112156863	0.098886319	-9.50174147	-10.0486379
Oxidation	20.38333		2370	2089.578558	33.74748346	33.20058703
	20.4		2240	1974.960324	33.50248018	32.95558375
	20.41667		2050	1807.441368	33.11753861	32.57064218
	20.43333		1910	1684.006348	32.81033367	32.26343724
	20.45		1790	1578.204902	32.52853031	31.98163388
	20.46667		1700	1498.853818	32.30448921	31.75759278
	20.48333		1640	1445.953095	32.14843848	31.60154205
	20.5		1590	1401.869159	32.01397124	31.46707481
	20.51667		1550	1366.60201	31.90331698	31.35642055
	20.53333		1510	1331.334862	31.78976947	31.24287304
	20.55		1480	1304.8845	31.70261715	31.15572072
	20.56667		1460	1287.250926	31.64352856	31.09663213
	20.58333		1450	1278.434139	31.61368002	31.06678359
	20.6		1450	1278.434139	31.61368002	31.06678359
Reduction	20.61667	21.8	0.042745098	0.037687443	-13.6911368	-14.23803325
	20.66667	20.1	0.039411765	0.034748514	-14.0437412	-14.59063762
	20.7	20.1	0.039411765	0.034748514	-14.0437412	-14.59063762
	20.75	20.1	0.039411765	0.034748514	-14.0437412	-14.59063762
	21	20.2	0.039607843	0.034921392	-14.0221881	-14.5690845
	21.25	20.3	0.039803922	0.03509427	-14.0007414	-14.54763781
	21.5	20.5	0.040196078	0.035440027	-13.9581632	-14.50505958
	21.75	20.8	0.040784314	0.035958661	-13.8950684	-14.44196484
	22	21.2	0.041568627	0.036650174	-13.8123432	-14.35923958
	22.5	21.8	0.042745098	0.037687443	-13.6911368	-14.23803325
	23	22.5	0.044117647	0.03889759	-13.5538766	-14.10077301
	23.5	23.1	0.045294118	0.03993486	-13.439582	-13.98647839
	24	23.2	0.045490196	0.040107738	-13.4208219	-13.96771834
	24.5	23.5	0.046078431	0.040626372	-13.3650231	-13.91191957
	25	23.9	0.046862745	0.041317885	-13.2917228	-13.83861918
	25.5	24.3	0.047647059	0.042009398	-13.219639	-13.76653545
Oxidation	25.66667		2380	2098.395345	33.76576957	33.21887314
	25.68333		2261	1993.475577	33.54300562	32.99610919
	25.7		1810	1595.838476	32.57678575	32.02988932
	25.71667		1630	1437.136308	32.12187604	31.57497961
	25.73333		1530	1348.968436	31.84691431	31.30001788
	25.75		1490	1313.701287	31.73186268	31.18496625
	25.76667		1460	1287.250926	31.64352856	31.09663213
	25.78333		1450	1278.434139	31.61368002	31.06678359
	25.8		1450	1278.434139	31.61368002	31.06678359
	25.81667		1450	1278.434139	31.61368002	31.06678359

Reduction	25.86667	24.4	0.047843137	0.042182276	-13.2018035	-13.74869993
	25.91667	20.8	0.040784314	0.035958661	-13.8950684	-14.44196484
	26	21	0.041176471	0.036304418	-13.8535088	-14.40040524
	26.25	21.6	0.042352941	0.037341687	-13.7311642	-14.27806068
	26.5	22.2	0.043529412	0.038378956	-13.612172	-14.15906845
	26.75	22.6	0.044313725	0.039070469	-13.5346174	-14.0815138
	27	22.9	0.044901961	0.039589103	-13.4773469	-14.02424337
	27.25	23.1	0.045294118	0.03993486	-13.439582	-13.98647839
Oxidation	27.33333		1632	1438.899665	32.12720154	31.58030511
	27.35		1378	1214.953271	31.39249218	30.84559575
	27.36667		1261	1111.796861	31.00715087	30.46025444
	27.38333		1192	1050.96103	30.76276255	30.21586612
	27.4		1150	1013.930524	30.6069784	30.06008197
	27.41667		1125	991.8885558	30.51152522	29.96462879
	27.43333		1109	977.7816963	30.44931546	29.90241903
	27.45		1103	972.4916241	30.42575512	29.87885869
	27.46667		1101	970.7282666	30.41787319	29.87097676
	27.48333		1099	968.9649092	30.40997692	29.86308049
Reduction	27.5	22.1	0.043333333	0.038206078	-13.631779	-14.17867545
	27.58333	17.1	0.033529412	0.029562169	-14.7457407	-15.29263709
	27.75	17.1	0.033529412	0.029562169	-14.7457407	-15.29263709
	28	17.4	0.034117647	0.030080803	-14.6702093	-15.21710571
	28.25	17.7	0.034705882	0.030599438	-14.5959691	-15.14286553
	28.5	17.9	0.035098039	0.030945194	-14.5471715	-15.09406788
	28.75	18	0.035294118	0.031118072	-14.5229767	-15.06987314
	29	18	0.035294118	0.031118072	-14.5229767	-15.06987314
	44.5	22.8	0.044705882	0.039416225	-13.4963533	-14.04324972
	44.75	22.8	0.044705882	0.039416225	-13.4963533	-14.04324972
Oxidation	45		1980	1745.723858	32.9666519	32.41975547
	45.01667		1872	1650.502557	32.72305844	32.17616201
	45.03333		1728	1523.540822	32.37543738	31.82854095
	45.05		1609	1418.621054	32.06556044	31.51866401
	45.06667		1509	1330.453183	31.7868924	31.23999597
	45.08333		1437	1266.972315	31.57456768	31.02767125
	45.1		1383	1219.361665	31.4082218	30.86132537
	45.11667		1339	1180.567801	31.26780577	30.72090934
	45.13333		1296	1142.655616	31.12605002	30.57915359
	45.15		1269	1118.850291	31.03461622	30.48771979
Reduction	45.16667	21.4	0.041960784	0.03699593	-13.771564	-14.31846046
	45.25	18.3	0.035882353	0.031636707	-14.4511909	-14.99808729
	45.5	17	0.033333333	0.029389291	-14.7712125	-15.31810898
	45.75	17.2	0.03372549	0.029735047	-14.7204173	-15.26731372
	46	17.5	0.034313725	0.030253681	-14.6453213	-15.1922177
	46.25	17.6	0.034509804	0.03042656	-14.6205751	-15.16747151
	46.5	17.7	0.034705882	0.030599438	-14.5959691	-15.14286553
	46.75	17.8	0.034901961	0.030772316	-14.5715017	-15.11839817

	46.91667	17.8	0.034901961	0.030772316	-14.5715017	-15.11839817
Oxidation	47		1958	1726.326926	32.91812687	32.37123045
	47.01667		1801	1587.903368	32.55513713	32.0082407
	47.03333		1623	1430.964557	32.1031852	31.55628877
	47.05		1474	1299.594428	31.68497484	31.13807841
	47.06667		1382	1218.479986	31.40508043	30.858184
	47.08333		1311	1155.880797	31.17602692	30.62913049
	47.1		1265	1115.323576	31.02090526	30.47400883
	47.11667		1234	1087.991536	30.9131516	30.36625517
	47.13333		1211	1067.712925	30.83144143	30.284545
	47.15		1200	1058.01446	30.79181246	30.24491603
Reduction	47.16667	19.1	0.03745098	0.033019732	-14.2653681	-14.81226452
	47.25	15.6	0.030588235	0.026968996	-15.1444558	-15.69135221
	47.5	15.5	0.030392157	0.026796118	-15.1723848	-15.71928121
	47.75	15.8	0.030980392	0.027314752	-15.0891309	-15.63602732
	48	16.1	0.031568627	0.027833387	-15.007443	-15.55433943
	48.25	16.3	0.031960784	0.028179143	-14.9538257	-15.50072215
	48.5	16.5	0.032352941	0.0285249	-14.9008623	-15.44775875
	48.75	16.6	0.03254902	0.028697778	-14.8746209	-15.42151731
Oxidation	49		1633	1439.781344	32.12986185	31.58296542
	49.01667		1512	1333.098219	31.79551791	31.24862148
	49.03333		1353	1192.911303	31.31297797	30.76608154
	49.05		1268	1117.968612	31.03119254	30.48429611
	49.06667		1185	1044.789279	30.7371835	30.19028707
	49.08333		1141	1005.995415	30.57285644	30.02596001
	49.1		1101	970.7282666	30.41787319	29.87097676
	49.11667		1074	946.9229413	30.31004281	29.76314638
	49.13333		1059	933.6977605	30.2489596	29.70206317
	49.15		1046	922.2359372	30.19531685	29.64842042
Reduction	49.16667	18.5	0.03627451	0.031982463	-14.4039845	-14.95088091
	49.25	13.2	0.025882353	0.02281992	-15.8699624	-16.41685888
	49.5	13.2	0.025882353	0.02281992	-15.8699624	-16.41685888
	49.75	13.3	0.026078431	0.022992798	-15.8371854	-16.38408178
	50	13.4	0.02627451	0.023165676	-15.8046538	-16.35155021
	50.25	13.5	0.026470588	0.023338554	-15.7723641	-16.31926051
	50.5	13.6	0.026666667	0.023511432	-15.7403127	-16.28720911
	50.75	13.7	0.026862745	0.023684311	-15.7084961	-16.25539252
	50.91667	13.7	0.026862745	0.023684311	-15.7084961	-16.25539252
	51	13.7	0.026862745	0.023684311	-15.7084961	-16.25539252
	68.5	15.8	0.030980392	0.027314752	-15.0891309	-15.63602732
	68.75	15.8	0.030980392	0.027314752	-15.0891309	-15.63602732
	68.91667	15.8	0.030980392	0.027314752	-15.0891309	-15.63602732
Oxidation	69		1685	1485.628637	32.26599905	31.71910262
	69.01667		1632	1438.899665	32.12720154	31.58030511
	69.03333		1533	1351.613472	31.85542155	31.30852512
	69.05		1453	1281.079175	31.62265614	31.07575971

	69.06667		1383	1219.361665	31.4082218	30.86132537
	69.08333		1330	1172.632693	31.23851641	30.69161998
	69.1		1280	1128.548757	31.0720997	30.52520327
	69.11667		1252	1103.861753	30.97604329	30.42914686
	69.13333		1224	1079.174749	30.87781418	30.33091775
	69.15		1201	1058.896138	30.79543007	30.24853364
Reduction	69.16667	16.3	0.031960784	0.028179143	-14.9538257	-15.50072215
	69.25	13.3	0.026078431	0.022992798	-15.8371854	-16.38408178
	69.5	13.5	0.026470588	0.023338554	-15.7723641	-16.31926051
	69.75	13.6	0.026666667	0.023511432	-15.7403127	-16.28720911
	70	13.7	0.026862745	0.023684311	-15.7084961	-16.25539252
	70.25	13.8	0.027058824	0.023857189	-15.6769109	-16.22380733
	70.5	13.9	0.027254902	0.024030067	-15.6455538	-16.19245019
	70.75	14	0.02745098	0.024202945	-15.6144214	-16.16131783
	71	14.1	0.027647059	0.024375823	-15.5835106	-16.13040706
	71.25	14.2	0.027843137	0.024548702	-15.5528183	-16.09971475
	71.5	14.2	0.027843137	0.024548702	-15.5528183	-16.09971475

Appendix B

The appendix B contains the results obtained from the redox cycle testing of all the 2-R cell samples and reference SOFC with calculated values Power output.

B.1 Test Results for 2-R Cell Sample-1

a. First reduction at 10 % Hydrogen

Table B.1: Table of I-V values for first reduction at 10 % Hydrogen for Specimen-1

Voltage (V)	Current (A)	Power (W)
0.55	1.280	0.704
0.6	1.110	0.666
0.65	0.980	0.637
0.7	0.830	0.581
0.75	0.700	0.525
0.8	0.550	0.44
0.85	0.420	0.357
0.9	0.31	0.279
0.95	0.19	0.1805
1.012	0.00	0

Voltage (V)	Current (A)	Power (W)
0.95	0.19	0.1805
0.9	0.30	0.27
0.85	0.41	0.3485
0.8	0.54	0.432
0.75	0.69	0.5175
0.7	0.83	0.581
0.65	0.98	0.637
0.6	1.10	0.66
0.55	1.25	0.6875

b. Second reduction at 10 % Hydrogen

Table B.2: Table of I-V values for second reduction at 10 % Hydrogen for Specimen-1

Voltage (V)	Current (A)	Power (W)
0.55	0.980	0.539
0.6	0.870	0.522
0.65	0.760	0.494
0.7	0.660	0.462
0.75	0.550	0.4125
0.8	0.480	0.384
0.85	0.350	0.2975
0.9	0.26	0.234
0.95	0.17	0.1615
1.012	0.00	0

Voltage (V)	Current (A)	Power (W)
0.95	0.17	0.1615
0.9	0.26	0.234
0.85	0.35	0.2975
0.8	0.46	0.368
0.75	0.54	0.405
0.7	0.65	0.455
0.65	0.75	0.4875
0.6	0.86	0.516
0.55	0.97	0.5335

c. First reduction at 100 % Hydrogen

Table B.3: Table of I-V values for first reduction at 100 % Hydrogen for Specimen-1

Voltage (V)	Current (A)	Power (W)
0.55	1.430	0.7865
0.6	1.260	0.756
0.65	1.100	0.715
0.7	0.940	0.658
0.75	0.790	0.5925
0.8	0.640	0.512
0.85	0.500	0.425
0.9	0.35	0.315
0.95	0.23	0.2185
1.034	0.00	0

Voltage (V)	Current (A)	Power (W)
0.95	0.23	0.2185
0.9	0.35	0.315
0.85	0.50	0.425
0.8	0.64	0.512
0.75	0.78	0.585
0.7	0.93	0.651
0.65	1.09	0.7085
0.6	1.24	0.744
0.55	1.40	0.77

d.Second reduction at 100 % Hydrogen

Table B.4: Table of I-V values for second reduction at 10 % Hydrogen for Specimen-1

Voltage (V)	Current (A)	Power (W)
0.55	0.980	0.539
0.6	0.870	0.522
0.65	0.760	0.494
0.7	0.660	0.462
0.75	0.550	0.4125
0.8	0.480	0.384
0.85	0.350	0.2975
0.9	0.26	0.234
0.95	0.17	0.1615
1.012	0.00	0

Voltage (V)	Current (A)	Power (W)
0.95	0.17	0.1615
0.9	0.26	0.234
0.85	0.35	0.2975
0.8	0.46	0.368
0.75	0.54	0.405
0.7	0.65	0.455
0.65	0.75	0.4875
0.6	0.86	0.516
0.55	0.97	0.5335

B.2 Test Results for 2-R Cell Sample-3

a. First reduction at 10 % Hydrogen

Table B.5: Table of I-V values for first reduction at 10 % Hydrogen for Specimen-3

Voltage (V)	Current (A)	Power (W)
0.55	2.250	1.2375
0.6	2.140	1.284
0.65	1.980	1.287
0.7	1.750	1.225
0.75	1.460	1.095
0.8	1.150	0.92
0.85	0.860	0.731
0.9	0.59	0.531
0.95	0.32	0.304
1.035	0.00	0

Voltage (V)	Current (A)	Power (W)
0.95	0.32	0.304
0.9	0.57	0.513
0.85	0.83	0.7055
0.8	1.13	0.904
0.75	1.41	1.0575
0.7	1.67	1.169
0.65	1.91	1.2415
0.6	2.09	1.254
0.55	2.21	1.2155

b. Second reduction at 10 % Hydrogen

Table B.6: Table of I-V values for second reduction at 10 % Hydrogen for Specimen-3

Voltage (V)	Current	Power (W)
0.55	2.160	1.188
0.6	2.000	1.200
0.65	1.820	1.183
0.7	1.590	1.113
0.75	1.340	1.005
0.8	1.080	0.864
0.85	0.810	0.689
0.9	0.55	0.495
0.95	0.31	0.295
1.035	0.00	0.000

Voltage (V)	Current	Power (W)
0.95	0.31	0.295
0.9	0.54	0.486
0.85	0.80	0.680
0.8	1.06	0.848
0.75	1.32	0.990
0.7	1.56	1.092
0.65	1.79	1.164
0.6	1.97	1.182
0.55	2.12	1.166

c. First reduction at 100 % Hydrogen

Table B.7: Table of I-V values for first reduction at 100 % Hydrogen for Specimen-3

Voltage (V)	Current (A)	Power (W)
0.55	4.660	2.563
0.6	4.300	2.58
0.65	3.720	2.418
0.7	3.010	2.107
0.75	2.480	1.86
0.8	1.970	1.576
0.85	1.480	1.258
0.9	1.03	0.927
0.95	0.60	0.57
1	0.28	0.28
1.04	0.00	0

Voltage (V)	Current (A)	Power (W)
1	0.28	0.28
0.95	0.60	0.57
0.9	1.03	0.927
0.85	1.46	1.241
0.8	1.93	1.544
0.75	2.42	1.815
0.7	2.93	2.051
0.65	3.62	2.353
0.6	4.18	2.508
0.55	4.51	2.4805

d. Second reduction at 100 % Hydrogen

Table B.8: Table of I-V values for second reduction at 10 % Hydrogen for Specimen-3

Voltage (V)	Current (A)	Power (W)
0.55	4.260	2.343
0.6	3.920	2.352
0.65	3.460	2.249
0.7	2.920	2.044
0.75	2.410	1.808
0.8	1.940	1.552
0.85	1.450	1.233
0.9	1.01	0.909
0.95	0.57	0.542
1	0.28	0.280
1.04	0.00	0.000

Voltage (V)	Current (A)	Power (W)
1	0.28	0.280
0.95	0.57	0.542
0.9	1.00	0.900
0.85	1.44	1.224
0.8	1.92	1.536
0.75	2.38	1.785
0.7	2.88	2.016
0.65	3.42	2.223
0.6	3.85	2.310
0.55	4.17	2.294

B.3 Test Results for 2-R Cell Sample-4

a. First reduction at 10 % Hydrogen

Table B.9: Table of I-V values for first reduction at 10 % Hydrogen for Specimen-4

Voltage (V)	Current (A)	Power (W)
0.55	2.250	1.2375
0.6	2.140	1.284
0.65	1.980	1.287
0.7	1.750	1.225
0.75	1.460	1.095
0.8	1.150	0.92
0.85	0.860	0.731
0.9	0.59	0.531
0.95	0.32	0.304
1.035	0.00	0

Voltage (V)	Current (A)	Power (W)
0.95	0.32	0.304
0.9	0.57	0.513
0.85	0.83	0.7055
0.8	1.13	0.904
0.75	1.41	1.0575
0.7	1.67	1.169
0.65	1.91	1.2415
0.6	2.09	1.254
0.55	2.21	1.2155

b. Second reduction at 10 % Hydrogen

Table B.10: Table of I-V values for second reduction at 10 % Hydrogen for Specimen-4

Voltage (V)	Current	Power (W)
0.55	2.160	1.188
0.6	2.000	1.200
0.65	1.820	1.183
0.7	1.590	1.113
0.75	1.340	1.005
0.8	1.080	0.864
0.85	0.810	0.689
0.9	0.55	0.495
0.95	0.31	0.295
1.035	0.00	0.000

Voltage (V)	Current	Power (W)
0.95	0.31	0.295
0.9	0.54	0.486
0.85	0.80	0.680
0.8	1.06	0.848
0.75	1.32	0.990
0.7	1.56	1.092
0.65	1.79	1.164
0.6	1.97	1.182
0.55	2.12	1.166

c. First reduction at 100 % Hydrogen

Table B.11: Table of I-V values for first reduction at 100 % Hydrogen for Specimen-4

Voltage (V)	Current (A)	Power (W)
0.55	4.660	2.563
0.6	4.300	2.58
0.65	3.720	2.418
0.7	3.010	2.107
0.75	2.480	1.86
0.8	1.970	1.576
0.85	1.480	1.258
0.9	1.03	0.927
0.95	0.60	0.57
1	0.28	0.28
1.04	0.00	0

Voltage (V)	Current (A)	Power (W)
1	0.28	0.28
0.95	0.60	0.57
0.9	1.03	0.927
0.85	1.46	1.241
0.8	1.93	1.544
0.75	2.42	1.815
0.7	2.93	2.051
0.65	3.62	2.353
0.6	4.18	2.508
0.55	4.51	2.4805

d. Second reduction at 100 % Hydrogen

Table B.12: Table of I-V values for second reduction at 10 % Hydrogen for Specimen-4

Voltage (V)	Current (A)	Power (W)
0.55	4.260	2.343
0.6	3.920	2.352
0.65	3.460	2.249
0.7	2.920	2.044
0.75	2.410	1.808
0.8	1.940	1.552
0.85	1.450	1.233
0.9	1.01	0.909
0.95	0.57	0.542
1	0.28	0.280
1.04	0.00	0.000

Voltage (V)	Current (A)	Power (W)
1	0.28	0.280
0.95	0.57	0.542
0.9	1.00	0.900
0.85	1.44	1.224
0.8	1.92	1.536
0.75	2.38	1.785
0.7	2.88	2.016
0.65	3.42	2.223
0.6	3.85	2.310
0.55	4.17	2.294

B.4 Test Results for Cell Sample-5, The Reference Sample

a. First reduction at 10 % Hydrogen

Table B.13: Table of I-V values for first reduction at 10 % Hydrogen for Specimen-5

Voltage (V)	Current (A)	Power (W)	Voltage (V)	Current (A)	Power (W)
0.55	0.570	0.3135	0.95	0.13	0.1235
0.6	0.510	0.306	0.9	0.17	0.153
0.65	0.450	0.2925	0.85	0.21	0.1785
0.7	0.380	0.266	0.8	0.26	0.208
0.75	0.330	0.2475	0.75	0.30	0.225
0.8	0.280	0.224	0.7	0.35	0.245
0.85	0.230	0.1955	0.65	0.40	0.26
0.9	0.17	0.153	0.6	0.45	0.27
0.95	0.13	0.1235	0.55	0.51	0.2805
1.04	0.00	0			

b. Second reduction at 10 % Hydrogen

Table B.14: Table of I-V values for second reduction at 10 % Hydrogen for Specimen-5

Voltage (V)	Current (A)	Power (W)	Voltage (V)	Current (A)	Power (W)
0.55	0.780	0.429	0.95	0.16	0.152
0.6	0.670	0.402	0.9	0.22	0.198
0.65	0.580	0.377	0.85	0.28	0.238
0.7	0.510	0.357	0.8	0.34	0.272
0.75	0.430	0.3225	0.75	0.41	0.3075
0.8	0.360	0.288	0.7	0.48	0.336
0.85	0.290	0.2465	0.65	0.54	0.351
0.9	0.22	0.198	0.6	0.62	0.372
0.95	0.16	0.152	0.55	0.72	0.152
1.04	0.00	0			